UNIVERSITÉ DE MONTRÉAL

CYLINDRICAL UNIDIRECTIONAL DIELECTRIC RADIATOR ARRAY FOR MILLIMETER-WAVE APPLICATIONS

WENLI HONG
DÉPARTEMENT DE GÉNIE ÉLECTRIQUE

ÉCOLE POLYTECHNIQUE DE MONTRÉAL

MÉMOIRE PRÉSENTÉ EN VUE DE L'OBTENTION
DU DIPLÔME DE MAITRISE ÈS SCIENCES APPLIQUÉES

(GÉNIE ÉLECTRIQUE)
DÉCEMBRE 2005

Your file Votre référence
ISBN: 978-0-494-16794-6
Our file Notre référence
ISBN: 978-0-494-16794-6

UNIVERSITÉ DE MONTRÉAL

ÉCOLE POLYTECHNIQUE DE MONTRÉAL

Ce mémoire Intitulé :

CYLINDRICAL UNIDIRECTIONAL DIELECTRIC RADIATOR ARRAY FOR MILLIMETER-WAVE APPLICATIONS

présenté par : HONG Wenli

en vue de l'obtention du diplôme de : Maîtrise ès Sciences Appliquées

a été dûment accepté par le jury d'examen constitué de :

M. JEAN-JACQUES Laurin, Ph.D., président

M. WU Ke, Ph.D., membre et directeur de recherche

M. VAHÉ Nerguizian, Ph.D., membre

ACKNOWLEDGEMENTS

Upon the time of completion of this thesis, I would like to express my sincere appreciation to my supervisor Professor Wu Ke, for his guidance and constant encouragement and support during the whole process of my research project. He has always been ready to give his time generously to discuss ideals and difficulties, and to provide invaluable advice. His keen technique insight and profound expertise have greatly benefited me and have been the driving force behind this research. I also wish to express special thanks to the member of my dissertation committee, Professor Jean-Jacques Laurin, Professor Vaché Nerguizian for their invaluable suggestions and precious time spent in reviewing this thesis and participating in the oral defense.

I would like to express my appreciation to those people in the Poly-Grames Research Centre, who have given me a great deal of help and support. My special thanks go to Professor Bosisio Renato G.,Cevdet Akyel, Jean-Jacques Laurin, Ghannouchi Fadhel, and Doctor Serioja-Ovidiu Tatu for their unforgettable teaching and useful discussion during my graduate study. My thanks also to Mr. Steve Dube, Jules Gauthier and Roch Brassard for the prototype fabrications, and also to Mr. Rene Archambault for the computer and measurement system management.

I also thank my (former) colleagues in Poly-Grames Research Centre, particularly Mr. Ping Yang, Dr. Duochuan Li, Mr. Xinyu Xu, Mr. Lin Li, Dr. Yves Cassivi and Dr. Guifu Gong, for their help and friendship.

Finally, I am greatly indebted to my wife, daughter, parents and brother in law for their support, endurance and deep understanding. Their love is the impetus of my hard work.

RÉSUMÉ

La croissance explosive sur le marché pour accès sans fil à large bande, en relation avec des applications d'onde millimétrique en particulier, a mené à une demande énorme d'antennes en ondes millimétriques rentables, plus performants, et moins coûteuses et a également stimulé beaucoup d'intérêt en recherchant des structures appropriées pour les dispositifs d'alimentation d'antenne. De tels circuits et antennes en ondes millimétriques sont utilisés pour construire l'équipement des locaux d'abonné (ELA) pour le service de distribution multipoint local (SDML) ou le service multipoint local de communication (SMLC) ainsi que d'autres systèmes d'onde millimétrique comprenant les capteurs avancés de radar anticollision de véhicule. Une des questions les plus importantes en faisant face à la conception des systèmes d'onde millimétrique est d'utiliser un module de circuit de haute performance et à faible coût.

L'objectif principal de ce travail est d'étudier et concevoir un nouveau radiateur diélectrique unidirectionnel cylindrique (RDUC) et des réseaux de RDUC. Basé sur le concept du guide conventionnel NRD et cylindrique DR, le RDUC et le réseau de RDUC sont proposés et étudiés théoriquement et expérimentalement. Le réseau de RDUC se compose d'un certain nombre de résonateurs diélectriques cylindrique et d'un guide NRD d'alimentation, qui a tous les avantages techniques de guide NRD et a un grand potentiel pour des applications de circuit en antenne a onde millimétrique et en combinateur de puissance spatial. L'alimentation du guide NRD se compose d'une transition de guide d'ondes métalliques au guide NRD, une jonction T de guide NRD, une courbure de 90° de guide NRD, qui sont proposés dans ce travail et des avantages spéciaux seront démontrés.

ABSTRACT

This thesis presents the new concept and technology of cylindrical unidirectional dielectric radiator (CUDR) and radiators array for applications in conjunction with microwave and millimeter wave circuits, which are based on low loss NRD-guide technology and high-Q cylindrical dielectric resonator technology. The associated feed blocks consists of NRD-guide components such as metal waveguide to NRD-guide transition, NRD-guide T-junction and NRD-guide bend, which allow the NRD-guide in direct coupling with the cylindrical dielectric resonators that can be arranged as cylindrical unidirectional dielectric radiators (CUDR). The structures have been investigated and verified both theoretically and experimentally.

The non-radiative dielectric guide (NRD-guide) is a low-loss transmission line having a unique feature that it can suppress radiation almost completely along bends and discontinuities. These two important features of the NRD-guide, namely, low transmission loss and absence of radiation from bends and discontinuities, make it suitable for realizing compact and high-performance millimeter-wave integrated circuits. The fields and propagation characteristics of the NRD-guide are discussed. Operating modes, dispersion and bandwidth characteristics are presented.

Dielectric resonators (DR) in cylindrical and rectangular shapes are commonly employed at microwave and millimeter-wave frequencies in the design of filters, oscillators, radiators, and tuning elements. Compared with the rectangular counterparts, the cylindrical resonators in the form of a pillbox (disk) or a ring are more often encountered in practice. Similar to the metallic cavity resonators, the dielectric

resonators can be excited with several modes. The basic characteristics defining a dielectric resonator are its resonant frequencies, Q-factors, and field distribution. The field analysis of dielectric rod and the eigenvalue equation for the dielectric rod are deduced and discussed. The modes and resonant frequencies of the parallel-plate dielectric resonator are presented.

The proposed NRD-guide feeder topology consists of a metal waveguide to an NRD-guide transition, LSM_{10}-to-LSE_{10} NRD-guide T-junction and LSE_{10}-to-LSM_{10} NRD-guide 90° bends. For the entire proposed structure, the TE_{01} mode of the rectangular waveguide at input port is split into two LSM_{10} modes of the NRD-guide and have 0° phase difference at the two outputs. This proposed structure is first described, then developed, analyzed and simulated with the help of commercial software Agilent HFSS. It is optimized for low return loss in achieving a good matching. Simulation and measurement results for this structure are presented.

Based on these circuit design and experiments, a promising dielectric antenna, namely the cylindrical unidirectional dielectric radiator (CUDR), which consists of a cylindrical dielectric resonator and NRD-guide feeder, is described. Analysis and experiment of such a cylindrical unidirectional dielectric radiator are also presented. It retains all the merits of NRD-guide and offers a number of unmatched advantageous features for millimeter-wave applications. Simulated and measured results of CUDR and CUDR array are given to illustrate future applications of those novel structures.

CONDENSÉ EN FRANÇAIS

RÉSEAU DE RADIATEUR DIÉLECTRIQUE UNIDIRECTINNEL CYLINDRIQUE POUR DES APPLICATIONS EN ONDE MILLIMETRIQUE

1. Introduction

La croissance explosive sur le marché pour accès sans fil à large bande, en relation avec des applications d'onde millimétrique en particulier, a mené à une demande énorme d'antennes en ondes millimétriques rentables, plus performants, et moins coûteuses et a également stimulé beaucoup d'intérêt en recherchant des structures appropriées pour les dispositifs d'alimentation d'antenne. De tels circuits et antennes en ondes millimétriques sont utilisés pour construire l'équipement des locaux d'abonné (ELA) pour le service de distribution multipoint local (SDML) ou le service multipoint local de communication (SMLC) ainsi que d'autres systèmes d'onde millimétrique comprenant les capteurs avancés de radar anticollision de véhicule. Une des questions les plus importantes en faisant face à la conception des systèmes d'onde millimétrique est d'utiliser un module de circuit de haute performance et à faible coût.

L'objectif principal de ce travail est d'étudier et concevoir un nouveau radiateur diélectrique unidirectionnel cylindrique (RDUC) et des réseaux de RDUC. Basé sur le concept du guide conventionnel NRD et cylindrique DR, le RDUC et le réseau de RDUC sont proposés et étudiés théoriquement et expérimentalement. Le réseau de

RDUC se compose d'un certain nombre de résonateurs diélectriques cylindrique et d'un guide NRD d'alimentation, qui a tous les avantages techniques de guide NRD et a un grand potentiel pour des applications de circuit en antenne a onde millimétrique et en combinateur de puissance spatial. L'alimentation du guide NRD se compose d'une transition de guide d'ondes métalliques au guide NRD, une jonction T de guide NRD, une courbure de 90° de guide NRD, qui sont proposés dans ce travail et des avantages spéciaux seront démontrés.

2. Propriétés fondamentales du guide diélectrique non radiatif (NRD)

Le guide diélectrique non radiatif, d'abord proposé par Yoneyama et Nishida, est une ligne de transmission à faible pertes ayant une caractéristique unique qu'il peut supprimer le rayonnement presque totalement le long des courbures et des discontinuités. Il se compose d'un guide de plaques parallèles avec une bande diélectrique insérée entre ces plaques. Structurellement, il est identique au guide en H sauf que la séparation entre les plaques est inferieure de la moitié de la longueur d'onde dans l'espace libre ($\lambda_0 / 2$).

Les deux caractéristiques importantes du guide NRD, les faibles pertes de transmission et l'absence du rayonnement des courbures et discontinuités, le rendent approprié à réaliser des circuits intégrés d'onde millimétrique compacts et de hautes performances.

Les modes d'un guide NRD sont habituellement classifiés aux modes de LSM et de LSE selon sa géométrie. Les modes LSM_{10} et LSE_{10} sont les plus inferieures des modes

LSM et *LSE* . Le mode LSM_{10} est choisi comme le mode fondamental de fonctionnement du guide de NRD à cause de ses faibles pertes de transmission, cependant, le LSE_{10} a une fréquence de coupure inférieure que le mode de fonctionnement désiré et il peut être utilisé pour coupler le mode LSM_{10} d'une branche du guide NRD à l'autre pour la conception et les applications au diviseur de puissance.

La constante de propagation du guide NRD peut être obtenue en analysant l'expression du champ et en résolvant l'équation caractéristique. Basé sur la description et les caractéristiques discutées de largeur de bande, un critère de conception du guide NRD peut également être obtenu.

3. Analyse des résonateurs cylindriques diélectriques

Les résonateurs sont des composants importants dans les circuits de communication micro-onde. Les résonateurs diélectriques (DR) de formes cylindriques et rectangulaires sont généralement utilisés aux fréquences de micro-onde et d'onde millimétrique dans la conception des filtres, des oscillateurs, des radiateurs, et des éléments d'accord. Comparés aux rectangulaires, les résonateurs cylindriques sous forme de pilulier (disque) ou d'anneau sont plus souvent rencontrés dans la pratique. Semblables aux résonateurs de cavité métalliques, les résonateurs diélectriques peuvent être excités avec plusieurs modes. Les caractéristiques de base définissant un résonateur diélectrique sont ses fréquences de résonance, facteurs Q, et sa distribution de champ.

La compréhension des ondes électromagnétiques dans le guide d'ondes diélectrique de tige est très utile dans la conception des résonateurs diélectriques. L'équation de

valeur propre et les valeurs propres du guide d'ondes diélectrique de tige peuvent être obtenues par l'analyse du champ et des conditions aux frontières. Nous pouvons calculer les fréquences de résonance du résonateur diélectrique de plaques parallèles lorsque les valeurs propres du résonateur diélectrique sont obtenues.

Les champs du résonateur cylindrique peuvent être divisés en modes constitutifs avec la variation azimutale représentée par l'un $\cos m\phi$ ou l'autre $\sin m\phi$ ou (m=0, 1, 2). Pour m=0, l'ensemble de modes peut être divisé en modes TE et modes TM . Ceux-ci sont désignés par les modes TE_{0np} et TM_{0np} .Pour m>0, les modes sont hybrides en nature et sont désignés par HEM_{mnp} . La plus faible fréquence de résonance appartient à la résonance de HEM_{111} , la suivante plus grande est de TE_{011} , et puis de HEM_{211} , de TM_{011} et etc. Les modes résonnants sont trouvés en résolvant les équations aux valeur propre avec les valeurs propres x_{mn} des différents modes. Les fréquences de résonance peuvent être déterminées par la constante diélectrique et les dimensions du résonateur diélectrique cylindrique et peuvent également être mesurées sur une gamme variable des valeurs ε_r et des paramètres dimensionnels en utilisant l'excitation de guide NRD. Quelques résultats typiques pour le résonateur diélectrique cylindrique de plaques parallèles sont présentés et récapitulés. Nous pouvons voir que les valeurs calculées de la fréquence de résonance sont inférieures aux résultats expérimentaux puisque ces fréquences de résonance normales sont affectées par la présence de l'alimentation.

4. Réseau d`alimentation du guide NRD

La topologie proposée d'alimentation du guide NRD se compose d'un guide d'ondes en métal à une transition de guide NRD, LSM10-à-LSE10 de guide NRD jonction en

T, et LSE10-à-LSM10 de guide NRD de 90^{o} de courbure. La première partie est une transition d'un guide d'ondes en métal à un guide NRD, qui convertit le mode TE_{01} du guide d'ondes rectangulaire en mode LSM_{10} du guide NRD. La deuxième partie est une jonction T LSM_{10}-à-LSE_{10} du guide NRD, qui a 180° de différence de phase entre les sorties. La troisième partie est un guide NRD LSE_{10}-à-LSM_{10} courbé à 90°, qui incluent un angle de courbure LSE_{10}-à-LSM_{10} de 90° à droite et un autre angle de courbure LSE_{10}-à-LSM_{10} de 90° à gauche et a 180°de différence de phase entre les sorties. Pour la structure proposée entière, le mode TE_{01} du guide d'ondes rectangulaire au port d'entrée est divisé en deux modes LSM_{10} du guide NRD et a 0° de différence de phase aux deux sorties.

La conception de la transition du guide d'ondes rectangulaire au guide NRD, qui sera appliquée dans ce projet, doit prévoir une conversion progressive du mode du guide d'ondes rectangulaire en mode du guide NRD. Cette transition est conçue et simulée aux fréquences de 26-30 GHz en utilisant le polystyrène comme matériel.

Les jonctions diélectriques T, sans compter qu'agir en tant que diviseurs de puissance, peuvent trouver des applications dans la conception des coupleurs 3dB, modulateurs, commutateurs, mélangeurs, et ainsi de suite. La jonction T du guide NRD est une structure diélectrique de forme T serrée entre les plaques parallèles en métal séparés par une distance de moins que la moitié d'une longueur d'onde, selon le principe du guide NRD.

La jonction T de guide NRD LSE_{10} -à- LSM_{10} est optimisé pour la bande de fréquence 26-29GHz. Les matériaux du polystyrène avec une constante

diélectrique $\varepsilon_r = 2.56$ sont utilisés. Pour obtenir un transfert optimum de mode du port d'entrée au port de sortie, la dimension conçue et la réponse en fréquence sont présentées. La puissance réfléchie au port d'entrée est alors au minimum de -17.8 dB. Le transfert en mode du mode LSM_{10} au port d'entrée au mode LSE_{10} aux ports de sortie demeure pratiquement constant, de -3.83 dB a -3.28 dB sur la plage de fréquences de 26 GHz to 30 GHz.

La courbure de 90° du guide NRD est appliquée dans la structure d'alimentation du guide NRD. On sait qu'il y a une conversion de mode entre les modes LSM_{10} et LSE_{10} dans les structures du guide NRD telles que les jonctions T et les courbures de 90°. Elle peut être optimisée de sorte que presque toute la puissance de mode LSE_{10} au port d'entrée est convertie en puissance de mode LSM_{10} aux ports de sorties. La jonction T du guide NRD ainsi que les courbures du guide NRD à un angle 90° à droite et à gauche sont utilisées pour former un diviseur de puissance en guide NRD. Le réseau d'alimentation du guide NRD a été proposé et développé. Les résultats simulés et mesurés ont montré le mécanisme opératoire et la performance préliminaire du l'alimentation du guide NRD.

5. Radiateur diélectrique cylindrique et rangée de radiateur

Il a été prouvé que le guide d'ondes NRD est l'un des modules les plus prometteurs dans des circuits d'onde millimétrique. Les antennes diélectriques ont l'avantage d'avoir de faible pertes, efficacité de rayonnant élevée, faible cout, simplicité mécanique, et elles sont particulièrement appropriées aux applications à des fréquences plus élevées. L'autre avantage principal des antennes diélectriques est qu'elles peuvent facilement être

intégrées avec les circuits intégrés diélectriques pour former les transmetteurs récepteurs frontaux.

Des antennes diélectriques résonatrices (ADRs), particulièrement les antennes diélectriques résonatrices cylindriques, ont été considérées pour des applications aux fréquences d'onde millimétrique, depuis que les investigations expérimentales systématiques sur ADRs ont été effectuées par Long et autres. Les ADRs partagent plusieurs des avantages des antennes diélectriques, y compris la petite taille, le profil bas, le poids léger, la grande largeur de bande, et la facilité de couplage à beaucoup de types de ligne de transmission. D'ailleurs, ADRs évitent les inconvénients inhérents aux antennes à plaques, telles que la perte élevée de conduction aux fréquences d'onde millimétrique, et la faible efficacité due à l'excitation d'onde de surface.

Dans cette thèse, on décrit une antenne diélectrique prometteuse, à savoir le radiateur diélectrique unidirectionnel cylindrique (RDUC), qui se compose d'une alimentation diélectrique cylindrique de résonateur et de guide NRD. Le RDUC est moisé entre deux plaques métalliques parallèles. C'est principalement une antenne diélectrique cylindrique alimentée par le guide NRD. Le principe de fonctionnement de RDUC est tout à fait semblable à celui du guide NRD et les antennes à onde de fuite, et est l'élément de rayonnement par résonance. Comme antenne, le RDUC est aisément connecté aux circuits passifs et actifs planaires ainsi qu'aux dispositifs NRD.

Il y a plusieurs façons d'exciter le mode résonnant de rayonnement, par exemple, par sonde d'alimentation coaxiale directe, par excitation planaire de couplage ruban-à-fente, ou par couplage direct au guide NRD. Dans ce projet, le guide NRD est choisi pour exciter le RDUC. Le mode d'opération dans le guide NRD est le mode LSM_{10}, qui

couple au résonateur diélectrique cylindrique par une discontinuité devant le guide NRD ou une discontinuité à proximité du guide NRD et excite le mode voulu dans le RDUC. Le mode HEM_{111} premier plus inferieure et le mode TE_{011} deuxième plus inferieure ont été excités dans le RDUC par différentes structures d'alimentation de guide NRD, à savoir, le couplage par devant et couplage par côté. La force du couplage entre le guide NRD et le RDUC peut être changée ou accordée en changeant la distance de discontinuité entre RDUC et l'alimentation de guide NRD.

Des prototypes du guide NRD proposé, alimentant les antennes diélectriques cylindriques de rayonnement, ont été établis et examinés. L'excellente efficacité de couplage peut être obtenue avec le mécanisme de couplage proposé. Les résultats mesurés pour les deux structures confirment l'exactitude de notre calcul des fréquences de résonance et sont également conformes aux résultats simulés. Les RDUCs ont un comportement de résonnance sur une largeur de bande étroite.

Les diagrammes de rayonnement de RDUC sont simulés et mesurés. L'accord entre les mesures et les simulations est bon. L'efficacité de couplage est élevée et une bonne adaptation peut être facilement obtenue. Les isolements entre les diagrammes Co-polaires et contra polaires, dans le plan E et dans le plan H, sont réalisés au-dessus de 23dB.

Pour augmenter la directivité de l'antenne, plusieurs RDUCs peuvent être cascadés pour former un réseau. Les éléments peuvent être alimentés par un seul ou plusieurs guides NRD. En augmentant la distance entre deux éléments adjacents de rayonnement la fréquence de résonance du réseau RDUC augmente, la largeur de bande devient étroite et les lobes secondaires prennent naissance. Le Changement du couplage mutuel

et l'accord de la fréquence de résonance du réseau RDUC peuvent être facilement faits et contrôlés en ajustant la distance entre les résonateurs diélectriques. Ce qui est un avantage significatif de ce type de réseaux d'antennes. Les résultats simulés et mesurés pour les deux structures de réseaux de RDUC sont présentés. L'accord entre les mesures et la simulation est bon. La moitié du faisceau de puissance dans le plan E du réseau de RDUC est plus étroit que celui d'un seul RDUC. Il y a des effets de lobes secondaires sur la plage intéressante du faisceau dans le plan E. Les résultats ont suggéré que l'antenne de CUDR puisse être utilisée pour faire une très bonne antenne directive avec de faibles pertes RF.

6. Conclusion

Dans cette thèse on présente de nouveau concept et technologie de réseaux radiateur et radiateur à diélectrique unidirectionnel cylindrique (RDUC) pour des applications en conjonction avec les circuits micro-ondes et d'ondes millimétriques, qui sont basés sur la technologie du guide NRD aux faibles pertes et la technologie de résonateur diélectrique cylindrique aux facteurs de qualité Q élevés. Les blocs d'alimentation associés sont basés sur les composants de guide NRD tels que la transition de guide d'ondes métallique au guide NRD, jonction T de guide NRD et la courbure de guide NRD, qui permettent un couplage directe du guide NRD avec des résonateurs diélectriques cylindriques qui peuvent être arrangés sous forme de radiateurs diélectriques unidirectionnels cylindrique (RDUC). Les structures ont été étudiées théoriquement et vérifiées expérimentalement. Les résultats expérimentaux démontrent l'utilité et les propriétés intéressantes des caractéristiques de rayonnement, qui conviennent aux applications en ondes millimétriques.

TABLE OF CONTENTS

ACKNOWLEDGEMENTS.....iv
RÉSUMÉ.....vi
ABSTRACT.....vii
CONDENSÉ EN FRANÇAIS.....ix
TABLE OF CONTENTS.....xix
LIST OF FIGURES.....xxii
LIST OF TABLES.....xxvi

CHAPTER I INTRODUCTION.....1
1.1 Brief Overview of Existing Millimeter-wave Circuits and Dielectric Antenna Technologies.....2
1.2 Objectives and Outline of the Thesis.....5

CHAPTER II NON-RADIATIVE DIELECTRIC (NRD) GUIDE.....9
2.1 Introduction.....10
2.2 Operating Principle and Field Expressions of NRD-guide.....11
2.3 Operating Modes, Dispersion and Bandwidth Characteristics 20
2.4 Technical Merits and Limitations of the NRD-guide Technology 24
2.5 Conclusion.....25

CHAPTER III ANALYSIS OF CYLINDRICAL DIELECTRIC RESONATORS.....26
3.1 Introduction.....27
3.2 Field Analysis and Eigenvalue Equation of Dielectric Rod 28
3.3 The Parallel-Plate Dielectric Resonator.....35
3.4 The Mode of the Dielectric Resonator 36
3.5 Experimental Result.....37

3.6 Conclusion.....39

CHAPTER IV NRD-GUIDE FEEDER NETWORK.....40
4.1 Introduction.....41
4.2 Transition from Rectangular Waveguide to NRD-guide.....44
4.2.1 Physical Description.....44
4.2.2 Experiments and Measured Results.....44
4.3 NRD-guide T-junction.....48
4.3.1 Description of NRD-guide T-junction.....48
4.3.2 Experiments and Results.....49
4.4 NRD-guide BEND.....51
4.4.1 Description of 90° NRD-guide Bend.....51
4.4.2 Experiments and Results.....52
4.5 Conclusion.....53

CHAPTER V CYLINDRICAL DIELECTRIC RADIATOR AND RADIATOR ARRAY.....56
5.1. Introduction.....57
5.2 Concept of Cylindrical Unidirectional Dielectric Radiator (CUDR).....58
5.2.1 Radiator Structure.....58
5.2.2 Feed Structure and Model Analysis.....60
5.3 Simulation and Measurement Results.....67
5.3.1 Front Coupling NRD-guide Feed Cylindrical Dielectric Radiator.....67
5.3.2 Side Coupling NRD-guide Fed Cylindrical Dielectric Radiator...73
5.4 Cylindrical Dielectric Radiator Array.....79
5.4.1 Multiple NRD-guide Front Coupling CUDR Array.....83
5.4.2 Single NRD-guide Side Coupling CUDR Array.....87

5.5 Conclusion.....90

CHAPTER VI CONCLUSIONS AND RECOMMENDATIONS.....91

6.1 Conclusion.....92

6.2 Suggestions for Future Work.....94

REFERENCES.....95

LIST OF FIGURES

Figure 1.1. (a) Cylindrical unidirectional dielectric radiators (CUDR) array with multiple NRD-guide feeder.....6

Figure 1.1. (b) Cylindrical unidirectional dielectric radiators (CUDR) array with single NRD-guide feeder.....6

Figure 2.1. Fig. 2.1 Basic NRD-guide structure.....11

Figure 2.2. The typical field lines in NRD-guide.....12

Figure 2.3. The transverse field of NRD-guide.....13

Figure 2.4. Operational diagram of NRD-guide: Dielectric used polystyrene ($\varepsilon_r = 2.56$), the operating region is between curve I and curve II.....22

Figure 2.5. (a) Relative bandwidth of NRD-guide as a function of a/λ_0 with dielectric polystyrene ($\varepsilon_r = 2.56$).....23

Figure 2.5. (b) The parameter b/λ_0 as a function of a/λ_0.....23

Figure 3.1. The parallel-plate cylindrical dielectric resonator.....28

Figure 3.2. The cylindrical coordinate system.....30

Figure 3.3. The dielectric rod waveguide 31

Figure 3.4. The parallel-plate dielectric resonator mode sequence.....37

Figure 3.5. The three-dimensional geometrical view of parallel-plate dielectric resonator.....38

Figure 4.1. The proposed topology NRD-guide feeder.....43

Figure 4.2. (a) 3-D Scheme of transition from metal waveguide WR-28 to NRD-guide.....45

Figure 4.2. (b) Cross-sectional scheme of transition from metallic waveguide WR-28 to NRD-guide.....46

Figure 4.3. (a) Simulated Return Loss S_{11} of metal waveguide to NRD-guide transition.....46

Figure 4.3. (b) Simulated Transmission $S_{21}$of Metal waveguide to NRD-guide transition.....47
Figure 4.4. Measured results of the proposed transition from metal waveguide to NRD-guide.....48
Figure 4.5. Physical topology of the NRD-guide T-junction and definition of the L....49
Figure 4.6. The return Loss of NRD-guide T-junction with main arm length L (mm).....50
Figure 4.7. LSM_{10} mode to LSE_{10} mode T-junction transmission S21 along frequencies (simulated).....51
Figure 4.8. Topology of NRD-guide 90° bend and definition of Lc 52
Figure 4.9. Physical topology of NRD-guide power splitter.....54
Figure 4.10. Simulated NRD-guide power splitter return loss and transmission S11 and S12.....55
Figure 5.1. Parallel-plate cylindrical dielectric resonator (CDR).....59
Figure 5.2. Cylindrical unidirectional dielectric radiator (CUDR).....60
Figure 5.3.Cylindrical unidirectional dielectric radiator fed by NRD-guide (front coupling).....61
Figure 5.4. Cylindrical dielectric radiator fed by NRD-guide (side coupling).....62
Figure 5.5. The typical lines HEM_{111} mode in cylindrical dielectric resonator.....63
Figure 5.6. (a) Side view of front coupling cylindrical unidirectional dielectric radiator.....64
Figure 5.6. (b) Top view of front coupling cylindrical unidirectional dielectric radiator.....64
Figure 5.7. Typical field line of TE_{011} mode in cylindrical dielectric resonator.....65
Figure 5.8. (a) Side view of side coupling cylindrical unidirectional dielectric radiator.....66
Figure 5.8. (b) Top view of side coupling cylindrical unidirectional dielectric radiator.....66

Figure 5.9. Simulated return loss versus frequency for different radiator position (d) with respect to the open edge while $d_1 = 1.5mm$ (front coupling).....69

Figure 5.10. Typical measured return loss response of an NRD-guide front coupling with cylindrical dielectric radiator for different radiator position (d), with $d_1 = 1.5mm$ and $\varepsilon_r = 2.56$ 70

Figure 5.11. (a) Simulated radiation pattern of front coupling radiator (E-plane).....71

Figure 5.11. (b) Simulated radiation pattern of front coupling radiator (H-plane).....72

Figure 5.12. (a) Measured radiation pattern of front coupling radiator in E-plane for $d_1 = 1.5mm$ and $d = 0.38mm$ 72

Figure 5.12. (b) Measured radiation pattern of front coupling radiator in H-plane for $d_1 = 1.5mm$ and $d = 0.38mm$ 73

Figure 5.13. Simulated return loss versus frequency for different position (d) of front coupling radiator while $d_2 = 1.01mm$ 75

Figure 5.14 Measured return loss response of an NRD-guide side coupling with cylindrical dielectric radiator for position $d = 0.38mm$ and $d_2 = 1.01mm$ ...75

Figure 5.15. (a) Simulated radiation pattern of side coupling radiator (E-plane).....77

Figure 5.15. (b) Simulated radiation pattern of side coupling radiator (H-plane).....77

Figure 5.16. (a) Measured radiation pattern of side coupling radiator in E-plane for $d_2 = 1.01mm$ and $d = 0.38mm$ 78

Figure 5.16. (b) Measured radiation pattern of side coupling radiator in H-plane for $d_2 = 1.01mm$ and $d = 0.38mm$ 78

Figure 5.17. (a) Three-dimensional (3D) geometrical transparent view of the proposed single NRD-guide side coupling with CUDR array.....80

Figure 5.17. (b) Top view of the proposed single NRD-guide side coupling with CUDR array.....81

Figure 5.18. (a) Three-dimensional (3D) geometrical transparent view of the proposed multiple NRD-guide front coupling with CUDR array.....82

Figure 5.18. (b) Top view of the proposed multiple NRD-guide front coupling with CUDR array.....83

Figure 5.19. Measured return loss of the two-elements CUDR array fed by multiple NRD-guide.....84

Figure 5.20. (a) Simulated E-plane of the two-elements CUDR array fed by the multiple NRD-guide with $d_1 = 1.5mm$, $d = 0.38mm$, and $s = 8.788mm$ 85

Figure 5.20. (b) Simulated H-plane patterns of the two-elements CUDR array fed by the multiple NRD-guide with $d_1 = 1.5mm$, $d = 0.38mm$, and $s = 8.788mm$ 86

Figure 5.21. (a) Measured E-plane patterns of the two-elements CUDR array fed by the multiple NRD-guide with $d_1 = 1.5mm$, $d = 0.38mm$, and $s = 8.788mm$ 86

Figure 5.21. (b) Measured H-plane patterns of the two-elements CUDR array fed by the multiple NRD-guide with $d_1 = 1.5mm$, $d = 0.38mm$, and $s = 8.788mm$ 87

Figure 5. 22. Measured return loss of the two-elements CUDR array fed by single NRD-guide with $d = 0.38mm$, $d_2 = 1.01mm$, and $s_1 = 10mm$ 105.....88

Figure 5.23. (a) Measured E-plane radiation pattern of CUDR array fed by single NRD-guide with $d_2 = 1.01mm$, $d = 0.38mm$, and $s_1 = 10mm$ 88

Figure 5.23. (b) Measured H-plane radiation pattern of CUDR array fed by single NRD-guide with $d_2 = 1.01mm$, $d = 0.38mm$, and $s_1 = 10mm$ 89

LIST OF TABLES

Table I. Typical Dielectric Material Properties.....5

Table II. Typical Resonant Frequencies and Modes of Cylindrical Dielectric Resonators.....38

CHAPTER I

INTRODUCTION

Explosive growth in broadband wireless access market in connection with millimeter-wave applications in particular has led to a huge demand for cost-effective, high performance, and low-cost millimeter-wave antennas and also stimulated much interest in searching for appropriate antenna feeder structures. Such millimeter-wave circuits and antennas are used to construct customer promises equipment (CPE) for the local multipoint distribution service (LMDS) or local multipoint communication service (LMCS) as well as other millimeter-wave systems including advanced vehicle collision-avoidance radar sensors. One of the most important issues in dealing with the design of the millimeter-wave systems is to make use of a high-performance circuit building block at low-cost.

1.1 Brief Overview of Existing Millimeter-wave Circuits and Dielectric Antenna Technologies

It has been known that conventional planar technologies, which are related to the microwave integrated circuits (MICs), miniaturized hybrid microwave integrated circuits (MHMICs), and monolithic microwave integrated circuits (MMICs), present many unparalleled advantages, namely, low profile, light weight, and conformable geometry [1]-[2]. However, they suffer from problems of increased conductor loss and stringent dimensional tolerances over millimeter-wave frequency range. Ohmic losses involved in antenna design are to greatly reduce the radiation efficiency and degrade the noise performance of receiver systems [3]-[4].

Generally speaking, one major problem encountered in use of planar transmission lines and metallic waveguide is that conductor losses increase with frequency. From the point of view of achieving a low transmission loss, dielectric guides present a very attractive solution at millimeter wave frequencies. Dielectric antennas have the merit of low loss, high radiating efficiency, low cost, mechanical simplicity, and they are particularly suitable for applications at higher frequencies [5]-[8]. Although dielectric waveguides have widely been used in integrated optical circuits and a large class of dielectric waveguides has even been proposed for millimeter wave and sub-millimeter wave applications, they are hardly considered as candidates to be integrated with planar circuits due to severe radiation losses at bends and discontinuities. This perception held until the invention of the non-radiative dielectric (NRD) waveguide [9]. The NRD-guide is well suitable for passive components because it can completely suppress the radiation loss along circuit bends and discontinuities. Since its inception in 1981, this technology has been used in the design and fabrication of a large class of integrated circuits and components such as filters, couplers, power dividers/ combiners, isolators, oscillators, as well as NRD receivers and transmitters [10]-[13], which have demonstrated superior electrical performance at millimeter wave frequencies because of its simplicity, ease of fabrication, and low loss nature. In particular, high-performance NRD-antennas, for example, NRD leaky-wave [14]-[16], and end-fire antennas [17], as well as NRD fed-slot antenna arrays [18] and slot coupling dielectric resonator antennas [19], have been also reported. Microstrip line excitation of aperture-coupled unidirectional dielectric radiator (UDR) array, which consists of a number of rectangular dielectric resonators, has been demonstrated in [6]-[8].

Resonators are important components in microwave and millimeter-wave communication circuits. Dielectric resonators (DR) in cylindrical and rectangular shapes are commonly employed at microwave and millimeter wave frequencies in

the design of filters, oscillators, and tuning elements. Compared with the rectangular resonator, cylindrical resonators in the form of a pill box (disk) are more often encountered in practice. Advantages of dielectric resonator come from their inherent combined properties that they have. They feature low-cost, small size and high quality, which may be approximated as lumped resonant elements for use in integrated microwave and millimeter-wave circuits. They bridge the gap between waveguide and planar technologies by providing excellent Q and temperature stabilities, comparable to those of Invar cavity resonators along with an integrability comparable to that of planar resonators. With outstanding design versatility, they are quite adaptable to various microwave and millimeter-wave requirements and coupling configurations. There are many approximate models such as magnetic wall model, Cohn model, Itoh and Rudokas model [20] to describe the characteristics of a DR. Such simple models are useful in understanding the operating principle of a DR, and they are helpful at initial stages of analysis or design.

Today, more low loss, high performance commercial dielectric materials become available for the design of NRD-guide based circuits and cylindrical dielectric resonator designs. Listed in Table I are several commonly used materials.

Table I. Typical Dielectric Material Properties

Material	Dielectric Constant	Loss δ
Teflon (PTFE) (f=100GHz)	2.07	0.0002
Rogers RT/Duroid 5880 (f=100GHz)	2.2	0.0009
Polyethylene (f=100GHz)	2.3	0.0003
Polystyrene (f=100GHz)	2.56	0.0003
Rogers TMM 3 (f=10GHz)	3.27	0.0016
Rogers TMM 6 (f=10GHz)	6.0	0.0018

1.2 Objectives and Outline of Thesis

The principal objective of this work is to investigate and design a novel cylindrical unidirectional dielectric radiator (CUDR) and CUDR arrays. Based on the concept of the conventional NRD guide and cylindrical DR, the CUDR and CUDR array are proposed and studied theoretically and experimentally. The CUDR array consists of a number of cylindrical dielectric resonators and an NRD guide feeder, as shown in Fig. 1(a) and (b), which retains all the technical merits of NRD guide and has a great potential for millimeter-wave antenna and space power combining circuit applications. The NRD-guide feeder consists of a metallic waveguide to NRD-guide transition, an NRD-guide T-junction, an NRD-guide 90° bend, which are proposed in this work and underlying advantages will be demonstrated.

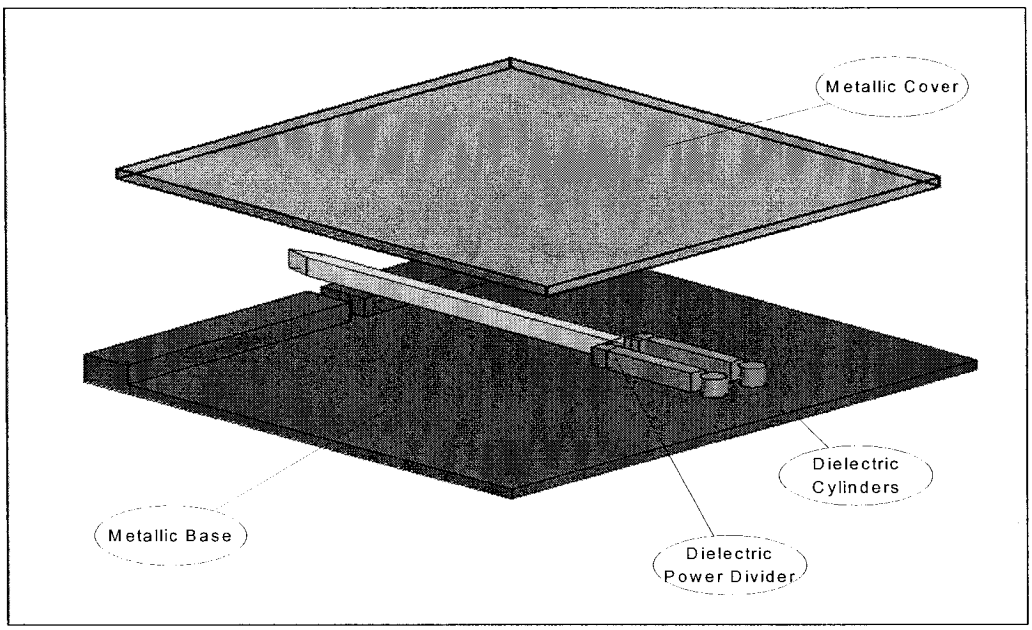

Fig. 1. (a) CUDR array with multiple NRD-guide feeder

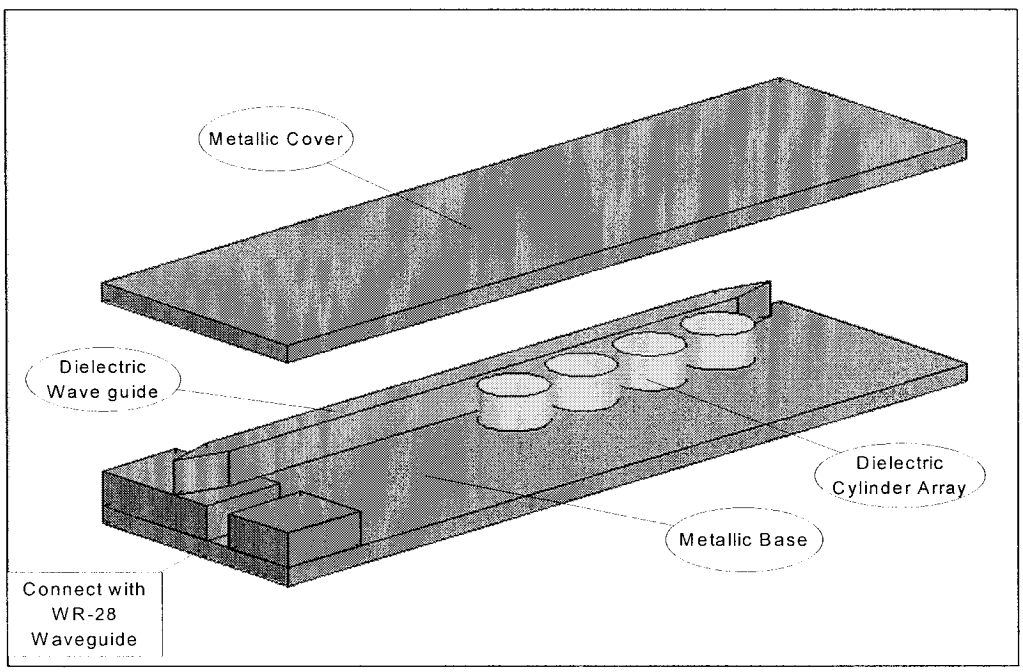

Fig. 1. (b) CUDR array with single NRD-guide feeder

This thesis consists of six chapters. Chapter II discusses the concept and fundamental properties of conventional NRD-guide. General analytical expressions for NRD-guide LSM and LSE modes are derived. Field and propagation characteristics of the NRD-guide are presented. Operation mode, and dispersion and bandwidth characteristics are also shown. Technical merits and limitations of the NRD-guide are also revealed. It is concluded that the NRD-guide structures are useful in the design of low-loss and low-cost integrated microwave and millimeter-wave circuits and antennas.

In Chapter III, the basic concept of the proposed cylindrical dielectric resonators (CDR) is introduced. The field analysis of dielectric rod and the eigenvalue equation for the dielectric rod are deduced and discussed. This analysis will be extended to the parallel-plate CDR. In addition, modes and resonant frequencies of the parallel-plate dielectric resonators are also discussed.

In Chapter IV, an NRD-waveguide feeder network, which consists of a metallic waveguide transition, an NRD-guide T-junction, and NRD-guide bends, is described, studied and simulated. Simulation and measurement results of this structure are presented. It is shown that a resonance problem within NRD-guide appears at metal-waveguide-to-NRD-guide transitions [25].

In Chapter V, the proposed promising dielectric antenna, namely, the CUDR, which consists of a CDR and an NRD-guide feeder, will be described. Simulated and measured results of CUDR will be presented. This new structure retains all the merits of NRD guide and offers a number of unmatched advantageous features in millimeter-wave applications. Simulated and measured results of CUDR and its array are provided to illustrate potential applications in future millimeter-wave systems.

Chapter VI provides our conclusions and suggestions for the future work in connection with the present work.

CHAPTER II

NON-RADIATIVE DIELECTRIC (NRD) GUIDE

2.1. Introduction

The non-radiative dielectric guide, first proposed by Yoneyama and Nishida [9], is a low-loss transmission line having a unique feature that it can suppress radiation almost completely along bends and discontinuities. It consists of a parallel-plate guide with a dielectric strip inserted between the plates (Fig. 2.1). Structurally, it is identical to the H-guide except that the plate separation is less than a half the free-space wavelength ($\lambda_0 / 2$).

In a conventional parallel-plate guide with air as the intervening medium, the TE modes, which have electric fields parallel to the metal plates, form low-loss modes. For a plate separation less than $\lambda_0 / 2$, such TE modes become cut off. In the NRD-guide, the presence of a dielectric strip enables electromagnetic waves to propagate along the strip whereas the radiated waves, if any, are suppressed because of the cut-off nature of the air-filled region.

The above two important features of the NRD-guide, namely, low transmission loss and absence of radiation from bends and discontinuities, make it suitable for realizing compact and high-performance millimeter-wave integrated circuits.

In this chapter, we will first derive general expressions for the hybrid-mode fields of a parallel-plate guide with a dielectric strip. The fields and propagation characteristics of the NRD-guide will be discussed. Operating modes, dispersion and bandwidth characteristics will be presented. Technical merits and limitations of the

NRD-guide will also be discussed.

2.2. Operating Principle and Field Expressions of NRD-guide

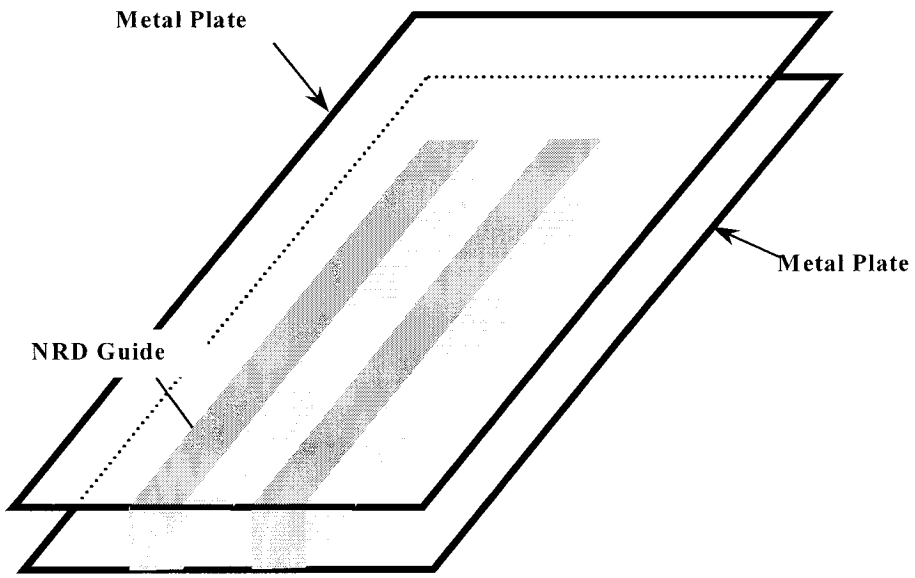

Fig. 2.1 Basic NRD-guide structure

The structure shown in Figure 2.1 operates as an NRD-guide when the spacing between the metal plates is less than a half the free-space wavelength ($a<\lambda_0/2$). With this condition, the modes of an NRD-guide generally classified into the two fundamental modes, namely LSM (longitudinal-section-magnetic) and LSE (longitudinal-section-electric), are non-radiative in nature. Field profiles of the lowest LSM mode (LSM_{10}) and LSE mode (LSE_{10}) are shown in Figure 2.2.

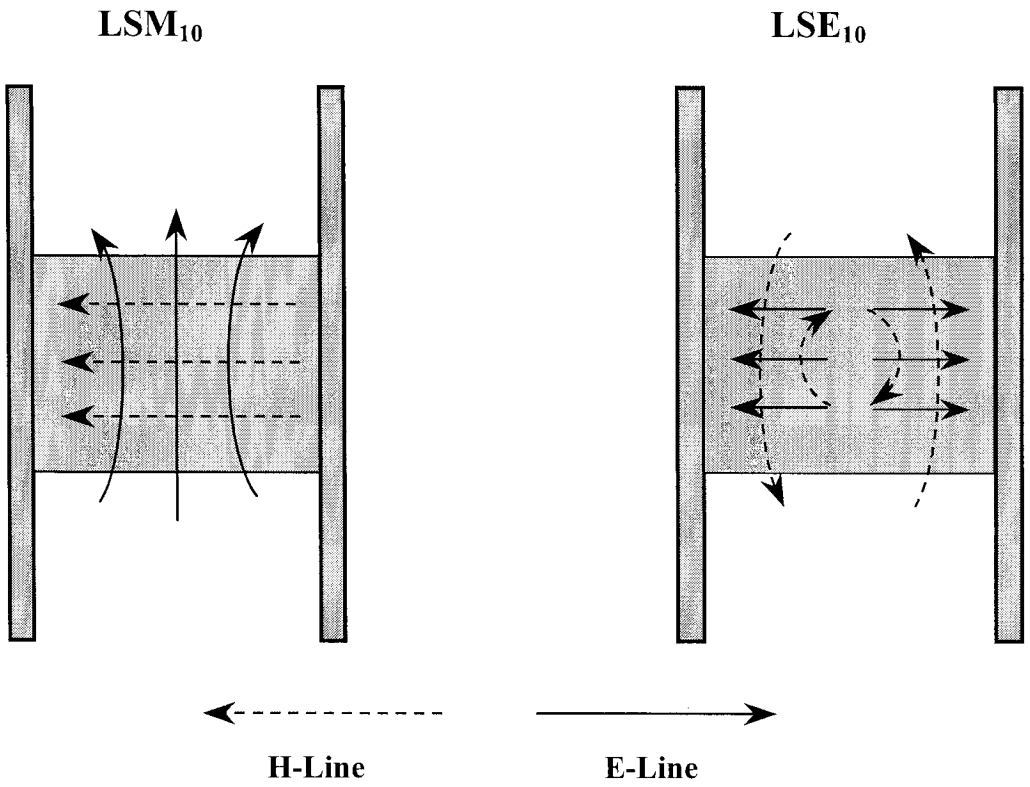

Figure 2.2 The typical field lines in NRD guide

Referring to the coordinate system shown in Figure 2.3, we assume wave propagation along the direction z of guide. The thickness and width of the dielectric waveguide are denoted by a and b, and the relative dielectric constant is ε_r. The analysis can be considerably simplified, if the hybrid modes in NRD-guide are considered by the fact that the LSM mode can be viewed as a result from the lowest TM surface wave mode bouncing back and forth between the parallel metal plates whereas the LSE mode can be regarded as being the TE surface wave mode confined between the metal plates.

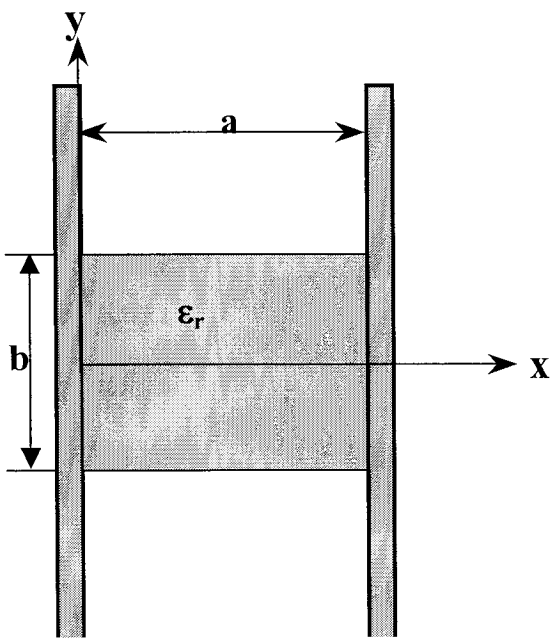

Figure 2.3 The transverse field of NRD guide

Normalized field expressions of the LSM and LSE mode are given below. The electromagnetic field of the LSM modes (Hy=0) satisfies the following equation [32].

$$(\nabla^2 + k^2)E_y = 0 \qquad (2.1\text{-a})$$

and other field components can be obtained by

$$(k^2 + \frac{\partial^2}{\partial y^2})E_x = \frac{\partial^2 E_y}{\partial y \partial x} \tag{2.1-b}$$

$$(k^2 + \frac{\partial^2}{\partial y^2})E_z = \frac{\partial^2 E_y}{\partial y \partial z} \tag{2.1-c}$$

$$(k^2 + \frac{\partial^2}{\partial y^2})H_x = -j\omega\varepsilon \frac{\partial E_y}{\partial z} \tag{2.1-d}$$

$$(k^2 + \frac{\partial^2}{\partial y^2})H_z = -j\omega\varepsilon \frac{\partial E_y}{\partial x} \tag{2.1-e}$$

in which

$$k^2 = \begin{cases} \varepsilon_r k_0^2, & |y| \le b/2 \\ k_0^2, & |y| \ge b/2 \end{cases} \tag{2.2-a}$$

$$\varepsilon = \begin{cases} \varepsilon_r \varepsilon_0 & |y| \le b/2 \\ \varepsilon_0 & |y| \ge b/2 \end{cases} \tag{2.2-b}$$

In the above equations, ε_0, μ_0, and k_0 are respectively permittivity, permeability, and wave-number of the free space, ε_r is the relative dielectric constant of the strip, and the upper and lower signs surrounding the air regions are defined by $y \ge b/2$ and

$y \le -b/2$. Thus the symmetric and anti-symmetric LSM field can be obtained from Eq.(2.1), which are symmetric and anti-symmetric about y=0. For the symmetric modes, the plane y=0 represents a magnetic wall, while for the anti-symmetric modes, it represent an electric wall. In our following investigation, our focus is the properties of the LSM_{10}, which is the fundamental mode in the NRD-guide. Therefore, only antisymmetric mode will be considered and studied. We can then obtain the following various field expressions of the anti-symmetric mode from equation (2.1):

For $|y| \le b/2$

$$E_x = -\frac{Aq}{h^2 \cos(qb/2)}\left(\frac{m\pi}{a}\right)\cos\left(\frac{m\pi}{a}x\right)\sin(qy)e^{-j\beta z} \tag{2.3-a}$$

$$E_y = -\frac{A}{\cos(qb/2)}\sin\left(\frac{m\pi}{a}x\right)\cos(qy)e^{-j\beta z} \tag{2.3-b}$$

$$E_z = j\frac{Aq\beta}{h^2 \cos(qb/2)}\sin\left(\frac{m\pi}{a}x\right)\sin(qy)e^{-j\beta z} \tag{2.3-c}$$

$$H_x = \frac{\omega\varepsilon_r\varepsilon_0 A\beta}{h^2 \cos(qb/2)}\sin\left(\frac{m\pi}{a}x\right)\cos(qy)e^{-j\beta z} \tag{2.3-d}$$

$$H_z = j\frac{\omega\varepsilon_r\varepsilon_0 A\beta}{h^2\cos(qb/2)}\left(\frac{m\pi}{a}\right)\cos\left(\frac{m\pi}{a}x\right)\cos(qy)e^{-j\beta z} \tag{2.3-e}$$

For $|y| \geq b/2$,

$$E_x = \mp\frac{\varepsilon_r Ap}{h^2}\left(\frac{m\pi}{a}\right)\cos\left(\frac{m\pi}{a}x\right)e^{-[p(|y|-b/2)+j\beta z]} \tag{2.4-a}$$

$$E_y = \varepsilon_r A\sin\left(\frac{m\pi}{a}x\right)e^{-[p(|y|-b/2)+j\beta z]} \tag{2.4-b}$$

$$E_z = \pm\frac{\varepsilon_r Ap\beta}{h^2}\sin\left(\frac{m\pi}{a}x\right)e^{-[p(|y|-b/2)+j\beta z]} \tag{2.4-c}$$

$$H_x = -\frac{\omega_0\varepsilon_0\varepsilon_r A\beta}{h^2}\sin\left(\frac{m\pi}{a}x\right)e^{-[p(|y|-b/2)+j\beta z]} \tag{2.4-d}$$

$$H_z = j\frac{\omega_0\varepsilon_0\varepsilon_r A}{h^2}\left(\frac{m\pi}{a}x\right)\sin\left(\frac{m\pi}{a}x\right)e^{-[p(|y|-b/2)+j\beta z]} \tag{2.4-e}$$

where

$$\beta^2 = h^2 - (m\pi / a)^2, \qquad m = 1,2,3,... \tag{2.5-a}$$

$$h^2 = \varepsilon_r k_0^2 - q^2 = k_0^2 + p^2 \tag{2.5-b}$$

where q and p are the first eigenvalues of the following characteristic equations, respectively:

$$q\tan(qb/2) = \varepsilon_r p \quad \text{(Symmetric modes)} \tag{2.6}$$

$$q\cot(qb/2) = -\varepsilon_r p \quad \text{(Anti-symmetric modes)} \tag{2.7}$$

$$p^2 + q^2 = (\varepsilon_r - 1)k_0^2 \tag{2.8}$$

Solving (2.5), (2.6), and (2.7), the propagation constant of LSM_{mn} mode of the NRD-guide is given by

$$\beta_{mn} = \sqrt{\varepsilon_r k_0^2 - (m\pi / a)^2 - q_n^2} = \sqrt{k_0^2 - (m\pi / a)^2 + p_n^2} \tag{2.9}$$

In a similar way, the fields for the LSE modes can be expressed as follows

For $|y| \le b/2$,

$$E_x = -\frac{\omega\mu_0 \hat{A}\hat{\beta}}{h^2 \cos(\hat{q}b/2)} \cos\left(\frac{m\pi}{a}x\right)\cos\left(\hat{q}y\right)e^{-j\hat{\beta}z} \tag{2.10-a}$$

$$E_y = 0 \tag{2.10-b}$$

$$E_z = -j\frac{\omega\mu_0 \hat{A}}{h^2 \cos(\hat{q}b/2)}\left(\frac{m\pi}{a}\right)\sin\left(\frac{m\pi}{a}x\right)\cos\left(\hat{q}y\right)e^{-j\hat{\beta}z} \tag{2.10-c}$$

$$H_x = \frac{\hat{A}\hat{q}}{h^2 \cos(\hat{q}b/2)}\left(\frac{m\pi}{a}\right)\sin\left(\frac{m\pi}{a}x\right)\sin\left(\hat{q}y\right)e^{-j\hat{\beta}z} \tag{2.10-d}$$

$$H_y = \frac{\hat{A}}{\cos(\hat{q}b/2)}\cos\left(\frac{m\pi}{a}x\right)\cos\left(\hat{q}y\right)e^{-j\hat{\beta}z} \tag{2.10-e}$$

$$H_z = j\frac{\hat{A}\hat{q}\hat{\beta}}{h^2 \cos(\hat{q}b/2)}\cos\left(\frac{m\pi}{a}x\right)\sin\left(\hat{q}y\right)e^{-j\hat{\beta}z} \tag{2.10-f}$$

For $|y| \geq b/2$,

$$E_x = -\frac{\omega\mu_0 \hat{A}\hat{\beta}}{\hat{h}^2}\cos\left(\frac{m\pi}{a}x\right)e^{-[\hat{p}(|y|-b/2)+j\hat{\beta}z]} \tag{2.11-a}$$

$$E_y = 0 \tag{2.11-b}$$

$$E_z = -j\frac{\omega\mu_0\hat{A}}{\hat{h}^2}\left(\frac{m\pi}{a}\right)\sin\left(\frac{m\pi}{a}x\right)e^{-[\hat{p}(|y|-h/2)+j\hat{\beta}z]} \tag{2.11-c}$$

$$H_x = \pm\frac{\hat{A}\hat{p}}{\hat{h}^2}\left(\frac{m\pi}{a}\right)\sin\left(\frac{m\pi}{a}x\right)e^{-[\hat{p}(|y|-h/2)+j\hat{\beta}z]} \tag{2.11-d}$$

$$H_y = \hat{A}\cos\left(\frac{m\pi}{a}x\right)e^{-[\hat{p}(|y|-h/2)+j\hat{\beta}z]} \tag{2.11-e}$$

$$H_z = \pm j\frac{\hat{A}\hat{p}\hat{\beta}}{\hat{h}^2}\cos\left(\frac{m\pi}{a}x\right)e^{-[\hat{p}(|y|-h/2)+j\hat{\beta}z]} \tag{2.11-f}$$

where

$$\hat{\beta}^2 = \hat{h}^2 - (m\pi/a)^2, \qquad m = 1,2,3,... \tag{2.12-a}$$

$$\hat{h}^2 = \varepsilon_r k_0^2 - \hat{q}^2 = k_0^2 + \hat{p}^2 \tag{2.12-b}$$

where $\hat{p}$ and $\hat{q}$ are the first eigenvalues of the following characteristic equations, respectively:

$$\hat{q}\tan(\hat{q}b/2) = \varepsilon_r \hat{p} \quad \text{(Symmetric modes)} \tag{2.13}$$

$$\hat{q}\cot(\hat{q}b/2) = -\varepsilon_r \hat{p} \quad \text{(Anti-symmetric modes)} \tag{2.14}$$

$$\hat{p}^2 + \hat{q}^2 = (\varepsilon_r - 1)k_0^2 \tag{2.15}$$

Solving (2.13), (2.14) and (2.15), the propagation constant of LSE_{mn} mode of the NRD-guide is given by

$$\hat{\beta}_{mn} = \sqrt{\varepsilon_r k_0^2 - (m\pi/a)^2 - \hat{q}_n^2} = \sqrt{k_0^2 - (m\pi/a)^2 + \hat{p}_n^2} \tag{2.16}$$

2.3. Operating Modes, Dispersion and Bandwidth Characteristics

Generally speaking, the modes of an NRD-guide are usually classified into the LSM and LSE modes according to its geometry. LSM_{10} and LSE_{10} modes are the lowest *LSM* and *LSE* modes. The LSM_{10} mode is selected as the fundamental operating mode of the NRD guide due to its lower transmission loss, and however, the LSE_{10} has a lower cut-off frequency than the desired operating mode and it can be used for coupling the LSM_{10} mode from one branch of the NRD-guide to another for the design and applications of power divider.

The design requirement of NRD-guide, in addition to non-radiative properties ($a < \lambda_0 / 2$), for the dominant LSM_{10} mode demands the following condition:

$$\lambda_{s1} / 2 < a < \lambda_{s2} \tag{2.17}$$

where $\lambda_{sn} = 2\pi / h_n$, h_n is the phase constant of the lowest LSM mode and can be obtained from equation (2.5-b).

Fig. 2.4 shows a typical operating diagram of an NRD guide using polystyrene ($\varepsilon_r = 2.56$) strip wherein the normalized parameter (b / λ_0) is plotted as a function of (a / λ_0). The single-mode (LSM_{10}) operating region is bound by the curves I: $\lambda_{s1} = 2a$ and II: $\lambda_{s2} = 2a$

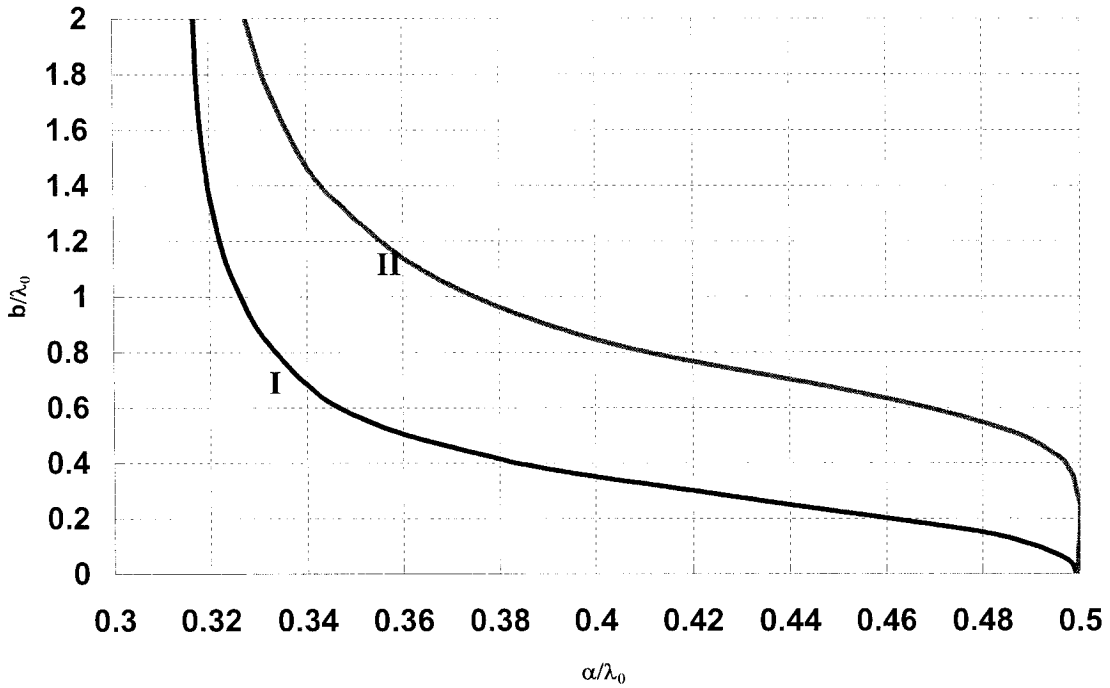

Fig. 2.4. Operational diagram of NRD-guide: Dielectric used polystyrene ($\varepsilon_r = 2.56$), the operating region is between curve I and curve II

Fig. 2.5 (a) shows the variation in relative bandwidth of the NRD for the dominant LSM_{10} mode as a function of parameter (a/λ_0) for polystyrene ($\varepsilon_r = 2.56$). There is a certain value of a/λ_0 at which the bandwidth reaches a maximum.

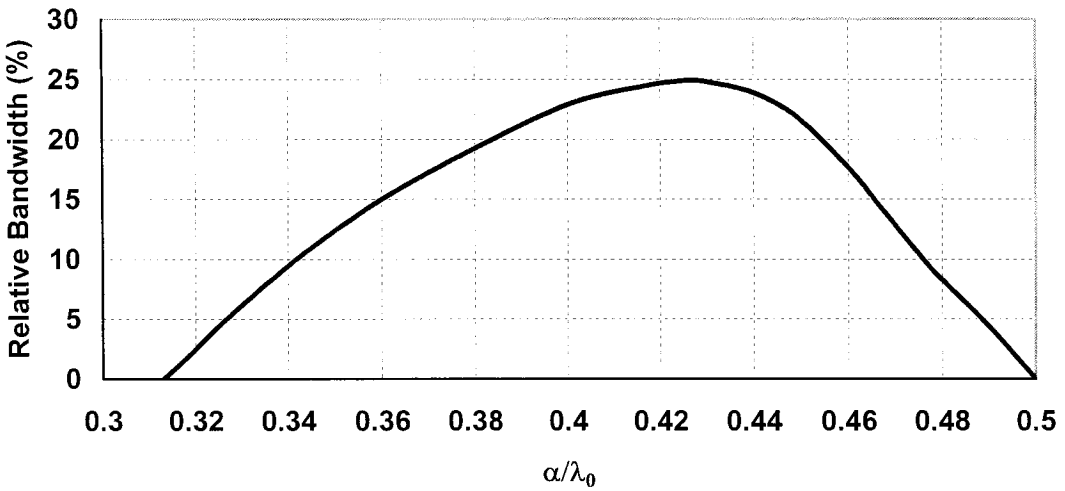

(a)

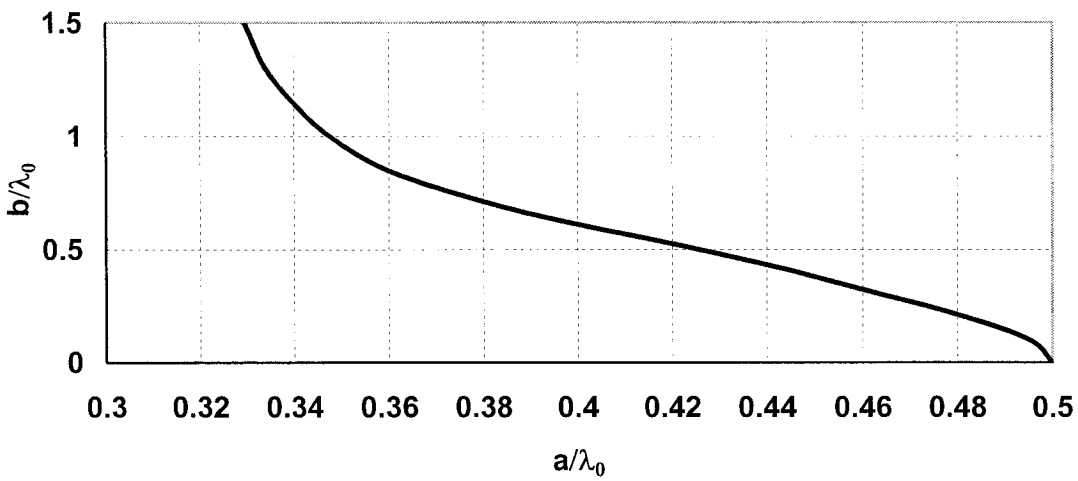

(b)

Fig. 2.5. (a) Relative bandwidth of NRD-guide as a function of a/λ_0 with dielectric polystyrene ($\varepsilon_r = 2.56$) (b) the parameter b/λ_0 as a function of a/λ_0

Based on the above description and discussed bandwidth characteristics, a design criterion of the NRD guide can be derived as follows

$$a / \lambda_0 \cong 0.45 \tag{2.18}$$

$$\sqrt{\varepsilon_r - 1} b / \lambda_0 = 0.4 \sim 0.6 \tag{2.19}$$

where λ_0 is the wavelength of free space.

2.4. Technical Merits and Limitations of the NRD-guide Technology

The NRD-guide based technology becomes attractive for use in a variety of microwave and in particular millimeter-wave circuits and systems. Since its inception in 1981, this technology has been used in the design and fabrication of a large class of integrated circuits and antennas that have demonstrated superior electrical performance at millimeter-wave frequencies [21]-[22].

Over the past years, a number of two-terminal active devices have already been used in the design of NRD-guide active circuits. However, an effective coupling from the NRD to planar circuits requires an additional effort since the impedance mismatch for this hybrid geometry is a severe problem. This is usually done by adding a thin dielectric sheet having an appropriate high permittivity in conjunction with certain dimensioned air-gap between the NRD-guide and the planar mount. Meanwhile, the NRD-guide, like any other dielectric waveguide, presents some difficult problems

when active device integration is required. It is detrimental to the development of a complete NRD-guide based functional system. It is difficult to achieve simultaneously overall required circuit performance by utilizing a single technology framework. In view of its advantages and disadvantages, the NRD technology is a good complement with respect to its planar counterpart. Obviously, the hybrid scheme based on combined planar/NRD waveguide technology is more appealing. The development of hybrid integration concept of planar circuit and NRD-guide aims at exploiting inherent complementary advantages of both planar circuit and NRD-guide while eliminating (at least partly if not completely) potential drawbacks of each building block [21]-[22]. These two different groups of structure can be designed and integrated well into a single building block so that the compactness and advantages of each line can be benefited.

2.5. Conclusion

We have presented general field expressions for the hybrid-modes LSM and LSE of NRD-guide. The fields and propagation characteristics of the NRD-guide are derived. Operating mode, dispersion and bandwidth characteristics are also presented. The technical merits and limitations of the NRD-guide are discussed. It can be found that the NRD-guide structures are very useful in the design for low-loss and low-cost integrated microwave and millimeter-wave circuits.

CHAPTER III

ANALYSIS OF CYLINDRICAL DIELECTRIC RESONATORS

3.1. Introduction

Resonators are important components in microwave communication circuits. Dielectric resonators (DR) in cylindrical and rectangular shapes are commonly employed at microwave and millimeter-wave frequencies in the design of filters, oscillators, radiators, and tuning elements. Compared with the rectangular counterparts, the cylindrical resonators in the form of a pillbox (disk) or a ring are more often encountered in practice. Similar to the metallic cavity resonators, the dielectric resonators can be excited with several modes. The basic characteristics defining a dielectric resonator are its resonant frequencies, Q-factors, and field distribution. It is important to know these properties for the lowest order resonant mode and few higher order modes in order to enable the selection of a proper mode for a particular application and the incorporation of a suitable coupling mechanism to excite the mode. Knowledge of field distribution also helps in devising suitable techniques for suppressing or eliminating undesired modes, which may interfere with the desired mode.

In this chapter, the basic concept of cylindrical dielectric resonator (CDR) is introduced. The field analysis of dielectric rod and the eigenvalue equation for the dielectric rod are deduced and discussed. The analysis is later limited to the case of parallel-plate cylindrical dielectric resonator with its cross section shown in Fig. 3.1. The modes and resonant frequencies of the parallel-plate dielectric resonator are also discussed.

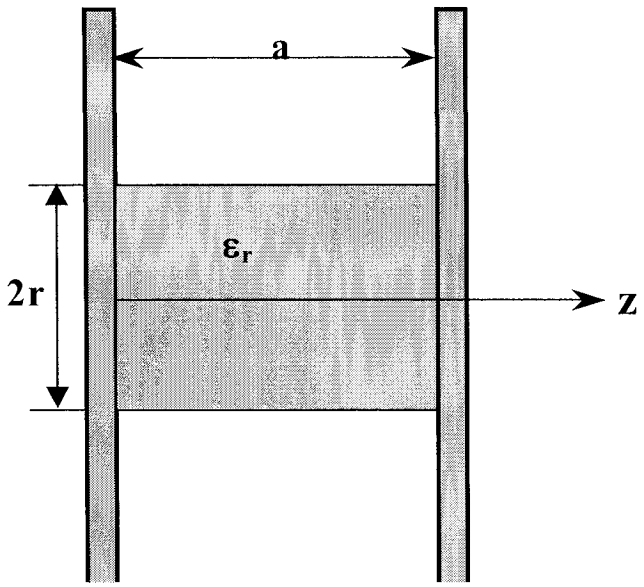

Figure 3.1 the parallel-plate cylindrical dielectric resonator

3.2. Field Analysis and Eigenvalue Equation of Dielectric Rod

An understanding of electromagnetic waves in dielectric rod waveguide is very helpful in the design of dielectric resonators. Just as a truncated hollow waveguide becomes a resonant cavity, the dielectric rod waveguide when truncated also becomes a dielectric resonator.

In a linear, homogeneous, and isotropic medium, the electric and magnetic fields satisfy Maxwell's two curl equation as follows

$$\nabla \times \vec{H} = j\omega\vec{E} + \vec{J}$$
$$\nabla \times \vec{E} = -j\omega\mu\vec{H} \tag{3.1}$$

Together with Gauss's law:

$$\nabla \bullet \varepsilon\vec{E} = \rho \tag{3.2}$$

The phasors $\vec{E}, \vec{H}$, and $\vec{J}$ in (3.1), (3.2) are, respectively, the electric field, magnetic field, and current density vectors. The constant scalars ε and μ are the permittivity and permeability of the medium, respectively, while ρ is the charge density.

We can obtain three vector Helmhotz or wave, equations such as

$$\left[\nabla^2 + k^2\right]\vec{E} = 0$$
$$\left[\nabla^2 + k^2\right]\vec{H} = 0 \tag{3.3}$$

where

$$k = \omega\sqrt{\mu\varepsilon} = \frac{2\pi}{\lambda} \tag{3.4}$$

is the wave-number of the medium and λ is the wavelength in the medium.

In the analysis of the dielectric rod waveguide, a cylindrical coordinate system shown in Fig. 3.2 is used for simplicity.

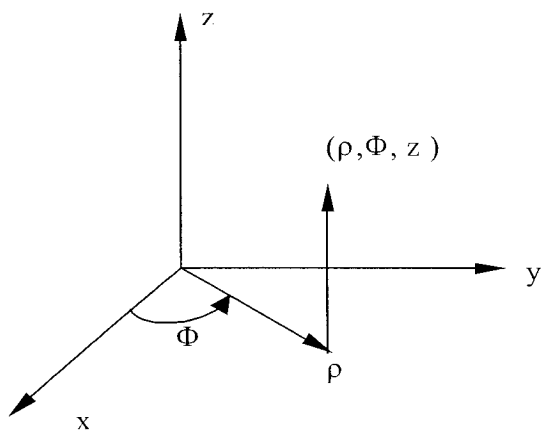

Fig. 3.2 The cylindrical coordinate system

The wave equation (3.3) with the Laplacian ∇^2 expressed in the cylindrical coordinate, is given by

$$\frac{1}{\rho}\frac{\partial}{\partial\rho}\left[\rho\frac{d}{d\rho}\psi\right]+\frac{1}{\rho^2}\frac{\partial^2}{\partial\phi^2}\psi+\frac{\partial^2}{\partial z^2}\psi+k^2\psi=0 \tag{3.5}$$

where ψ stands for either longitudinal field component.

In essence, the method of separation of variables seeks a solution of (3.5) of the form

$$\psi(\rho,\phi,z) = P(\rho)F(\phi)Z(z) \tag{3.6}$$

$$\frac{1}{Z}\frac{d^2Z}{dz^2} = -\beta^2 \tag{3.7}$$

$$\frac{1}{F}\frac{d^2F}{d\phi^2} = -m^2 \tag{3.8}$$

$$\rho\frac{d}{d\rho}\left[\rho\frac{d}{d\rho}P\right] + \left[\left(k_\rho\rho\right)^2 - m^2\right]P = 0 \tag{3.9}$$

where β and m are constants and

$$k^2{}_\rho = k^2 - \beta^2 \tag{3.10}$$

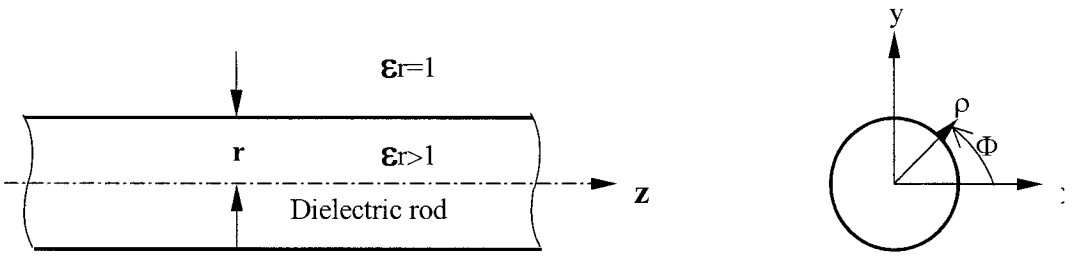

Fig. 3.3 The dielectric rod waveguide

Let's consider the dielectric rod waveguide shown in Fig. 3.3. The rod material is assumed to be a perfect dielectric characterized by the real scalar permittivity $\varepsilon=\varepsilon_0\varepsilon_r$ and the real scalar permeability μ_0.

Inside the rod, E_z and H_z are finite at the origin, and they are periodic with a period of 2π with respect to ϕ, which are to represent waves traveling in the positive z-direction. These requirements are met by choosing E_z and H_z in the form as follows

$$\vec{E}_{z1} = AJ_m(k_{\rho 1}\rho)\begin{bmatrix}\cos(m\phi)\\ \sin(m\phi)\end{bmatrix}e^{-j\beta z}$$
$$\vec{H}_{z1} = BJ_m(k_{\rho 1}\rho)\begin{bmatrix}\sin(m\phi)\\ \cos(m\phi)\end{bmatrix}e^{-j\beta z} \qquad (3.11)$$

where m is an integer, A, B are the amplitude coefficients, J_m is the Bessel function of the first kind and m^{th} order, and

$$k^2_{\rho 1} = k^2 - \beta^2 \qquad (3.12)$$

in (3.12) $k = k_0\sqrt{\varepsilon_r}$ is the wave number of the dielectric, where k_0 is the wave number of free space. Outside the rod, E_z and H_z are similarly periodic with the period of 2π with respect to ϕ, and they represent traveling waves along the z-axis. However, unlike the component inside, they are exponentially decaying in the ρ direction, if the rod is a waveguide. Thus,

$$\vec{E}_{Z2} = CK_m(k_{\rho 2}\rho)\begin{bmatrix}\cos(m\phi)\\ \sin(m\phi)\end{bmatrix}e^{-j\beta z}$$
$$\vec{H}_{Z2} = DK_m(k_{\rho 2}\rho)\begin{bmatrix}\sin(m\phi)\\ \cos(m\phi)\end{bmatrix}e^{-j\beta z} \tag{3.13}$$

where K_m is the modified Bessel function of the second kind and m^{th} order, and

$$k^2_{\rho 2} = \beta^2 - k_0^2 \tag{3.14}$$

The transverse field components inside the rod are expressed as

$$\vec{E}_{\rho 1} = \frac{1}{k^2_{\rho 1}}[-j\beta k_{\rho 1}AJ'_m(k_{\rho 1}\rho) - j\omega\mu_0 m\frac{B}{\rho}J_m(k_{\rho 1}\rho)]\cos(m\phi)e^{-j\beta Z}$$
$$\vec{H}_{\rho 1} = \frac{1}{k^2_{\rho 1}}[-j\omega\varepsilon\ m\frac{A}{\rho}J_m(k_{\rho 1}\rho) - j\beta k_{\rho 1}BJ'_m(k_{\rho 1}\rho)]\sin(m\phi)e^{-j\beta Z}$$
$$\vec{E}_{\phi 1} = \frac{1}{k^2_{\rho 1}}[j\beta m\frac{A}{\rho}J_m(k_{\rho 1}\rho) + j\omega\mu_0 k_{\rho 1}BJ'_m(k_{\rho 1}\rho)]\sin(m\phi)e^{-j\beta Z} \tag{3.15}$$
$$\vec{H}_{\phi 1} = \frac{1}{k^2_{\rho 1}}[-j\omega\varepsilon\ k_{\rho 1}AJ'_m(k_{\rho 1}\rho) - j\beta m\frac{B}{\rho}J_m(k_{\rho 1}\rho)]\cos(m\phi)e^{-j\beta Z}$$

whereas those outside the rod are given by

$$\vec{E}_{\rho 2} = \frac{-1}{k^2_{\rho 2}}[-j\beta k_{\rho 2} CK'_m(k_{\rho 2}\rho) - j\omega\mu_0 m\frac{D}{\rho}K_m(k_{\rho 2}\rho)]\cos(m\phi)e^{-j\beta Z}$$
$$\vec{H}_{\rho 2} = \frac{-1}{k^2_{\rho 2}}[-j\omega\varepsilon_0 m\frac{C}{\rho}K_m(k_{\rho 2}\rho) - j\beta k_{\rho 2} DK'_m(k_{\rho 2}\rho)]\sin(m\phi)e^{-j\beta Z}$$
$$\vec{E}_{\phi 2} = \frac{-1}{k^2_{\rho 2}}[j\beta m\frac{C}{\rho}K_m(k_{\rho 2}\rho) + j\omega\mu_0 k_{\rho 2} DK'_m(k_{\rho 2}\rho)]\sin(m\phi)e^{-j\beta Z} \quad (3.16)$$
$$\vec{H}_{\phi 2} = \frac{-1}{k^2_{\rho 2}}[-j\omega\varepsilon_0 k_{\rho 2} CK'_m(k_{\rho 2}\rho) - j\beta m\frac{D}{\rho}K_m(k_{\rho 2}\rho)]\cos(m\phi)e^{-j\beta Z}$$

J'_m is the derivative of Bessel function of the first kind and m^{th} order while K'_m is the derivative of the modified Bessel function of the second kind and m^{th} order.

The solution of the following equation at ρ=r can be obtained with the boundary conditions $E_{Z1}=E_{Z2}$, $H_{Z1}=H_{Z2}$, $E_{\phi 1}=E_{\phi 2}$, $H_{\phi 1}=H_{\phi 2}$,

$$F_1(x)F_2(x) - F_3^2(x) = 0 \quad (3.17)$$

where

$$F_1(x) = \frac{J'_m(x)}{x} + \frac{K'_m(y)J_m(x)}{\varepsilon_r y K_m(y)}$$
$$F_2(x) = \frac{J'_m(x)}{x} + \frac{K'_m(y)J_m(x)}{y K_m(y)} \quad (3.18)$$
$$F_3(x) = \frac{\beta r m}{k_0 r\sqrt{\varepsilon_r}}J_m(x)\left[\frac{1}{x^2} + \frac{1}{y^2}\right]$$

and

$$x = k_{\rho 1} r = \sqrt{(k_0 r)^2 \varepsilon_r - \left[\frac{r}{a} p\pi\right]^2}$$
$$y = k_{\rho 2} r = \sqrt{(k_0 r)^2 (\varepsilon_r - 1) - x^2} \tag{3.19}$$

Equation (3.19) is called eigenvalue equation for the dielectric rod whose zeros x are called eigenvalues of the dielectric rod waveguide. There are only a finite number of eigenvalues for any specified m. Another subscript n is, therefore, needed to enumerate the eigenvalue by x_{mn}. It then becomes convenient to denote the eigenvalues by x_{mn}. The fields (E_{mn}, H_{mn}) corresponding to x_{mn} are called the modes of dielectric rod waveguide [20].

3.3. The Parallel-Plate Dielectric Resonator

When a cylindrical dielectric rod waveguide is enclosed between two parallel metal plates with the length a as shown in Fig 3.1, a standing wave pattern is created in the z-direction. Furthermore, the normal component of magnetic field must vanish at the surface of perfect conductor, whereas that of the electric field becomes proportional to the surface charge density there.

Consequently, $\beta a = \frac{2\pi}{\lambda_g} a = p\pi$ (3.20)

where λ_g is the wavelength of the dielectric rod waveguide, and p is an integer. Thus, the height a is an integral multiple of half a wavelength,

$$a = p\frac{\lambda_g}{2}, p = 1, 2, \cdots \tag{3.21}$$

From (3.19) and (3.20), the value of x at resonance is determined by

$$x_{mn}^{\ 2} = (k_0 r)_{mn}^{\ 2} \varepsilon_r - \left(\frac{r}{a} p\pi\right)^2 \tag{3.22}$$

The resonant frequencies of the parallel-plate dielectric resonator can be given by

$$f_{mnp} = \frac{150}{\pi r}(k_0 r)_{mnp} \tag{3.23}$$

where r is measured in millimeter.

3.4. The Mode of the Dielectric Resonator

The fields of the cylindrical resonator can be divided into constituent modes with azimuthal variation represented by either $\cos m\phi$ or $\sin m\phi$ (m=0, 1, 2,$\cdots$). For m=0, the set of modes can be divided into TE modes and TM modes. These are designated as TE_{0np} and TM_{0np} modes. For m>0, the modes are hybrid in nature and are

designated as HEM_{mnp} . The lowest resonant frequency belongs to the HEM_{111} resonance, the next higher is TE_{011}, and then HEM_{211}, TM_{011}, and etc. The resonant modes are found by solving equations (3.17) and (3.18) with the eigenvalues x_{mn} of various modes. Fig. 3.4 shows some of the resonant modes sequence of the parallel-plate dielectric resonator.

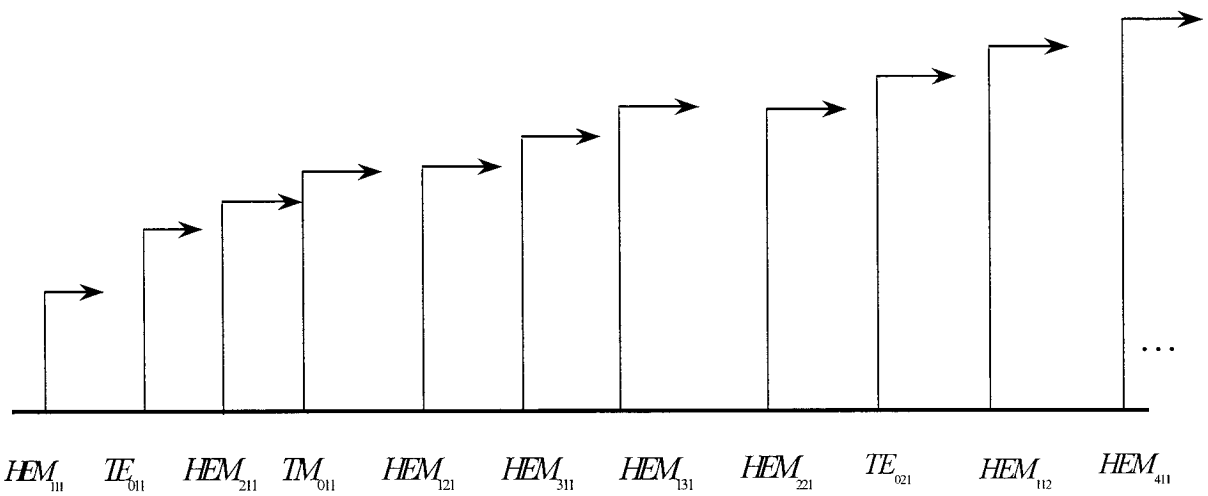

Fig. 3.4 The parallel-plate dielectric resonator mode sequence

3.5. Experimental Result

Fig. 3.5 shows a three-dimensional (3D) view of the proposed parallel-plate cylindrical dielectric resonator, which consists of a dielectric cylinder sandwiched between two parallel metallic plates. Some typical results for the parallel-plate cylindrical dielectric resonator are summarized in Table II.

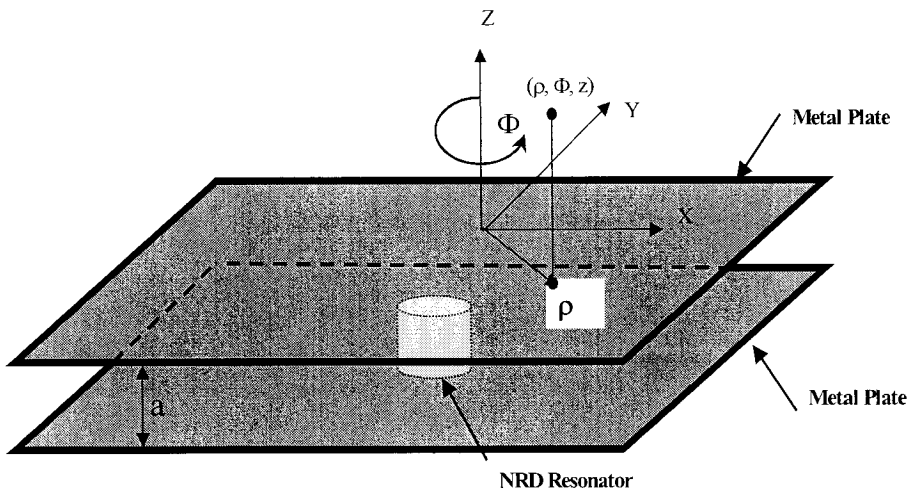

Fig. 3.5 The three-dimensional geometrical view of parallel-plate dielectric resonator

Table II Typical Resonant Frequencies and Modes of Cylindrical Dielectric Resonators

Material	Dielectric Constant	Dimension of CDR		Resonant Mode	Resonant Frequencies (GHz) (Calculated)	Resonant Frequencies (GHz) (Measured)
		Height a (mm)	Radius r (mm)			
Teflon	2.08	4.953	2.6	HEM_{111}	28.047	28.1
Teflon	2.08	4.953	3.0	HEM_{111}	27.093	N/A
Polystyrene	2.56	4.953	2.4	HEM_{111}	27.074	27.28
Polystyrene	2.56	4.953	2.4	TE_{011}	33.034	N/A
Polystyrene	2.56	4.953	4	HEM_{111}	23.303	N/A
Polystyrene	2.56	4.953	4	TE_{011}	27.342	27.62

The resonant frequencies were measured over a varying range of ε_r values and dimensional parameters using NRD-guide excitation. The calculated and measured values are shown in Table II, which can be seen that the calculated values of resonant frequency are lower than the experimental results since these natural resonant frequencies are affected by the presence of NRD-guide feed.

3.6. Conclusion

The cylindrical dielectric resonator (CDR) has been studied analytically and experimentally. Electromagnetic fields and eigenvalue equation of the dielectric rod are presented. Detailed results provide us a basic concept and also a design guideline for the parallel-plate cylindrical dielectric resonator. The operating modes and resonant frequencies in the CDR can be determined as long as the dimensions of CDR are given.

CHAPTER IV

NRD-GUIDE FEEDER NETWORK

4.1. Introduction

The nonradiative dielectric (NRD) waveguide is a promising technology for millimeter-wave applications. Various types of NRD-guide components have been proposed and developed [23] including filters, couplers, antennas, and hybrid planar NRD circuits [24].

As described in Chapter II, the two fundamental hybrid modes are the LSE_{10} and LSM_{10} modes in an NRD-guide. The LSM_{10} mode is usually preferred because it has low-loss transmission property and it is the dominant TMy-type mode, while the LSE_{10} mode is the second TEy mode after the LSE_{10} mode. Mode conversion between the LSE_{10} and LSM_{10} mode is omnipresent in NRD-guide bends [25] and misalignments [26]. The useful relationship between the radius of bend and the conversion loss for the LSE_{10} mode has been developed [27]. This analysis has shown that, for a very sharp bend and T-junction, the LSM_{10} mode can almost completely be converted into its LSM_{10} counterpart. For this reason, the development of NRD-guide T-junction [28]-[30] and 90° bend have led to a topology that were optimized for the complete modal conversion of an LSM_{10} mode input signal into LSE_{10} mode signals at the output ports. They were also shown that a T-junction splitting an LSE_{10} mode into two LSM_{10} signals and a 90° bend converting an LSE_{10} mode into an LSM_{10} signal was also feasible [30]-[31]. A useful property of that type of NRD-guide T-junctions is the phase difference between the two outputs. Due to the electromagnetic field configuration of the LSE_{10} and LSM_{10} modes, an LSM_{10}-to-LSE_{10} mode conversion T-junction will have 180° phase difference between the outputs, and an LSE_{10}-to-LSM_{10} mode conversion T-junction will have 0° phase difference between the two outputs. Otherwise, for both an LSM_{10}-to-LSE_{10} mode conversion and an LSE_{10}-to-LSM_{10} mode conversion, the right

angle 90° bend and left angle 90° bend will have 180° phase difference between the outputs.

The proposed NRD-guide feeder topology consists of a metal waveguide to an NRD-guide transition, LSM_{10}-to-LSE_{10} NRD-guide T-junction and LSE_{10}-to-LSM_{10} NRD-guide 90° bends, as shown in the Fig.4.1. The first part is a metal waveguide to an NRD-guide transition, which converts the TE_{01} mode of the rectangular waveguide to the LSM_{10} mode of the NRD-guide. The second part is LSM_{10}-to-LSE_{10} NRD-guide T-junction, which have 180° phase difference between the outputs. The third part is LSE_{10}-to-LSM_{10} NRD-guide 90° bends, which include one right angle LSE_{10}-to-LSM_{10} 90° bend and one left angle LSE_{10}-to-LSM_{10} 90° bend and have 180° phase difference between the outputs. For the entire proposed structure, the TE_{01} mode of the rectangular waveguide at input port is split into two LSM_{10} modes of the NRD-guide and have 0° phase difference at the two outputs.

In this chapter, an NRD-waveguide feeder network, which consists of metal waveguide transitions, NRD-guide T-junctions and NRD-guide bends, is first described, then analyzed and simulated. Simulation and measurement results for this structure are presented. It is shown that a resonance problem within the NRD-guide appears with metal waveguide-to-NRD-guide transitions [25].

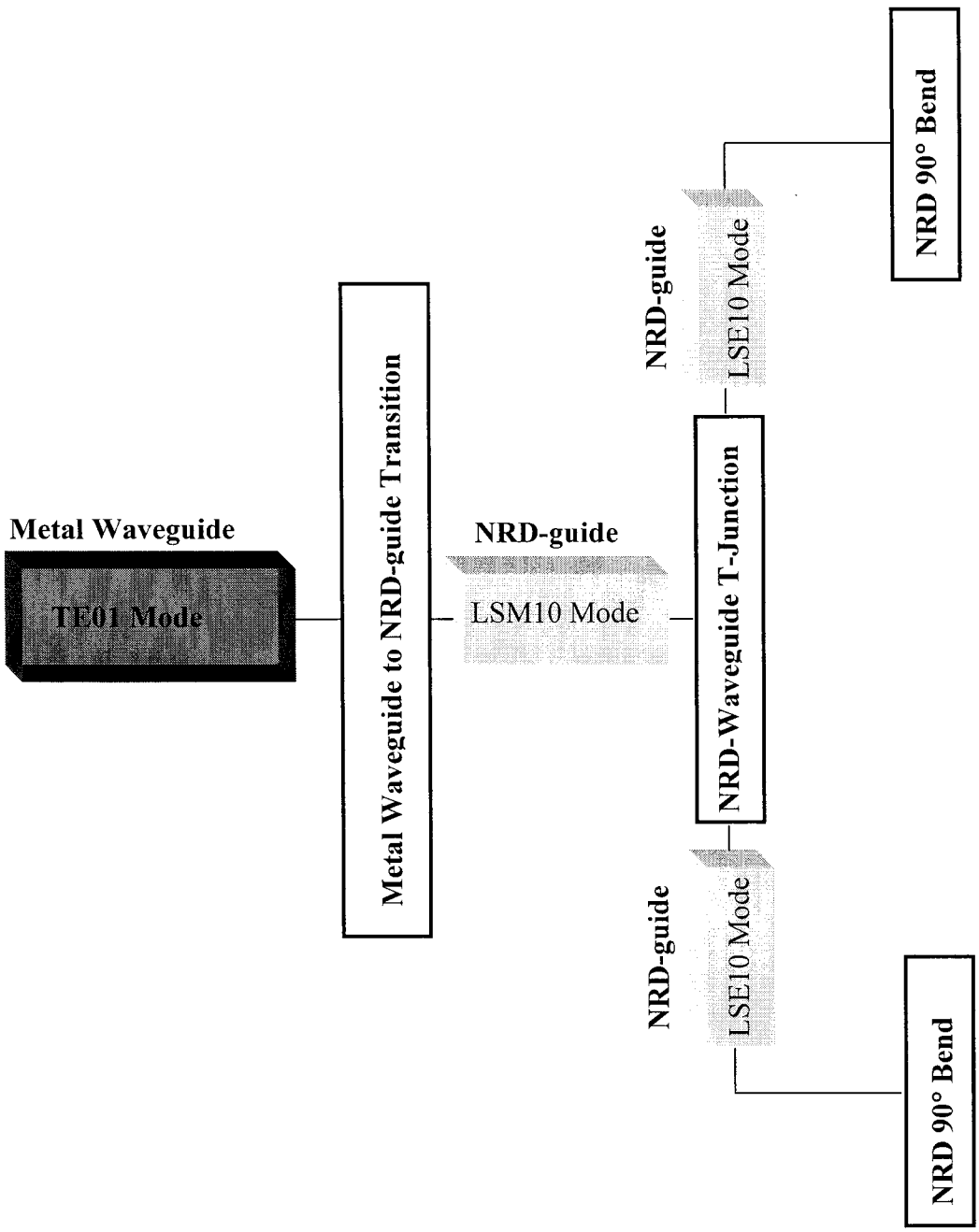

Fig. 4.1 The proposed topology NRD-guide feeder

4.2. Transition from Rectangular Waveguide to NRD-guide

4.2.1 Physical Description

The NRD-guide is commonly excited by a rectangular metallic waveguide or a stripline. The design of the transition from rectangular waveguide to NRD-guide, which will be applied in this project, must provide for a gradual conversion of the TE_{01} mode of the rectangular waveguide to the LSM_{10} mode of the NRD-guide. The transition shown in Fig. 4.2(a) consists of two sections. The first section is a transition from a standard rectangular waveguide to a reduced-length dielectric-filled metallic waveguide. The metallic walls of the waveguide are equal to dielectric in width and the linear dielectric taper along width approximates a specified impedance match. For ease of fabrication, the dielectric strip was taper linearly from 0 to b over the length l. The cross-sectional dimensions of the dielectric at the end of this first section are shown in Fig. 4.2(b) where both b and c are constant that are the same as those of the dielectric in the NRD-guide. The second section of the transition is from the dielectric-filled waveguide to NRD-guide, where the width is now kept constant at the plate separation value of b. The dielectric height is kept constant at a. The TE_{01} mode that exists in the uniformly filled waveguide is gradually converted to the dominant NRD-guide mode, LSM_{10} mode.

4.2.2 Experiments and Measured Results

This transition was designed and simulated over 26-30 GHz frequency range. The design and theoretical procedure were reported [30]. As mentioned above, the

composite transition consists of two sections as shown in Fig. 4.2. The first part of transition between standard rectangular waveguide WR-28 of inner dimensions $7.112 \times 3.556mm$ to a dielectric-filled metallic waveguide of dimensions $4.953 \times 3.556mm$, which was the same as those of dielectric stripe b =3.556 mm in width and a =4.953 mm in thickness. The dielectric used was Polystyrene with $\varepsilon_r = 2.56$, which was chosen for its low-loss properties as well as its excellent machinaebility. The dielectric tapers inside the waveguide are linearly varied in H-plane for ease of machining, while the dielectric taper length l approximates a specified impedance match to maintain a good mode matching. Our goal is to optimize the load so it can provide a sufficient attenuation in the frequency of interest. The dimension is obtained for the length of dielectric taper in metallic waveguide l =6.5mm. The optimized result by Ansoft HFSS is given by Fig. 4.3, indicating a minimum attenuation level of 0 dB achievable over the bandwidth, and input port reflected power below – 30dB.

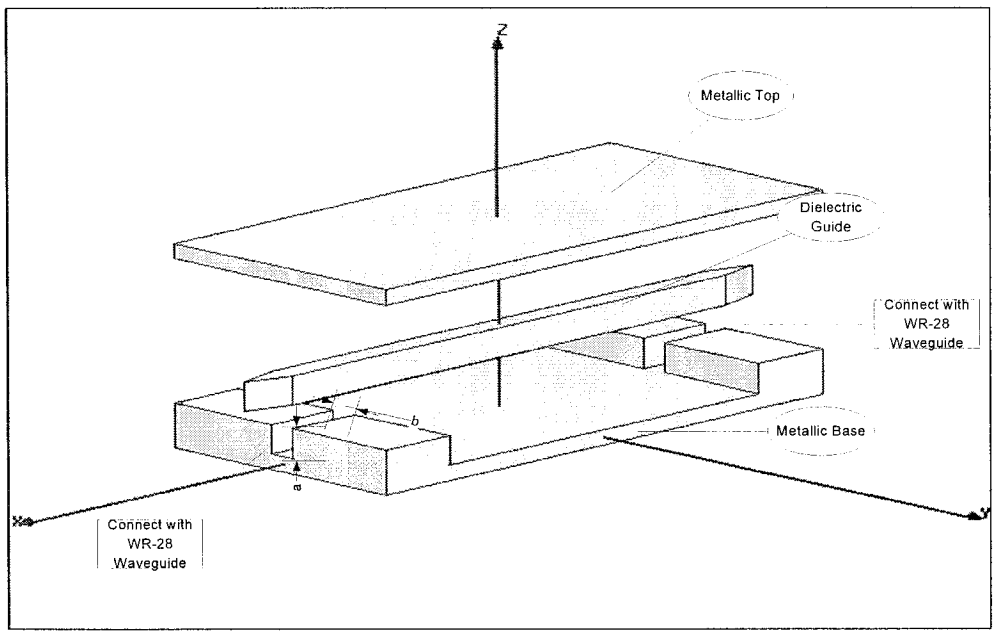

Fig. 4.2 (a) 3-D Scheme of transition from metal waveguide WR-28 to NRD-guide

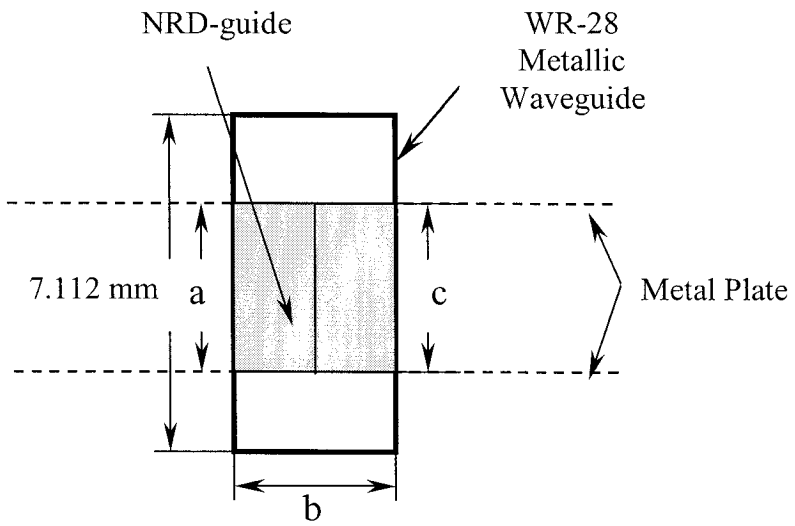

Fig. 4.2 (b) Cross-sectional scheme of transition from metallic waveguide WR-28 to NRD-guide

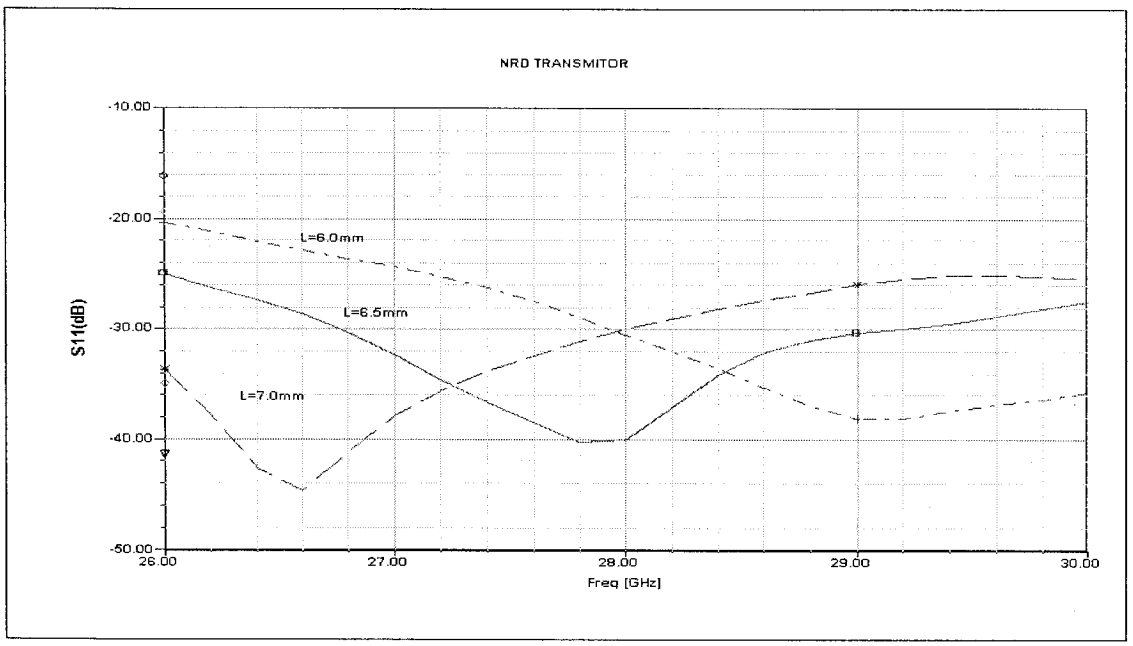

Fig. 4.3 (a) Simulated return loss S_{11} of metal waveguide to NRD-guide transition with different taper length of L

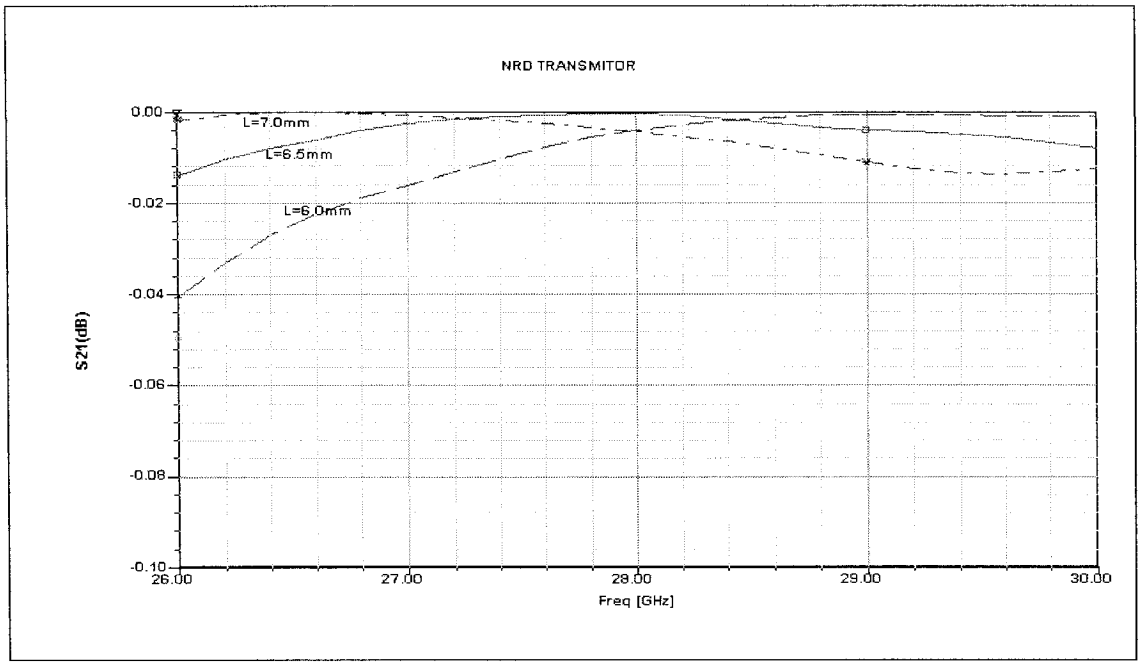

Fig. 4.3 (b) Simulated Transmission S_{21} of Metal waveguide to NRD-guide transition

Fig. 4.4 gives measured results of the proposed transition from the rectangular waveguide to NRD-guide. The transition was constructed using a polystyrene strip. It shows that there are noticeable spikes in measurement of the transition. They are similar to the case in which the spikes appear when an NRD-guide bend is terminated by LSM_{10} mode waveguide transition, reported by Yoneyama *et al.* [25], this construction results in an LSE_{10} mode cavity having resonance at discrete frequencies. At resonance, the LSE_{10} mode signal, which is linked to the LSM_{10} mode signal through the mode conversion, cannot propagate in the structure, resulting in a high insertion loss for the LSM_{10} mode at these frequencies.

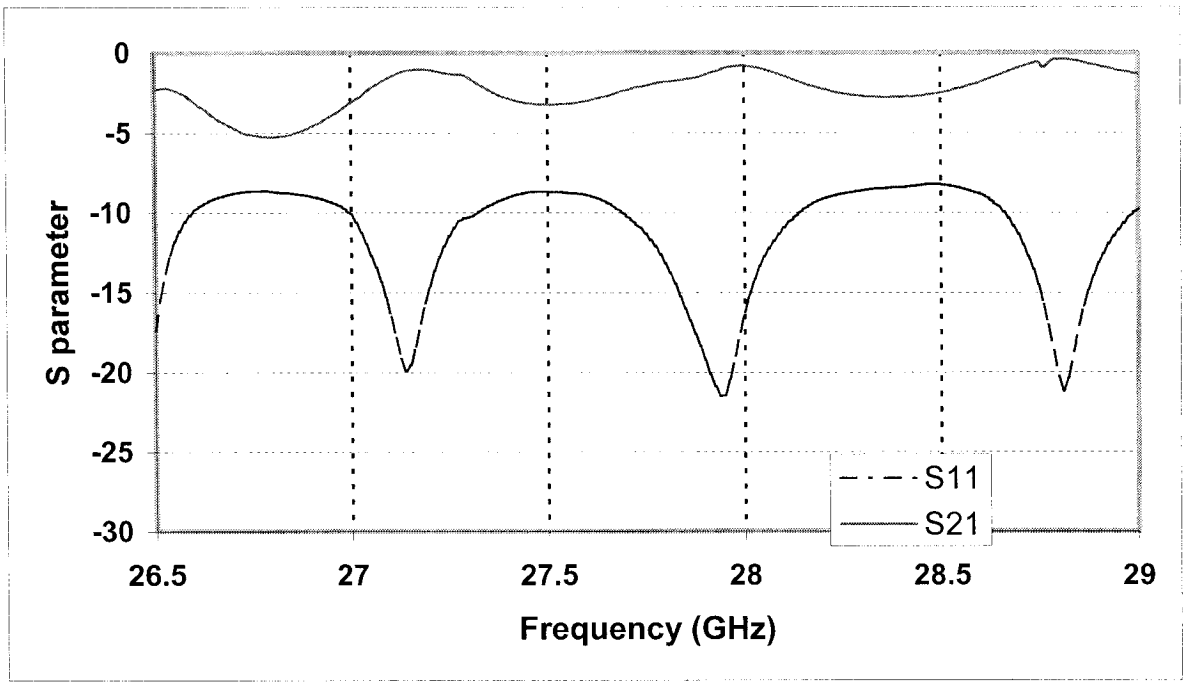

Fig. 4.4. Measured results of the proposed transition from metal waveguide to NRD-guide with different taper length of L

4.3. NRD-guide T-junction

4.3.1. Description of NRD-guide T-junction

Dielectric T-junctions, beside acting as power dividers, can find applications in the design of 3dB couplers, modulators, switches, mixers, and so on. The NRD-guide T-junction is a dielectric T-shaped structure sandwiched between parallel metal plates separated by a distance of less than half a wavelength, according to the principle of NRD-guide. There exits LSM_{10} mode at the input port that is converted to an LSE_{10} mode at the two output ports, which have 180° phase difference. As is well known, any lossless three-port network cannot be simultaneously matched at all ports,

matching was attempted only at input port to extract half the amount of input power from two output ports. For this purpose, the fabricated T-junction was provided with an optimal length L of the main arm, shown in Fig. 4.5.

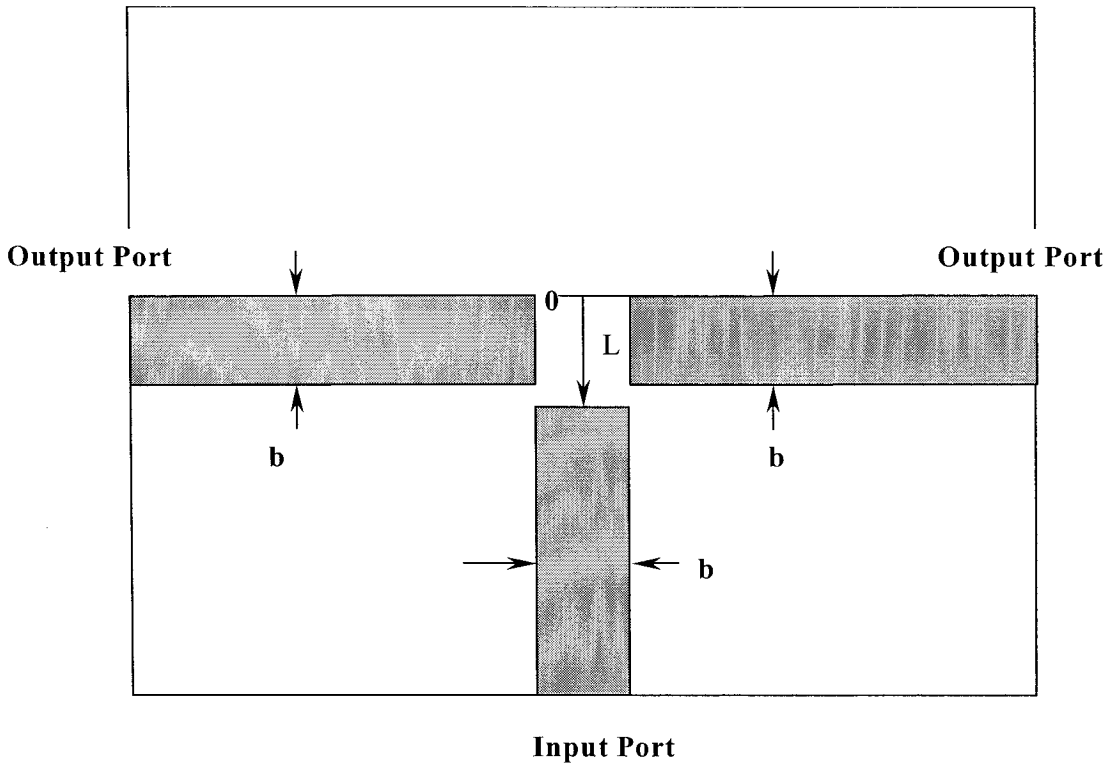

Fig. 4.5 Physical topology of the NRD-guide T-junction and definition of the L

4.3.2 Experiments and Results

The LSE_{10}-to-LSM_{10} NRD-guide T-junction is optimized for the frequency band of interest. In this project, the frequency band is 26-29 GHz. Polystyrene material with the dielectric constant of $\varepsilon_r = 2.56$ is used. The resulting dimensions of the T-junction (see Fig.4. 5) are a=4.953mm in height and b=3.556mm in width for the three

arms of T-junction. To obtain an optimum mode transfer from input port to output ports, the designed dimension and frequency response are presented. The simulation results of the overall NRD-guide T-junction are presented in Fig. 4.6 and Fig. 4.7, and Fig.4.6 shows that the return loss of input port is a function of the length L and L=b=3.556 mm is critical point. For this dimension, the LSM_{10} mode at the input port is equally divided in amplitude into two LSE_{10} modes at output ports. The reflected power at input port is then minimal at –17.8 dB and is only related to mode LSM_{10}. The transmissions of S_{21} and S_{31} of the T-junction are investigated as a function of frequencies from 26 GHz to 30 GHz while L= 3.556 mm. The mode transfer from LSM_{10} mode at input port to LSE_{10} mode at output ports remains practically constant, from -3.83 dB to -3.28 dB at frequencies range from 26 GHz to 30 GHz.

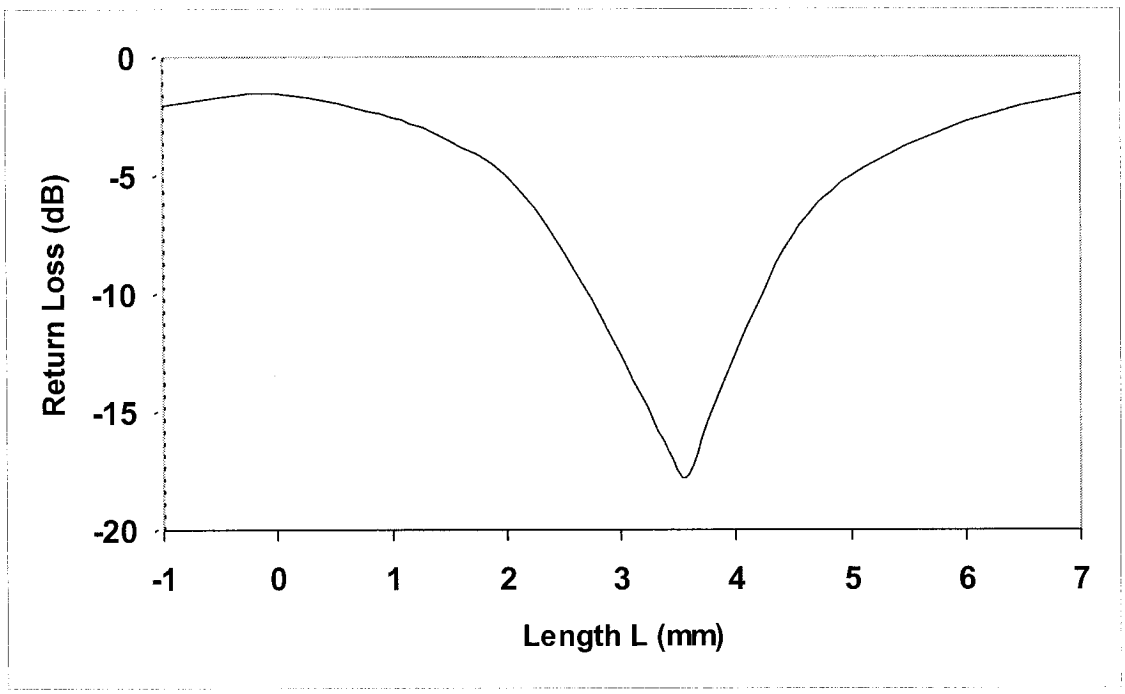

Fig. 4.6 The return Loss of NRD-guide T-junction with main arm length L (mm)

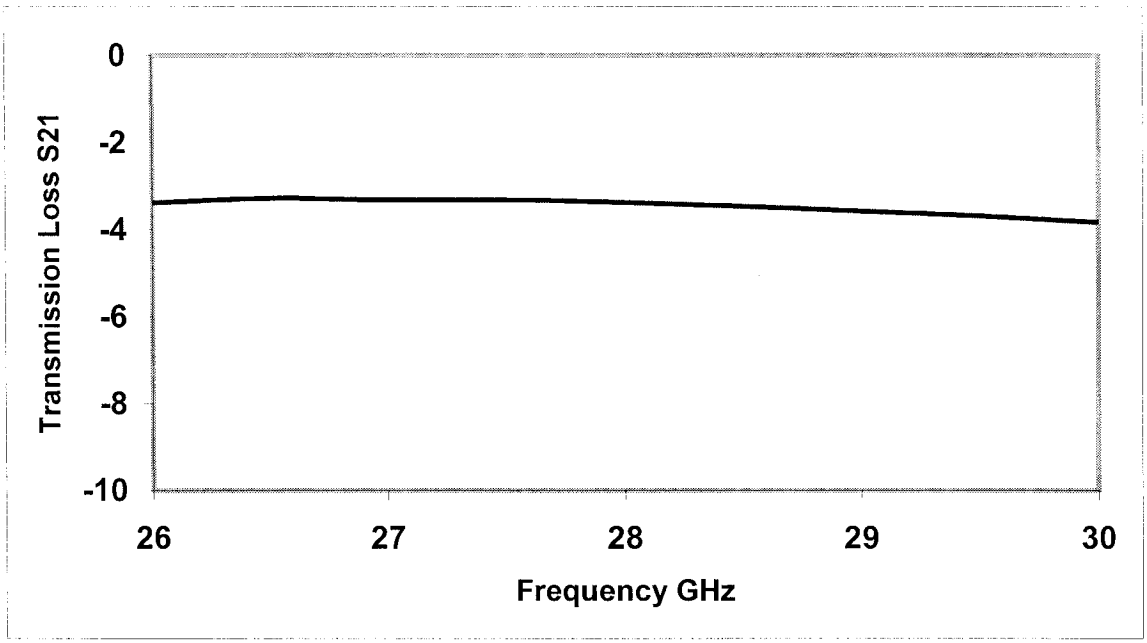

Fig. 4.7 LSM_{10} mode to LSE_{10} mode T-junction transmission S21 along frequencies while L=3.556mm (simulated)

4.4. NRD-guide Bend

4.4.1 Description of 90° NRD-guide Bend

In the case of an NRD-guide bend, since the structure is basically nonradiative, any loss caused by bends is due to reflection at the transition between the straight guide and the curve guide. Thus the minimum radius of bend permissible in practice is determined by the tolerable reflection. The NRD-guide 90° bends is applied in the NRD-guide feeder structure. It is known that there is a mode conversion between LSM_{10} and LSE_{10} modes in the NRD-guide structures such as T-junctions or 90° bends. This mode conversion cannot be eliminated without using a special measure like mode

suppressor. However, it can be optimized such that nearly all the power of LSE_{10} mode at the input port is converted into the LSM_{10} mode power at output port. Using the design procedure described in [32], which gives an adequate dimension of 90° NRD-guide sharp bends for optimum mode conversion, we constructed an NRD-guide bend, as shown in Fig. 4.8. Lc is a critical dimension that affects LSE_{10} mode to LSM_{10} conversion. The LSE_{10} mode is mainly converted to LSM_{10} mode but a small part with optimum value Lc.

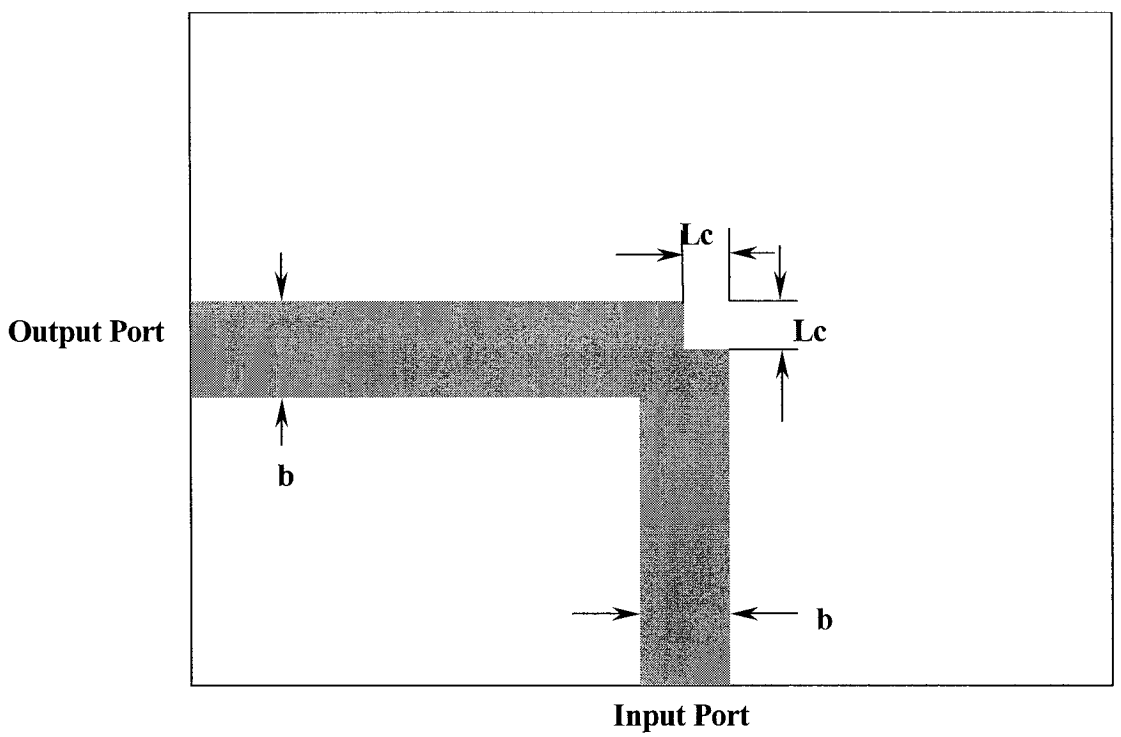

Fig. 4.8 Topology of NRD-guide 90° bend and definition of Lc

4.4.2. Experiments and Results

L-shaped polystyrene strips ($\varepsilon_r = 2.56$) with $a = 4.953mm$ in height and $b = 3.556mm$ in width, sandwiched into two parallel metal plates, are used to construct 90° right angle and left angle NRD-guide bends at a center frequency of 27.5 GHz while Lc was optimized to be 2.781 mm. The NRD-guide T-junction as well as NRD-guide 90° right angle and left angle bend are used to form an NRD-guide power splitter, shown in Fig. 4.9. The LSM_{10} mode at the input port is equally divided in amplitude into two LSM_{10} modes with 0° phase difference at the two output ports. Simulation results that do not include the dielectric loss are given in Fig. 4.10, which show an insertion loss of about 0.7 dB for the *LSM* to *LSE* mode and *LSE* to *LSM* mode conversions as well as direct *LSM* to *LSE* mode and *LSE* to *LSM* mode transfer level below –13 dB. The simulated results demonstrated that a low transmission loss and a good return loss could be achieved with the proposed concept. In this experiment, one input port of the proposed structure is connected to the metallic waveguide through a transition from the metallic waveguide to NRD-guide, while the other two output ports of the device work as LSM_{10} mode NRD-guide, which will couple with the cylindrical dielectric resonators and feed them.

4.5. Conclusion

The NRD-guide feeder network, which consists of metallic waveguide transition, NRD-guide T-junction and NRD-guide bends, has been proposed and developed. Simulated and measured results have shown the operating mechanism and preliminary performance of the NRD-guide feeder. The resonance and spikes have been discussed. The experiments have verified the low-loss characteristics of this structure and the performances of NRD-guide transition, T-junction and bend have demonstrated

potential applications for the construction of millimeter-wave circuits.

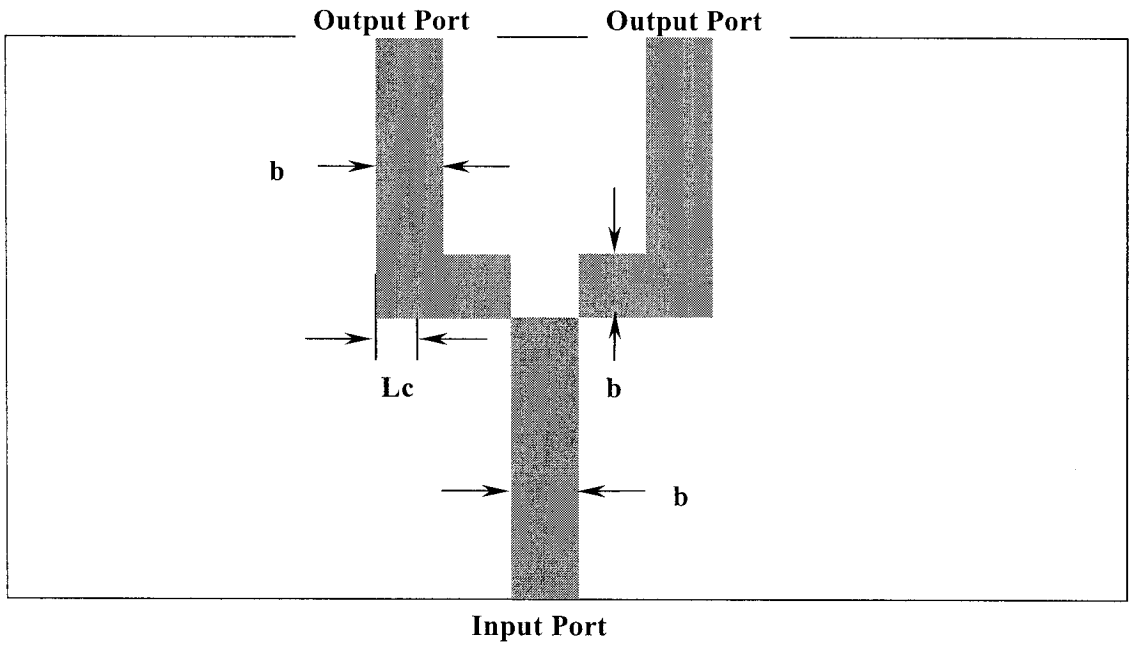

Fig. 4.9 Physical topology of NRD-guide power splitter

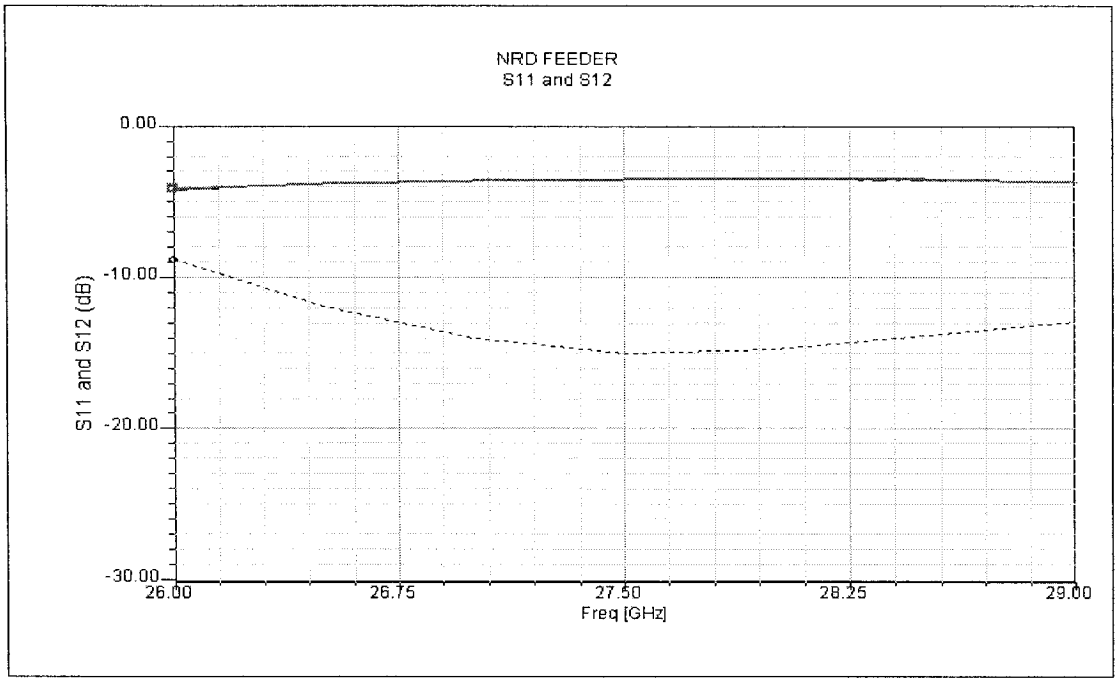

Fig. 4.10 Simulated NRD-guide power splitter return loss and transmission S11 and S12

CHAPTER V

CYLINDRICAL DIELECTRIC RADIATOR AND RADIATOR ARRAY

5.1. Introduction

As discussed in the previous chapters, the NRD waveguide has been demonstrated to be one of the most promising building blocks in millimeter-wave circuits because of its simplicity, ease of fabrication, and low loss nature. Dielectric antennas have the merit of low loss, high radiating efficiency, low cost, mechanical simplicity, and they are particularly suitable for the applications at higher frequencies. Other major advantage of dielectric antennas is that they can easily be integrated with dielectric integrated circuits to form transmitter/receiver front ends.

A number of authors have recently described new antenna configurations in NRD waveguide [6]-[8], [33]. These antennas all fall into the broad category of antennas that radiate either as open-ended single or coupled NRD waveguides or as the unidirectional radiator (UDR). Other antennas in NRD waveguide make use of a variety of radiating mechanisms, such as radiation through slots in the conducting plane [34]-[36], leaky-wave structures using various schemes [37]-[39], and radiation from variously terminated guides [40]. All these antennas have the common advantage, namely, that they can be integrated directly into an NRD waveguide circuit.

Dielectric resonator antennas (DRAs), especially cylindrical dielectric resonator antennas, have been considered for applications at millimeter-wave frequencies, since systematic experimental investigations on DRAs were carried out by Long et al. [41]. DRAs share many of the advantages of dielectric antennas, including small size, low profile, lightweight, and ease of coupling to many types of transmission line. In addition, DRAs exhibit a relatively large bandwidth. Moreover, DRAs avoid the inherent disadvantages of patch antennas, such as high conduction loss at millimeter-wave frequencies, and low efficiency due to surface wave excitation. The

excitation methods such as aperture-coupled feed and coaxial probe have been presented. [41]-[43].

In this chapter, a promising dielectric antenna, namely the cylindrical unidirectional dielectric radiator (CUDR), which consists of a cylindrical dielectric resonator and NRD-guide feeder, will be described. Analysis and experiment of such a cylindrical unidirectional dielectric radiator will be presented. It retains all the merits of NRD-guide and offers a number of unmatched advantageous features for millimeter-wave applications. Simulated and measured results of CUDR and CUDR array are given to illustrate future applications of those novel structures.

5.2. Concept of Cylindrical Unidirectional Dielectric Radiator (CUDR)

5.2.1 Radiator Structure

The CUDR is sandwiched between two parallel metallic plates (distance=**a**). It is basically a cylindrical dielectric antenna fed by NRD-guide (height=**a**, width=**b**). To understand better its operating principle, let's consider a dielectric cylinder inserted two infinitely extended metallic plates, which effectively forms a dielectric resonator. As is well known, if the two parallel metal plates are separated by a distance smaller than one-half of the free–space wavelength, electromagnetic waves with the electric fields parallel to the plates cannot propagate between them because of the cutoff properties. This structure then becomes a high-Q dielectric resonator, as shown in Fig. 5.1. Resonant characteristics and electromagnetic fields have already been discussed in chapter III. If the metal plates have finite extent and the cylindrical dielectric

resonator is located in a close proximity of the plate edges, as shown in Fig. 5.2, the complete non-radiating condition is no longer satisfied and the electromagnetic energy begins to radiate toward the open space, mostly in the x-direction from the aperture while suppressed in other directions due to the cutoff properties of the NRD structure. It is then become a CUDR. The operating principle of CUDR is quite similar to that NRD-guide and leaky-wave antennas, and is a resonance type of radiating element. As an antenna, the CUDR is readily connected to planar passive and active circuits as well as NRD components.

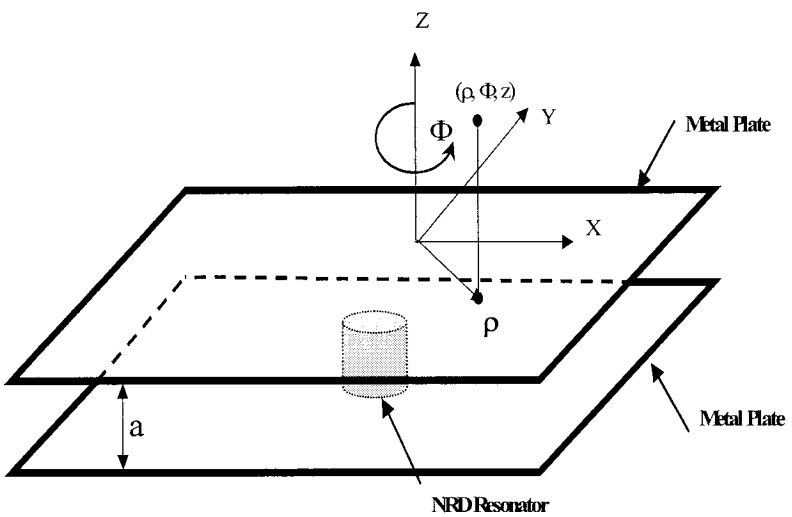

Fig.5.1 Parallel-plate cylindrical dielectric resonator (CDR)

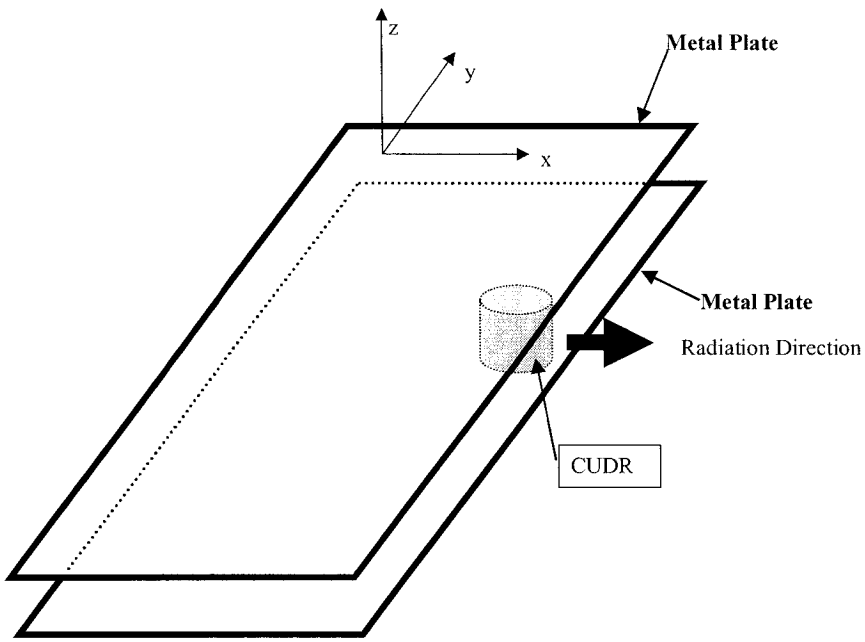

Fig. 5.2 Cylindrical unidirectional dielectric radiator (CUDR)

5.2.2. Feed Structure and Model Analysis

It is well known that the radiation field of antenna can be determined if the electromagnetic field distribution at the aperture are known. In the modeling of CUDR, the two parallel metal plates of the structure are first assumed to extend to infinite in x-direction, thereby resulting in a typical cylindrical dielectric resonator. The efficient numerical technique proposed in [18] is extended for analysis of the cylindrical dielectric resonator. The field expression has been deducted and presented in chapter III. The resonant frequencies can be determined by the dielectric constant and the dimensions of the cylindrical dielectric resonator (CDR) (radius=**r**, height=**a**). Once the proposed resonant frequency is given, the mode of the cylindrical dielectric resonator

and the field expression can be obtained, and the equivalent current distribution on the radiating aperture is obtained to calculate the radiation properties.

There are several ways to excite the resonant radiating mode, for example, direct coaxial feeding probe, planar strip-to-slot coupling excitation, and NRD-guide direct coupling. In this project, NRD-guide is chosen to excite the CUDR. As mentioned in chapters II and III, the operation mode in NRD-guide is LSM_{10} mode, which couples with the cylindrical dielectric resonator through a gap in front of NRD-guide or a gap in proximity to the NRD-guide and excites the mode of interest in CUDR, as shown in Fig. 5.3 and Fig. 5.4.

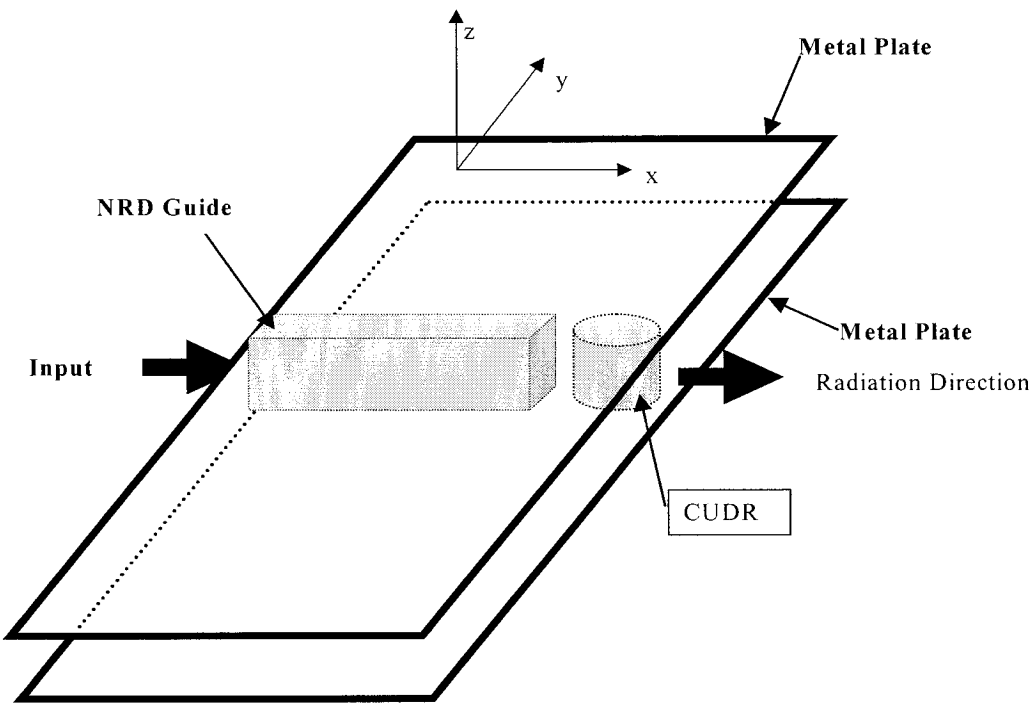

Fig. 5.3 Cylindrical unidirectional dielectric radiator fed by NRD-guide (front coupling)

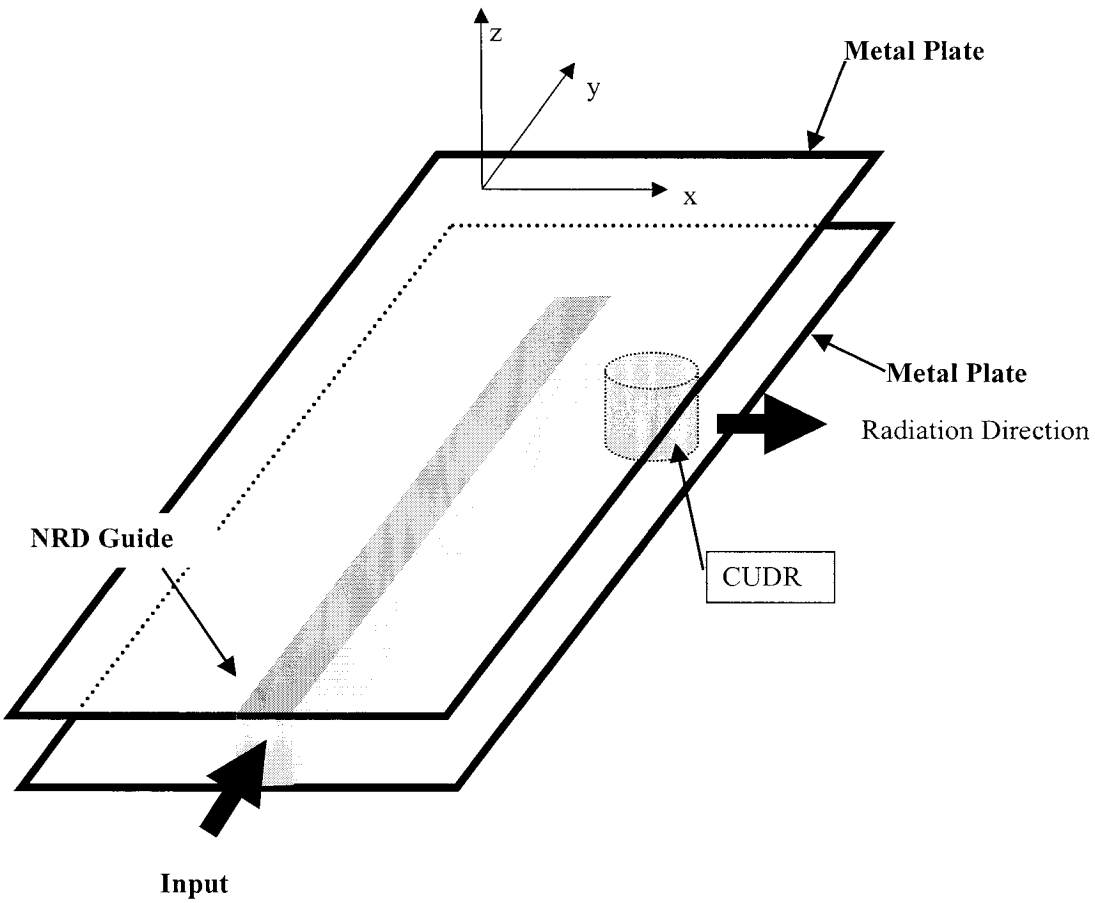

Fig. 5.4 Cylindrical dielectric radiator fed by NRD-guide (side coupling)

A. Front Coupling

A cylindrical dielectric radiator placed between two parallel metallic plates and located in the front end of NRD-guide is coupled by NRD-guide through a gap at the end of NRD-guide, shown in Fig. 5.3. This coupling scheme excites HEM_{111} mode (see Fig. 5.5) in the CUDR. For the HEM_{111} mode, the inner electromagnetic fields are given by (3.11) and (3.15) and outer electromagnetic fields are given by (3.13) and

(3.16).

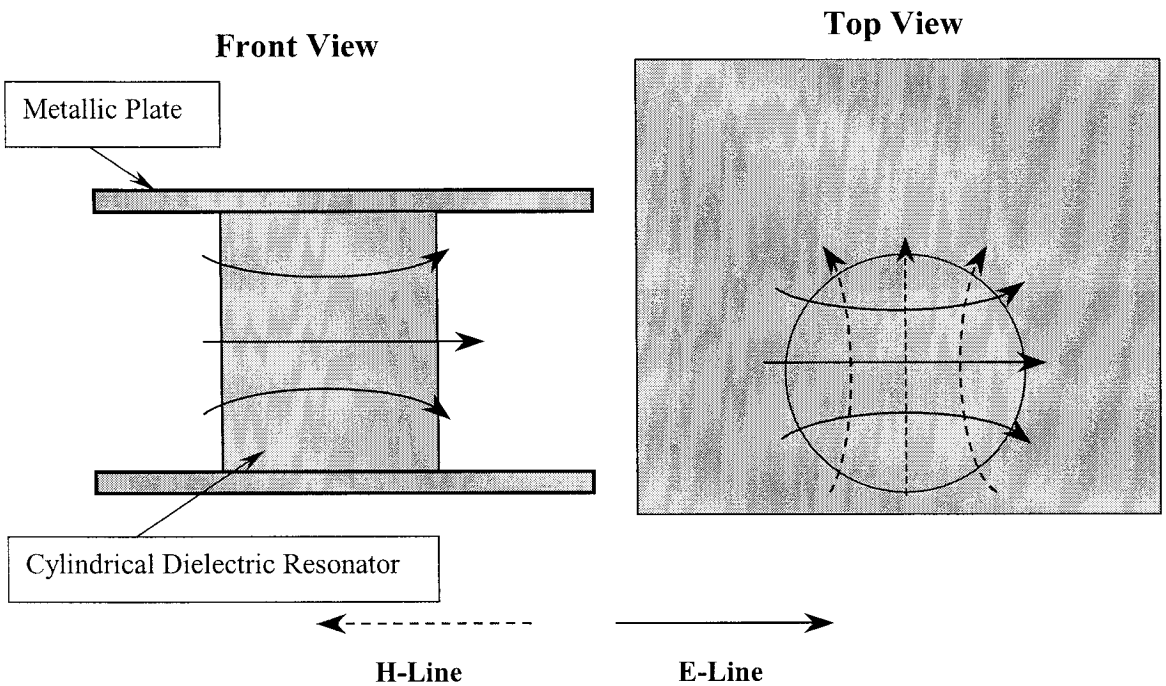

Figure 5.5 The typical field lines HEM_{111} mode in cylindrical dielectric resonator

The CUDR is kept symmetrical and coupled with the NRD-guide through the front coupling gap. It is basically a cylindrical dielectric radiator fed by the NRD-guide (height=**a**, width=**b**). The cylindrical dielectric radiator (radius=**r**, height=**a**) is located in a close proximity (distance=**d**) to the edges of the two parallel plates. The gap distance between the cylindrical dielectric resonator and the feeding NRD guide is d_1, as shown in Fig.5.6 (a) and Fig.5.6 (b). The coupling strength between the NRD-guide and CUDR can be changed or tuned by varying gap distance d_1.

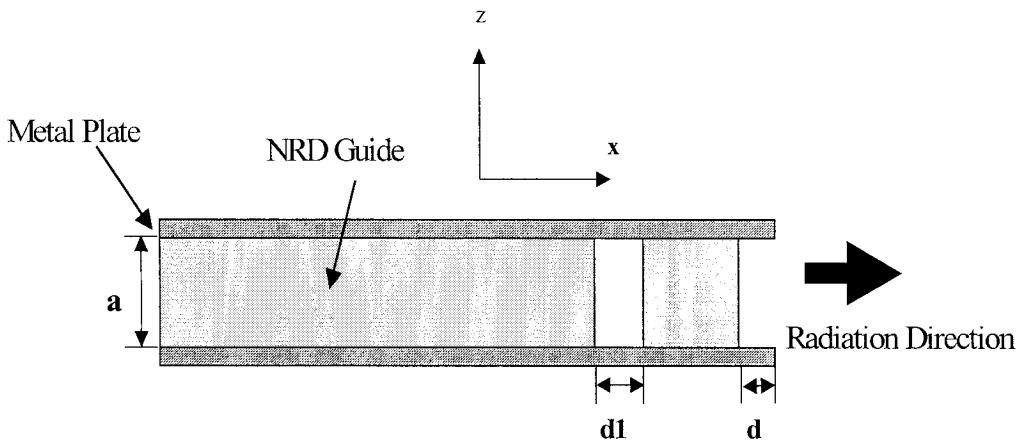

Fig. 5.6 (a) Side view of front coupling cylindrical unidirectional dielectric radiator

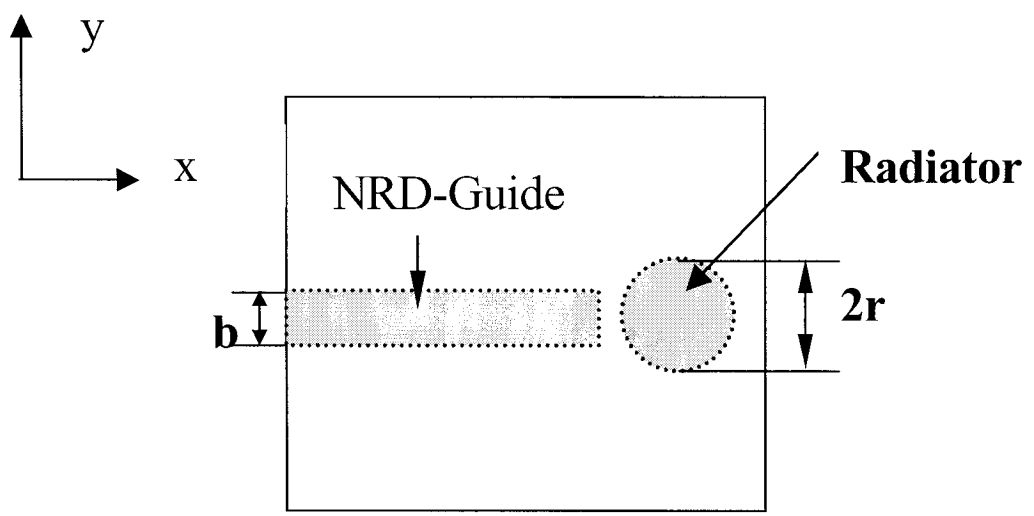

Fig. 5.6 (b) Top view of front coupling cylindrical unidirectional dielectric radiator

B. Side Coupling

The cylindrical dielectric radiator placed between the two parallel metallic plates and located at the side of NRD-guide is coupled by the NRD-guide through a gap at the side of NRD-guide, as shown in Fig. 5.4. The operation mode in the NRD-guide is LSM_{10} mode, which excites the TE_{011} mode (see Fig. 5.7) in the cylindrical dielectric radiator. For TE_{011} mode, the inner electromagnetic fields are given by (3.11) and (3.15) while the outer electromagnetic fields are given by (3.13) and (3.16).

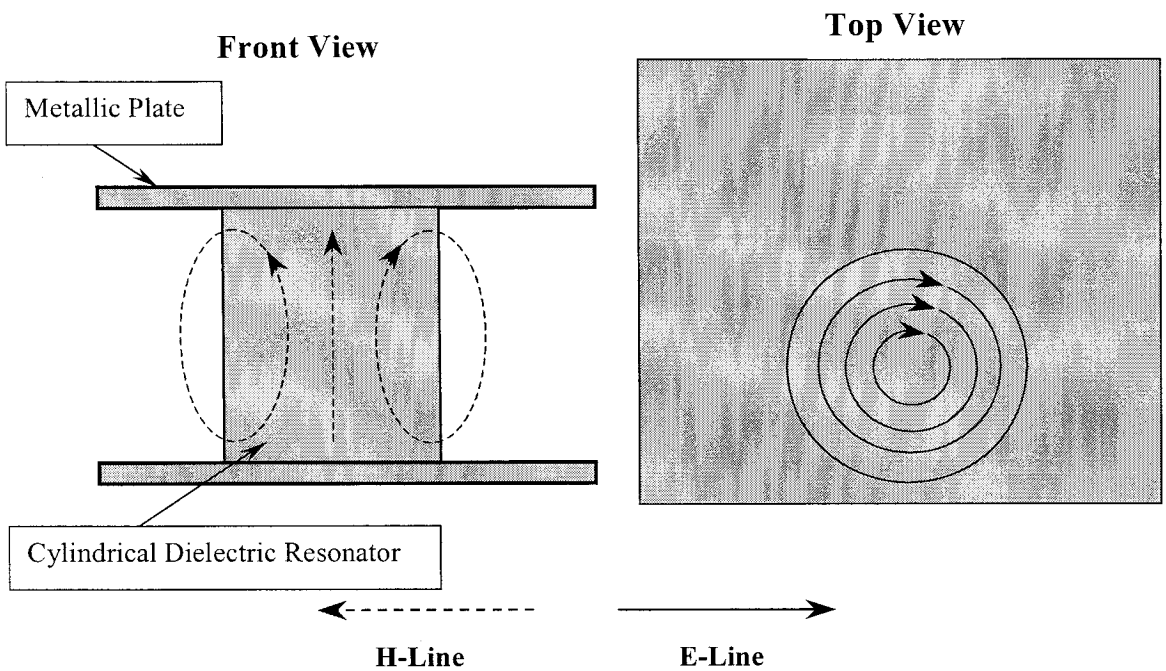

Figure 5.7 The typical field lines of TE_{011} mode in cylindrical dielectric resonator

The CUDR is placed next to the NRD-guide and coupled with the NRD-guide through a side-coupling gap. This is another cylindrical dielectric radiator fed by the NRD guide (height=**a**, width=**b**). The cylindrical dielectric radiator (radius=**r**, height=**a**) is also located in a close proximity (distance=**d**) to the edges of the two parallel

plates. The gap distance between the cylindrical dielectric resonator and feeding NRD guide is d_2, as shown in Fig.5.8 (a) and Fig.5.8 (b). The coupling strength between the NRD-guide and CUDR can also be controlled by varying gap distance d_2.

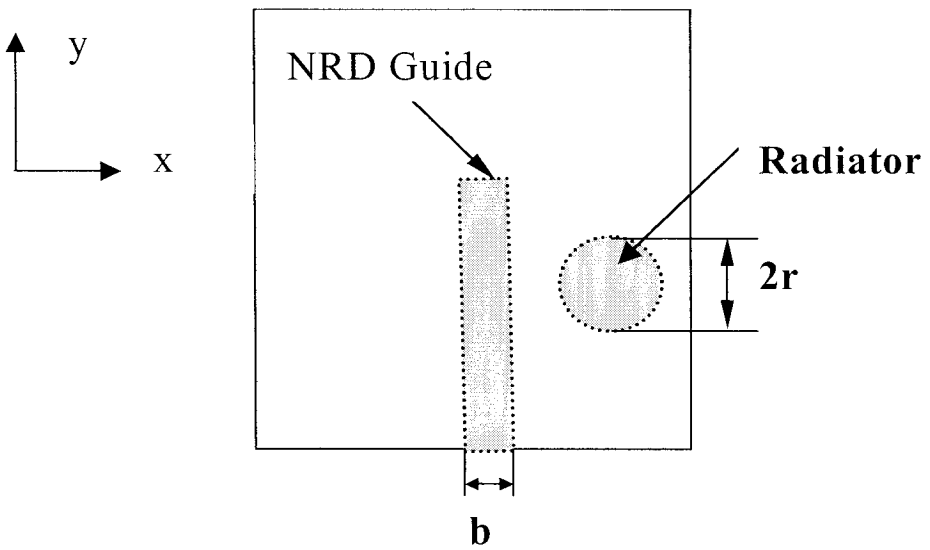

Fig. 5.8 (a) Side view of side coupling cylindrical unidirectional dielectric radiator

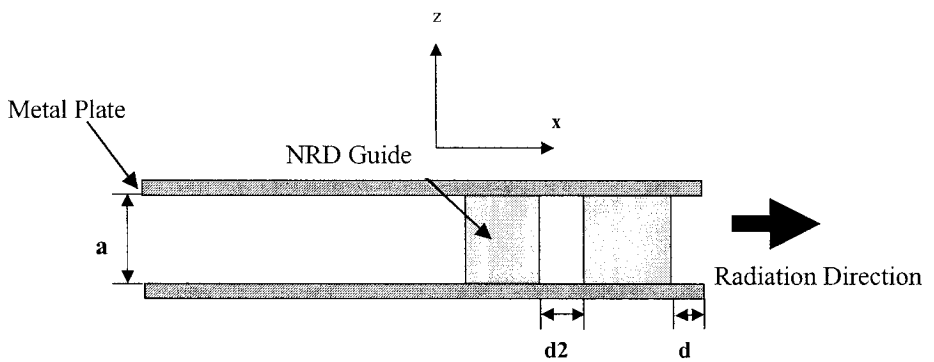

Fig. 5.8 (b) Top view of side coupling cylindrical unidirectional dielectric radiator

5.3. Simulation and Measurement Results

Prototypes of the proposed NRD-guide fed cylindrical dielectric radiator antennas were built and tested. Polystyrene material with dielectric constant $\varepsilon_r = 2.56$ was used to fabricate the NRD-guide and cylindrical dielectric radiator for its low loss and ease of fabrication. The lowest HEM_{111} mode and the second lowest TE_{011} mode were excited in the CUDR by different NRD-guide feeding structures, namely, the front coupling and side coupling. The dimensions of CUDR can be calculated by (3.17), (3.18), (3.22) and (3.23) while the resonant frequencies and modes can be determined. For both of the two feeding structures, the distance between the NRD-guide feeder and the cylindrical dielectric radiator are d_1 and d_2, respectively; and the distance of the cylindrical dielectric radiator with respect to the metal plate edge is d, as shown in Fig. 5.6 and Fig. 5.8. The adequate choices of d, d_1 and d_2 are critical in exciting the wanted mode in the cylindrical dielectric radiator as well as also in obtaining a good impedance matching. There exist optimal ranges of d, d_1 and d_2 for the maximum coupling and also the best possible impedance matching.

5.3.1. Front Coupling NRD-guide Feed Cylindrical Dielectric Radiator

As described above, the front coupling NRD-guide fed cylindrical dielectric radiator, which consists of an NRD-guide feeder and a cylindrical resonator used as radiator is made of polystyrene ($\varepsilon_r = 2.56$) with height of 4.953 mm, the NRD-guide width of 3.556 mm and the resonator radius of 2.4 mm. As discussed in Chapter III, the resonant frequency of the cylindrical dielectric resonator is known to be 27.047 GHz as

well as the desired resonance mode HEM_{111} is excited while its dimension is determined.

Generally speaking, the input impedance of the radiator depends on various geometrical and electrical parameters such as position of radiator, distance with respect to the NRD-guide feeder, dielectric constant and frequency. In this case, the position of radiator (d) and the distance between the radiator and NRD-guide feeder (d_1) are merely considered to demonstrate that the impedance matching can be achieved by an adequate choice. In the following, the return loss S_{11} at the feeding port is used to interpret the impedance matching behavior instead of the conventional input impedance. Fig. 5.9 displays the frequency-dependent magnitude of return loss S_{11} as a function of radiator position d with respect to the open edge while the distance between the radiator and NRD-guide feeder is fixed with $d_1 = 1.5mm$. It is observed that a good impedance match can be achieved by choosing an appropriate distance, almost a quarter wavelength ($d_1 = 1/4\lambda_g$), between the radiator and the NRD-guide feeder. Once this distance is given, it is also possible to have an impedance matching simply by varying the position (d) with respect to the edge of metal plates.

An HP8510 C Network Analyzer was used for the return loss measurement of antenna over the connector interface with a one-port calibration procedure. The typical measured return loss response of an NRD-guide front coupling with the cylindrical dielectric radiator for different radiator position (d), while $d_1 = 1/4\lambda_g = 1.5mm$, is shown in Fig. 5.10. The results show that the measured resonance frequencies for $d_1 = 1.5mm$, $d = 0.30mm, 0.4mm, 0.50mm$ are 27.378, 27.380, and 27.381 GHz, respectively, which are close to the calculated value of 27.034 GHZ. These confirm the accuracy of our calculation in Chapter III and are also consistent with the

simulated results shown in Fig. 5.10. Excellent coupling efficiency can be obtained with the proposed coupling mechanism. For $d_1 = 1.5mm$, and $d = 0.30mm, 0.4mm, 0.50mm$, the minimum return losses are obtained with 34 dB, 44 dB, and 36dB, respectively. The bandwidth and coupling strength can be changed by adjusting d and d_1. Typically, the resonant CUDR has a narrow bandwidth behavior. The 10dB return loss bandwidth can be estimated at the range of 0.2 to 0.6 GHz by adjusting the radiator position (d)

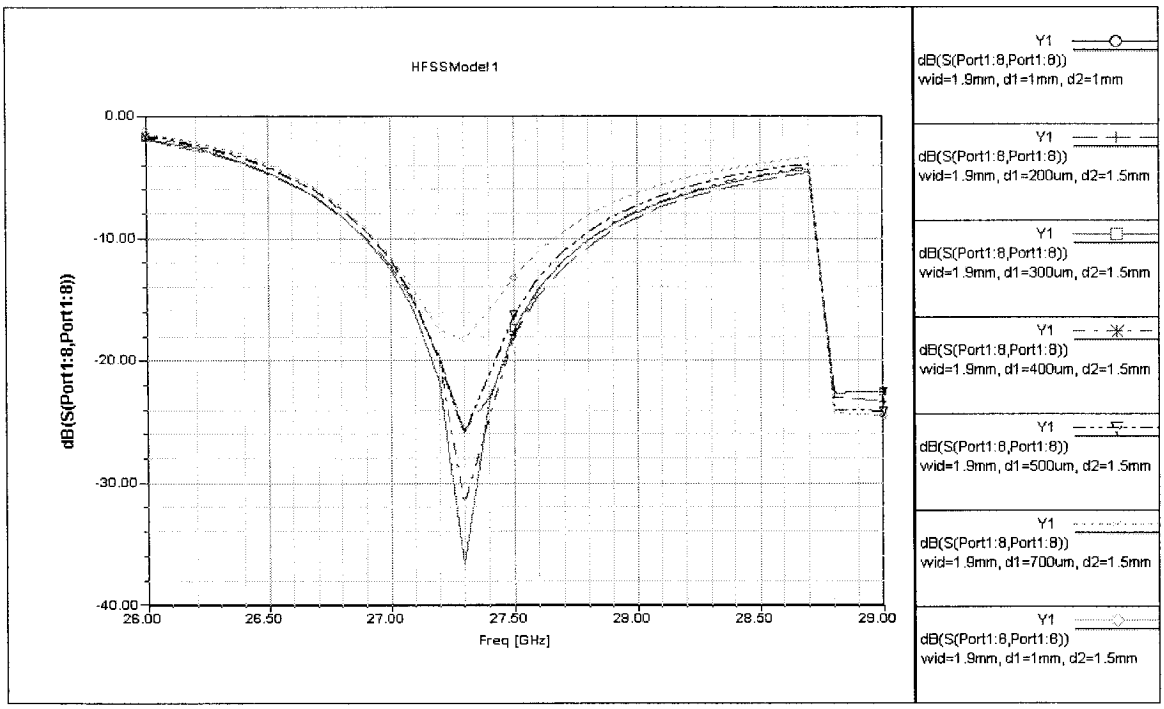

Fig. 5.9 Simulated return loss versus frequency for different radiator position (d) with respect to the open edge while $d_1 = 1.5mm$ (front coupling)

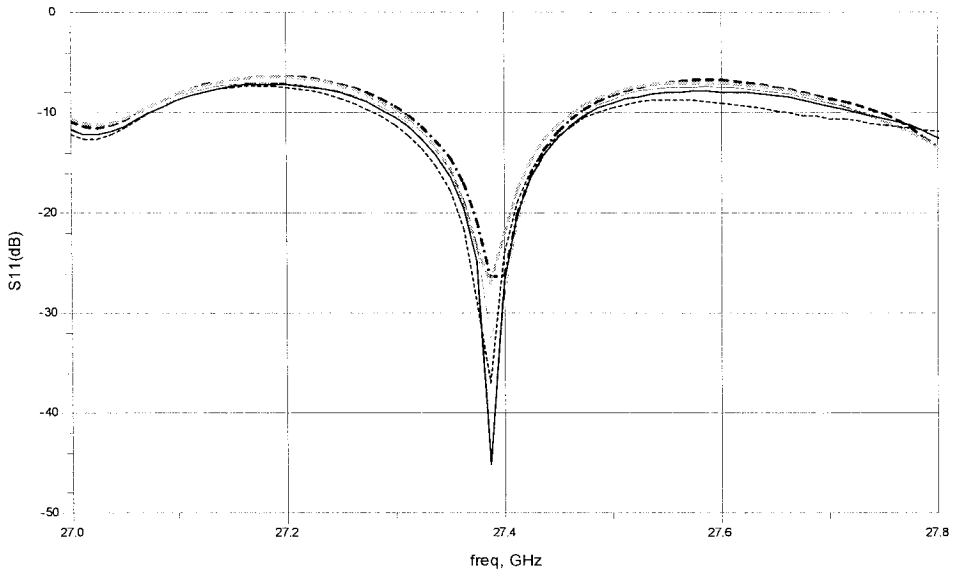

Fig. 5.10 Typical measured return loss response of an NRD-guide front coupling with cylindrical dielectric radiator for different radiator position (d), with $d_1 = 1.5mm$ and $\varepsilon_r = 2.56$

The radiation patterns of CUDR are simulated by HFSS. Fig. 5.11 (a) and (b) show the E plane (xy plane) and H plane (xz plane) co-polar and cross-polar patterns over 180°, respectively, for the case of $d = 0.38mm$ and $d_1 = 1.5mm$. They also indicate that the half power beam width (88°) in H-plane is much larger than that in E-plane (41°).

The MI-3000 system is used to measure the radiation patterns of CUDR. The measured radiation pattern of CUDR fed by the NRD-guide with $d_1 = 1.5mm$ and $d = 0.38mm$ is illustrated in Fig. 5.12 (a) and 5.12 (b), showing that the gain for

this antenna is measured to be 10.8 dB, as well as the half power beam widths are 40° in E-plane and 79° in H-plane. The agreement between the measurement and simulation is quite good. The coupling efficiency is high and a good matching can easily be obtained. As shown in Fig. 5.12 (a) and (b), an isolation of about 25 dB between the E-plane co-polar and cross-polar patterns can be achieved. Meanwhile, the isolation between the H-plane co-polar and cross-polar patterns is about 23 dB. In both case, there are virtually no side-lobe effects over the range of interest and this radiator exhibits a clean linear polarization.

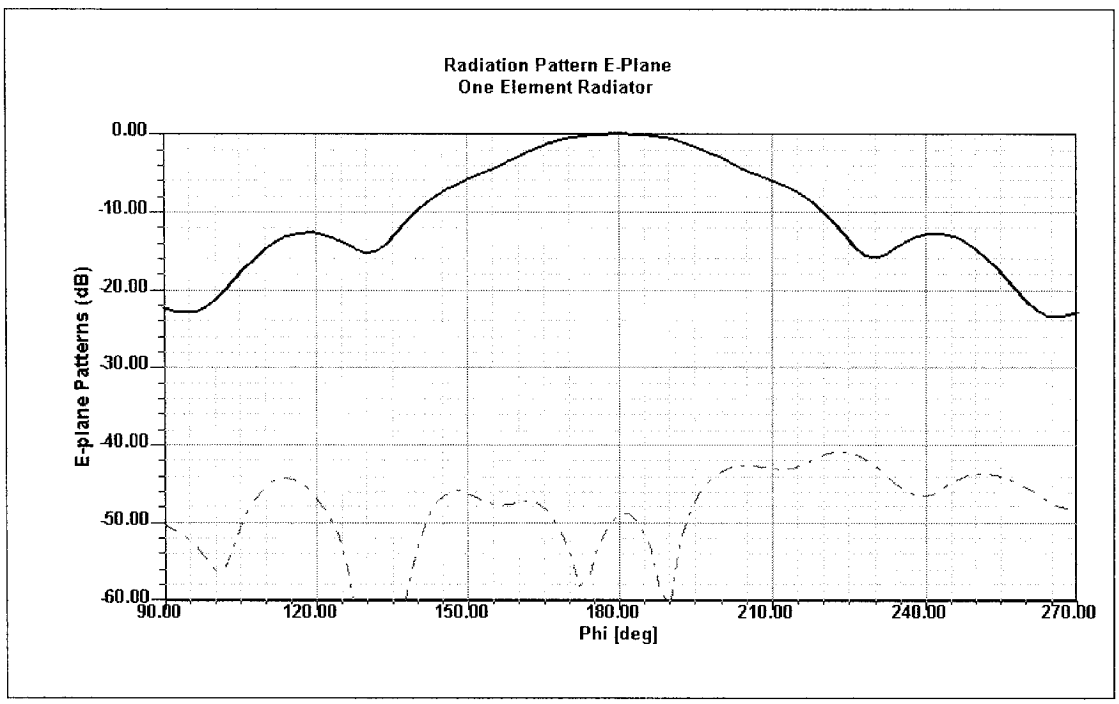

Fig. 5.11 (a) Simulated radiation pattern of front coupling radiator (E-plane)

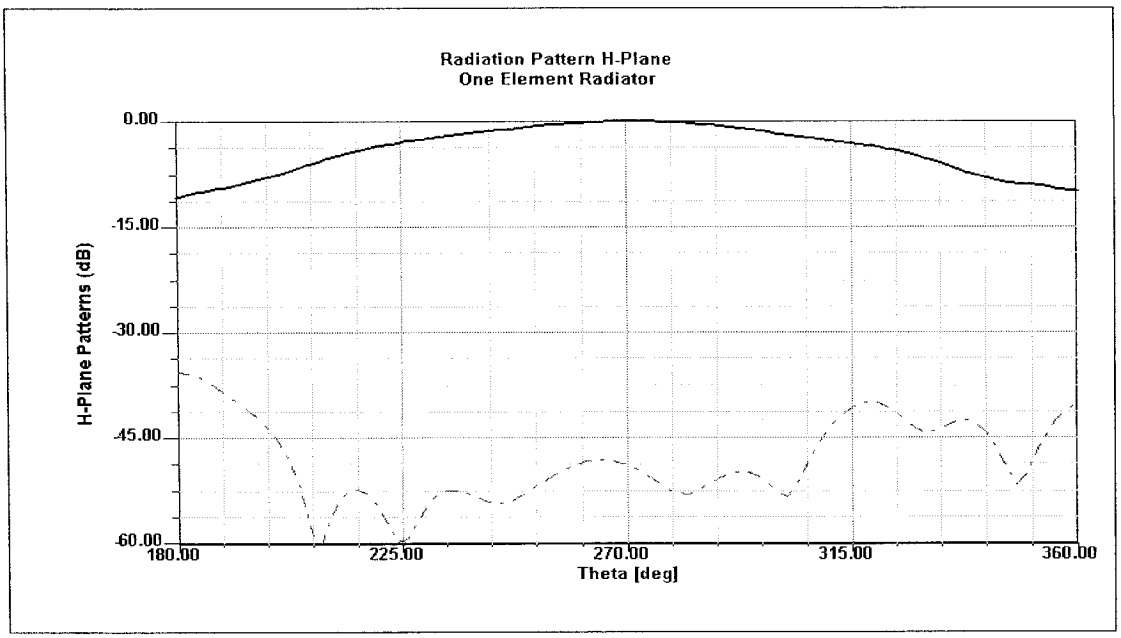

Fig. 5.11 (b) Simulated radiation pattern of front coupling radiator (H-plane)

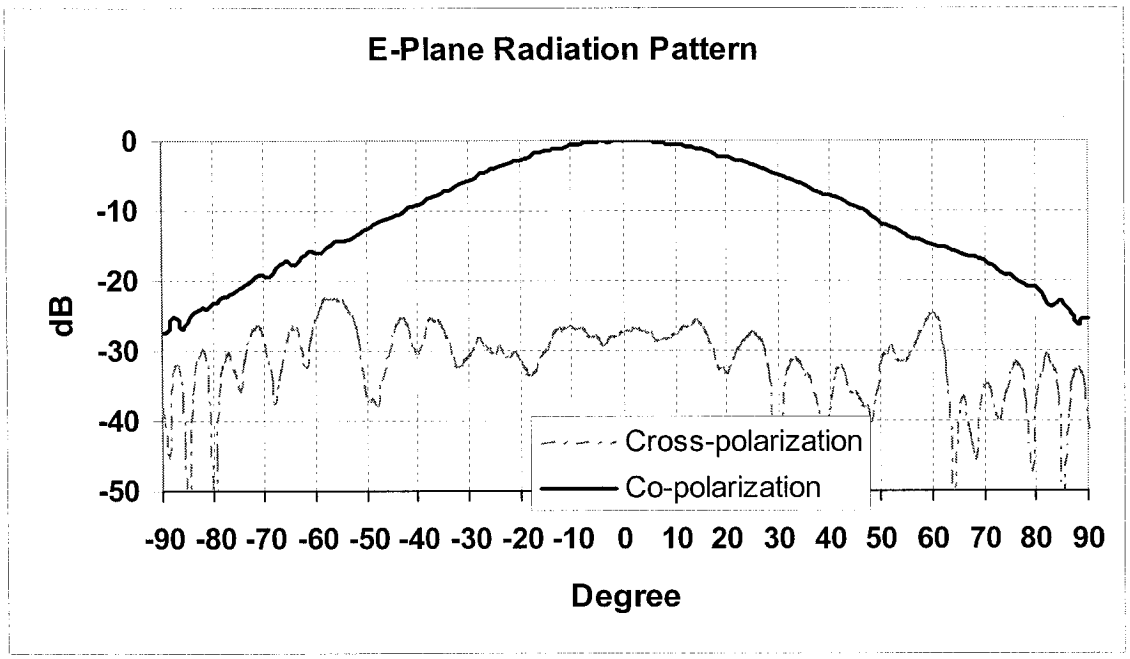

Fig. 5.12 (a) Measured radiation pattern of front coupling radiator in E-plane for $d_1 = 1.5mm$ and $d = 0.38mm$

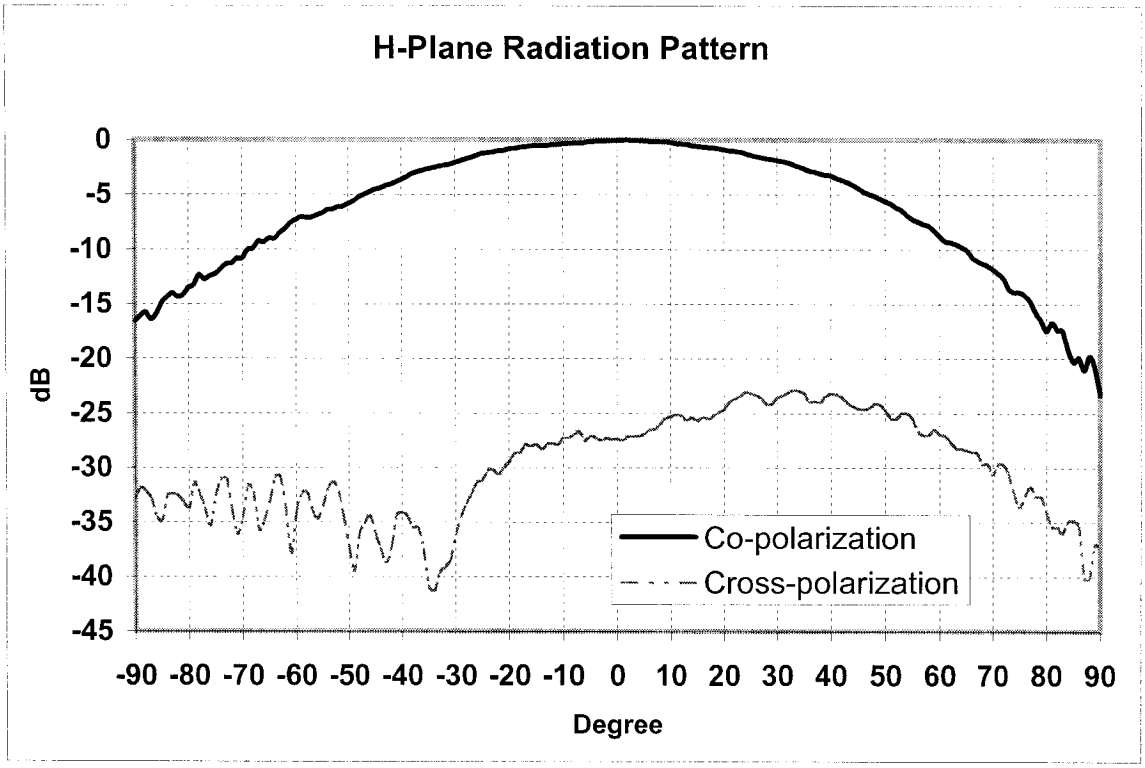

Fig. 5.12. (b) Measured radiation pattern of front coupling radiator in H-plane for $d_1 = 1.5mm$ and $d = 0.38mm$

5.3.2. Side Coupling NRD-guide Fed Cylindrical Dielectric Radiator

Similar to the front coupling structure, the side coupling NRD-guide fed cylindrical dielectric radiator, which consists of an NRD-guide feeder and a cylindrical resonator used as radiator also made of polystyrene ($\varepsilon_r = 2.56$) with height of 4.953 mm, the NRD-guide width of 3.556 mm as well as the resonator radius of 4.0 mm. In this case, the resonant frequency of the cylindrical dielectric resonator is known to be 27.342 GHz as well as the desired resonance mode TE_{011} is excited.

The input impedance of radiator is also determined by geometrical and electrical parameters. The coupling between the radiator and the NRD-guide feeder can be controlled by varying the distance between the radiator and the NRD-guide feeder (d_2). The position of radiator (d) is also considered to demonstrate that the impedance matching can be achieved by an adequate choice. Fig. 5.13 shows the frequency-dependent magnitude of return loss S_{11} as a function of the radiator position d with respect to the open edge while the distance between the radiator and NRD-guide feeder was $d_2 = 1.01mm$.

Typical measured return loss response of an NRD-guide side coupling with the cylindrical dielectric radiator for $d = 0.38mm$ and $d_2 = 1.01mm$, is shown in Fig. 5.14. The results show that the measured resonance frequency for $d_2 = 1.01mm$ and $d = 0.38mm$ is 27.921 GHz, which is close to the calculated valued of 27.342 GHz. This confirms the accuracy of our calculation in chapter III and is also consistent with the simulated result shown in Fig. 5.13. Excellent coupling efficiency can be obtained with the proposed coupling mechanism. There exits an optimal range d_2 to obtain the maximum coupling. For $d_2 = 1.01mm$ and $d = 0.38mm$, the minimum return loss is 25 dB. The bandwidth and coupling strength can be changed by adjusting ranges d and d_2.

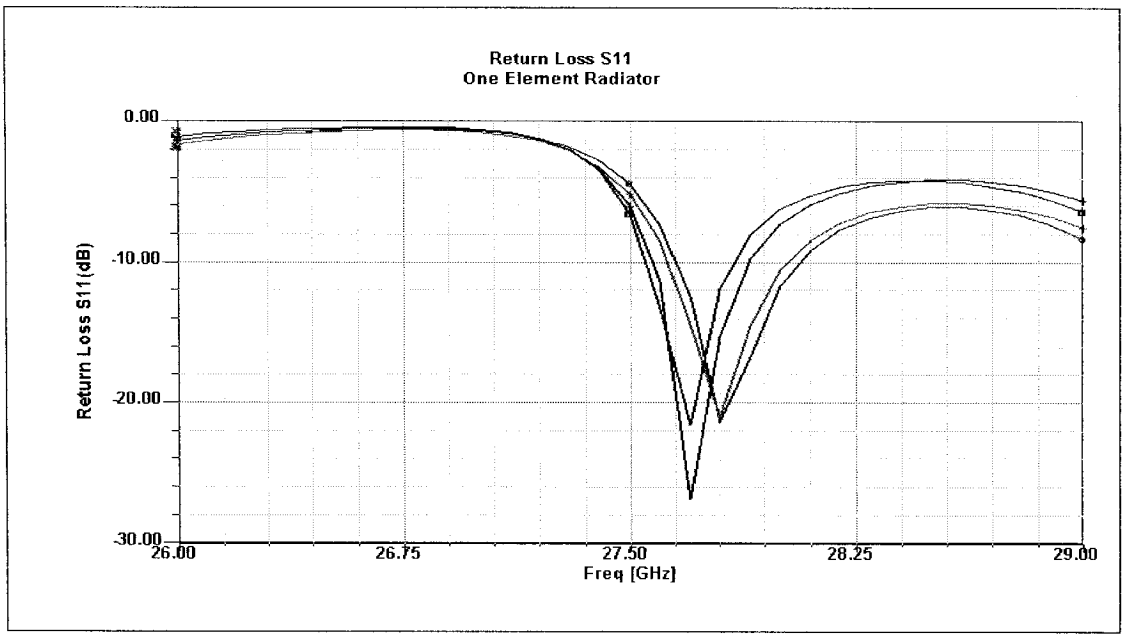

Fig. 5.13 Simulated return loss versus frequency for different position (d) of front coupling radiator while $d_2 = 1.01mm$

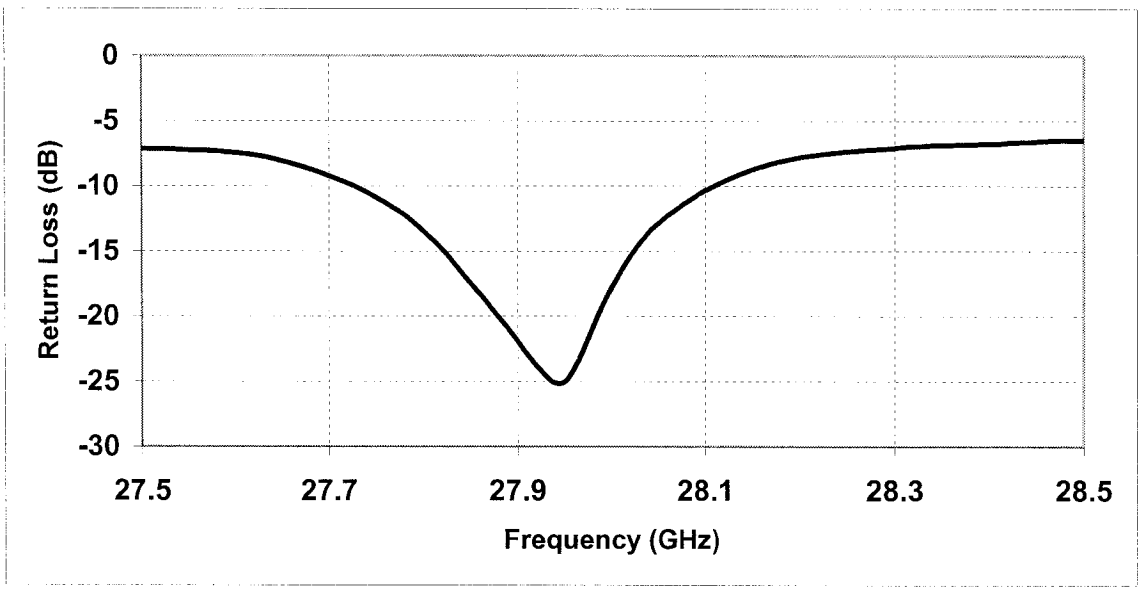

Fig. 5.14 Measured return loss response of an NRD-guide side coupling with cylindrical dielectric radiator for position $d = 0.38mm$ and $d_2 = 1.01mm$

Fig. 5.15 (a) and (b) show the E plane (xy plane) and H plane (xz plane) co-polar and cross-polar patterns over 180°, respectively, simulated by HFSS for $d = 0.38mm$ and $d_2 = 1.01mm$. They also indicate that the half power beam width (96°) in H-plane is much larger than that in E-plane (57°).

The measured radiation pattern of CUDR fed by the NRD-guide with $d_2 = 1.01mm$ and $d = 0.38mm$ is illustrated in Fig. 5.16 (a) and 5.16 (b), which shows that realized gain for this antenna is measured as 14.1 dB, as well as the half power beam widths are 51° in E-plane and 84° in H-plane. The agreement between the measurement and simulation is good. The coupling efficiency is high and good matching can easily be obtained. As shown in Fig. 5.16 (a) and (b), an isolation of about 15 dB between the E-plane co-polar and cross-polar patterns can be achieved. Meanwhile, the isolation between the H-plane co-polar and cross-polar pattern is about 20 dB. In both case, there are virtually slight side-lobe effects over the range of interest. The main beam direction of the radiation pattern in E-plane appears with slight shifting.

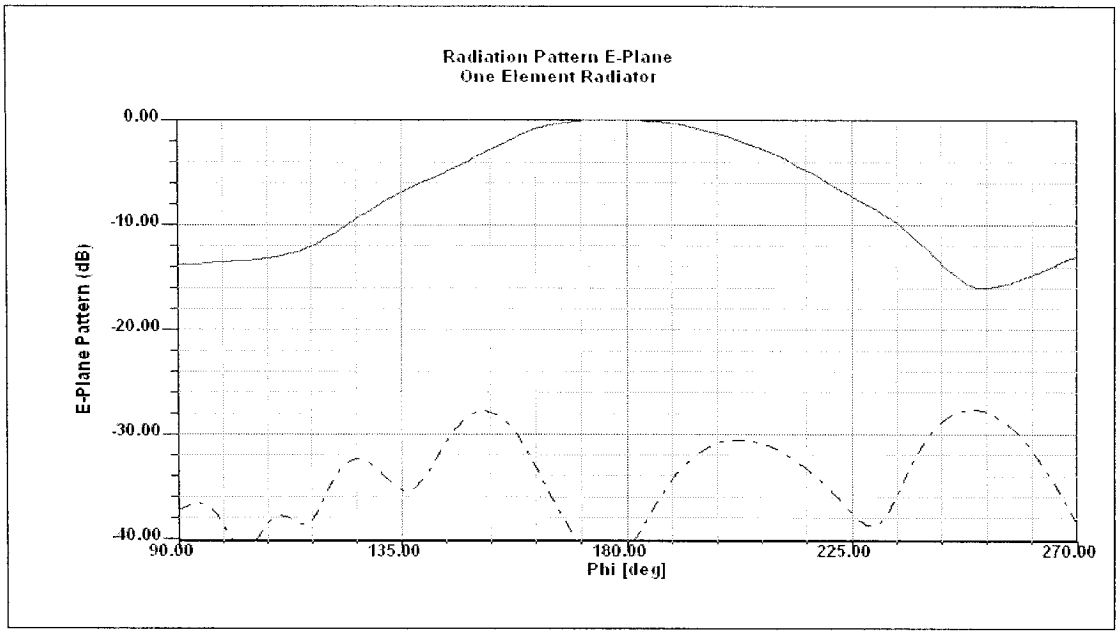

Fig. 5.15 (a) Simulated radiation pattern of side coupling radiator (E-plane)

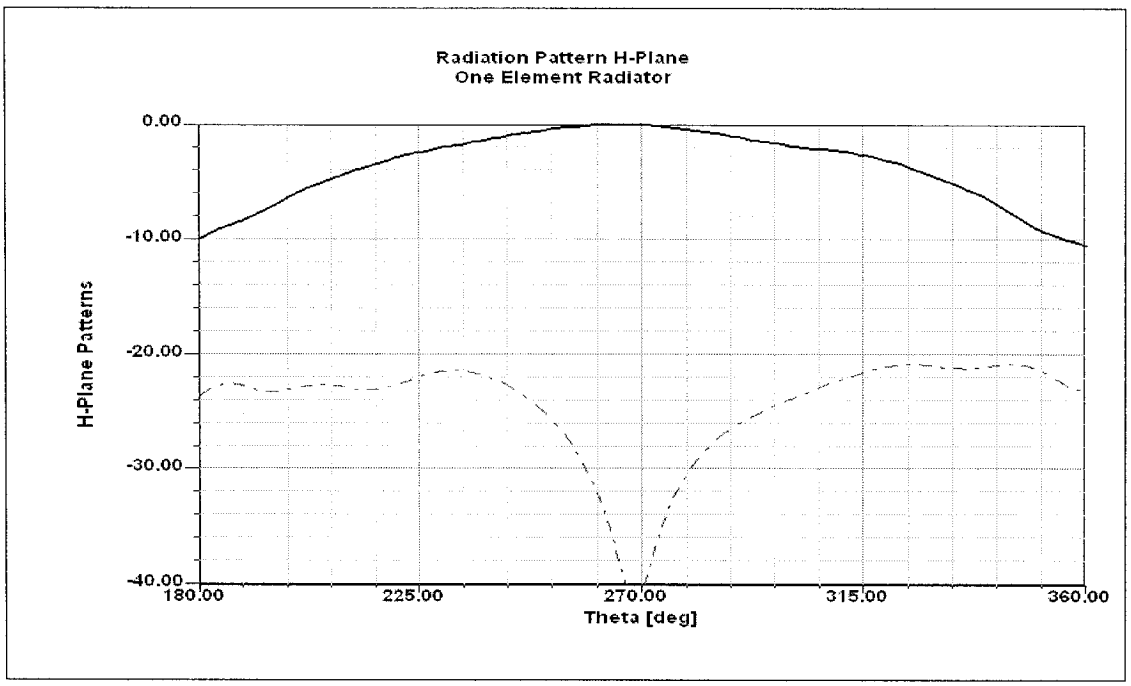

Fig. 5.15 (b) Simulated radiation pattern of side coupling radiator (H-plane)

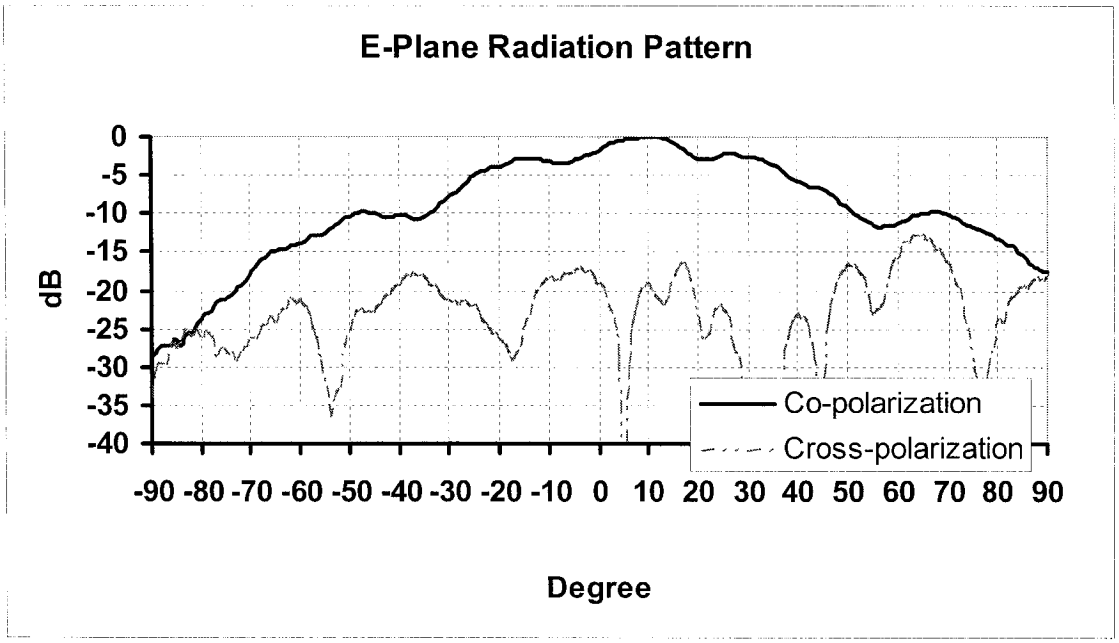

Fig. 5.16. (a) Measured radiation pattern of side coupling radiator in E-plane for $d_2 = 1.01mm$ and $d = 0.38mm$

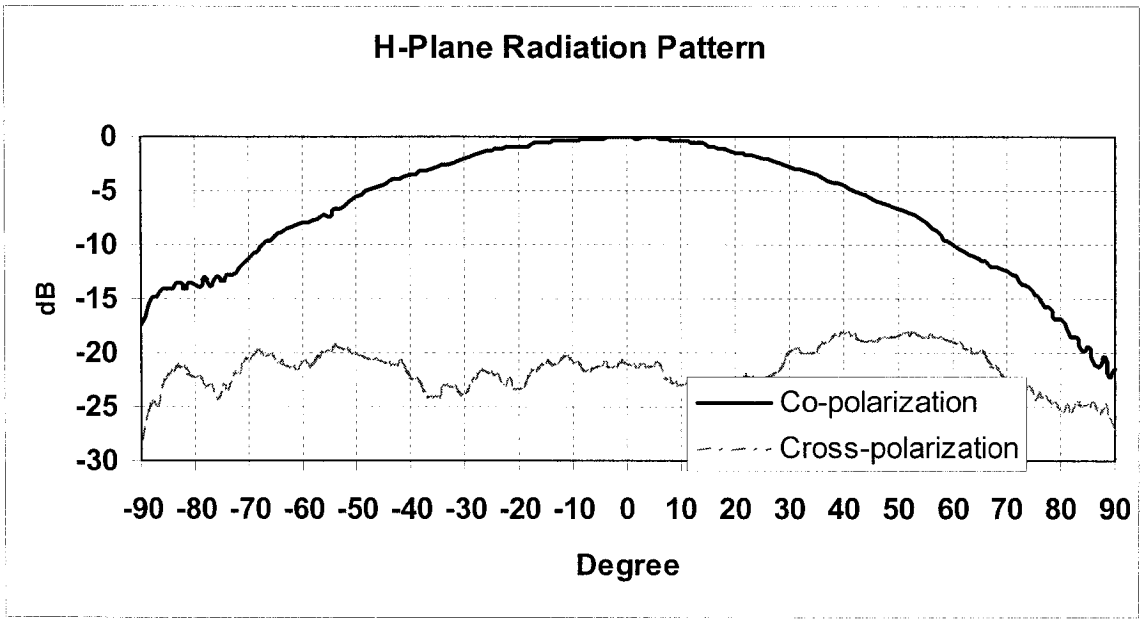

Fig. 5.16. (b) Measured radiation pattern of side coupling radiator in H-plane for $d_2 = 1.01mm$ and $d = 0.38mm$

5.4. Cylindrical Dielectric Radiator Array

To increase the directivity of antenna, multiple CUDRs may be cascaded to form an array. The elements can be fed by a single NRD-guide or multiple NRD-guide, the three-dimensional (3D) geometrical transparent view of the proposed single and multiple NRD-guide coupling schemes with CUDR arrays is shown in Fig. 5.17 (a) and 5.18 (a), as well as the top view of single and multiple NRD-guide coupling arrangement with CUDR arrays is shown in Fig. 5.17 (b) and 5.18 (b). The distance from the NRD-guide feeder to radiators are still denoted as d_1 or d_2; the position of radiators with respect to the edge of two metal plates is d; distances between two adjacent radiators are s or s_1. With the increasing of s or s_1, the resonant frequency of CUDR array increases; the bandwidth becomes narrow with emerging side lobes. The changing in mutual coupling and the tuning in resonant frequency of CUDR array can be easily done and controlled by adjusting the distance s between the dielectric resonators. This is a significant advantage of this type of antenna arrays [7].

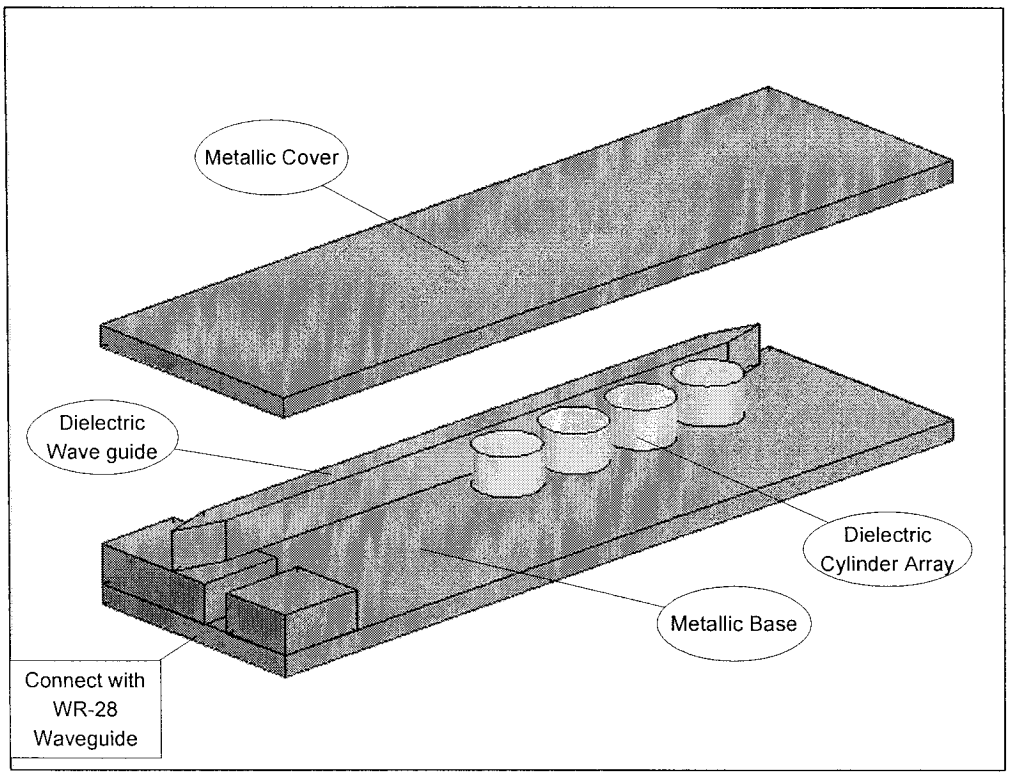

Fig. 5.17 (a) Three-dimensional (3D) geometrical transparent view of the proposed single NRD-guide side coupling with CUDR array

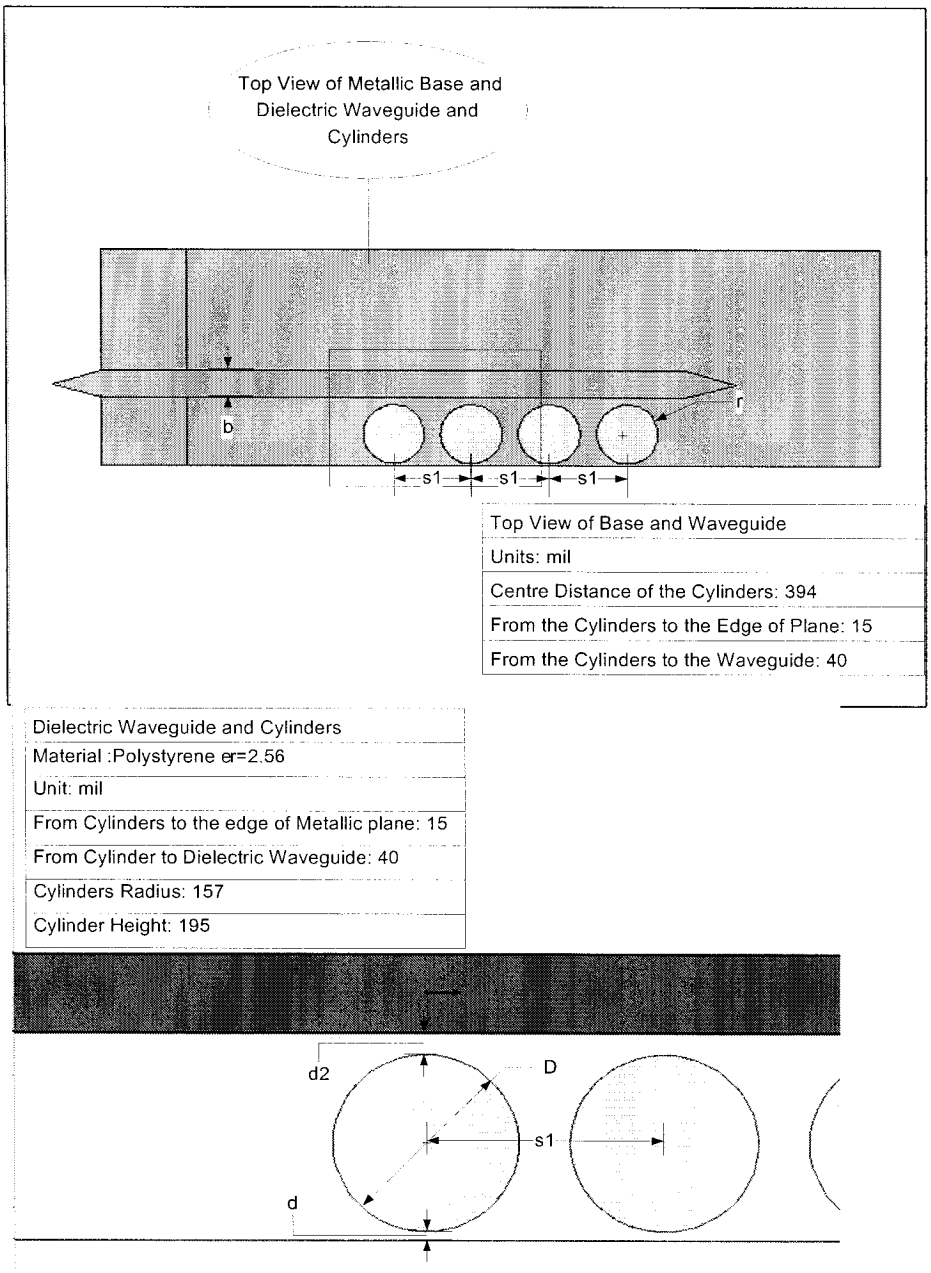

Fig. 5.17 (b) Top view of the proposed single NRD-guide side coupling with CUDR array

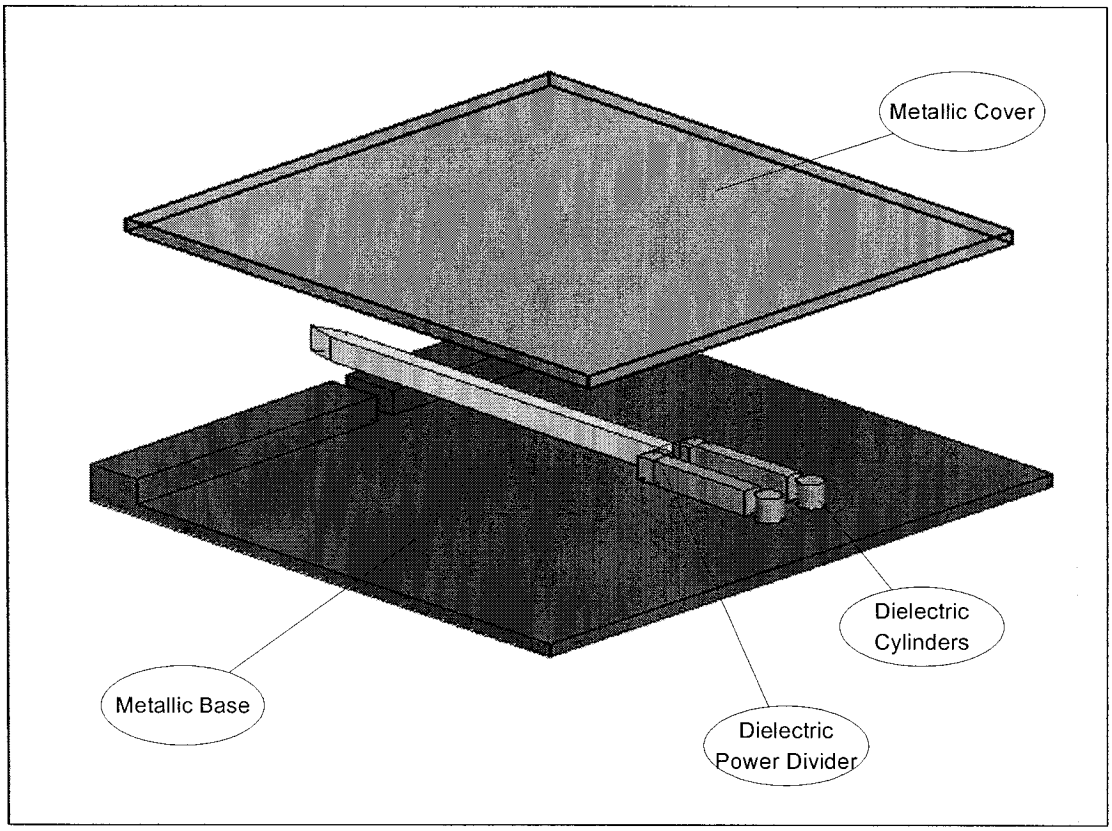

Fig. 5.18 (a) Three-dimensional (3D) geometrical transparent view of the proposed multiple NRD-guide front coupling with CUDR array

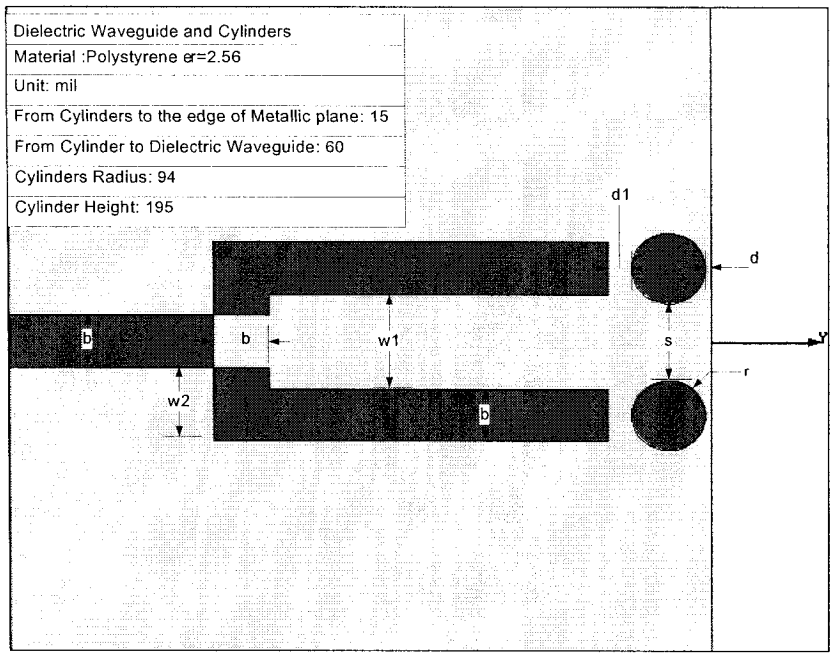

Fig. 5.18 (b) Top view of the proposed multiple NRD-guide front coupling with CUDR array

5.4.1 Multiple NRD-guide Front Coupling CUDR Array

CUDRs fed by a multiple NRD-guide that consists of an NRD-guide T-junction and two NRD-guide 90° bends described in a previous chapter. The proposed structure has been illustrated in Fig. 5. 18. The dielectric radiators and NRD-guide are made of polystyrene ($\varepsilon_r = 2.56$) with height of 4.953 mm, the NRD-guide width of 3.556 mm and the radiators radius of 2.4 mm, while $d_1 = 1.5mm$, $d = 0.38mm$, and $s = 8.788mm$. The resonant frequency of cylindrical dielectric resonator remains to be 27.047 GHz as well as the desired resonance mode HEM_{111} is excited.

The measured return loss of the two-elements CUDR array fed by the multiple NRD-guide is presented in Fig. 5.19. It shows that 10 dB return loss bandwidth of two elements array is 0.3 GHz with a center frequency 27.38 GHz, which agrees with the calculated values of 27.047 GHz.

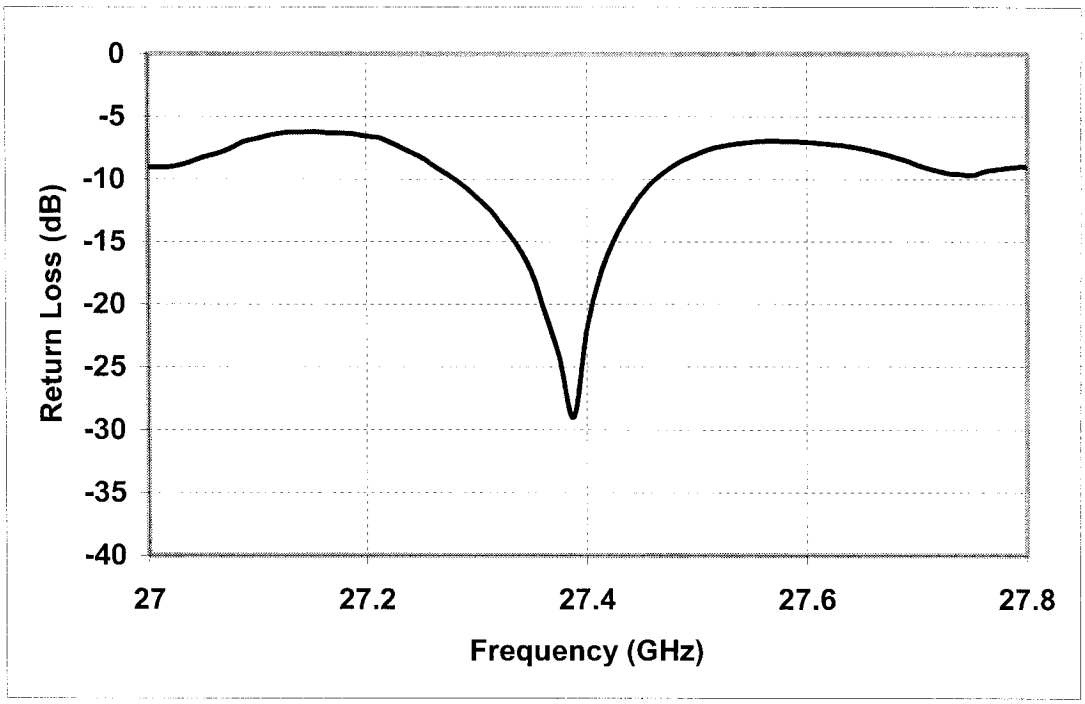

Fig. 5.19 Measured return loss of the two-elements CUDR array fed by multiple NRD-guide

The simulated E-plane and H-plane patterns of the two-elements CUDR array with $d_1 = 1.5mm$, $d = 0.38mm$, and $s = 8.788mm$ are shown in Fig. 5.20 (a) and (b). The MI-3000 system was used to measure the radiation patterns of CUDR array. The measured radiation patterns of the structure fed by the multiple NRD-guide with $d_1 = 1.5mm$ and $d = 0.38mm$ at the center frequency of 27.4GHz are shown in Fig. 5.21 (a) and (b), which can be found that antenna array gain is measured to be 11.4 dB,

as well as the half power beam widths are 25° in E-plane and 75° in H-plane. The agreement between the measurement and simulation is good. As shown in Fig. 5.21 (a) and (b), an isolation of about 25 dB between the E-plane co-polar and cross-polar patterns can be achieved. Meanwhile, the isolation between the H-plane co-polar and cross-polar patterns is about 23 dB. There are side-lobe effects over the range of interest in the E-plane beam.

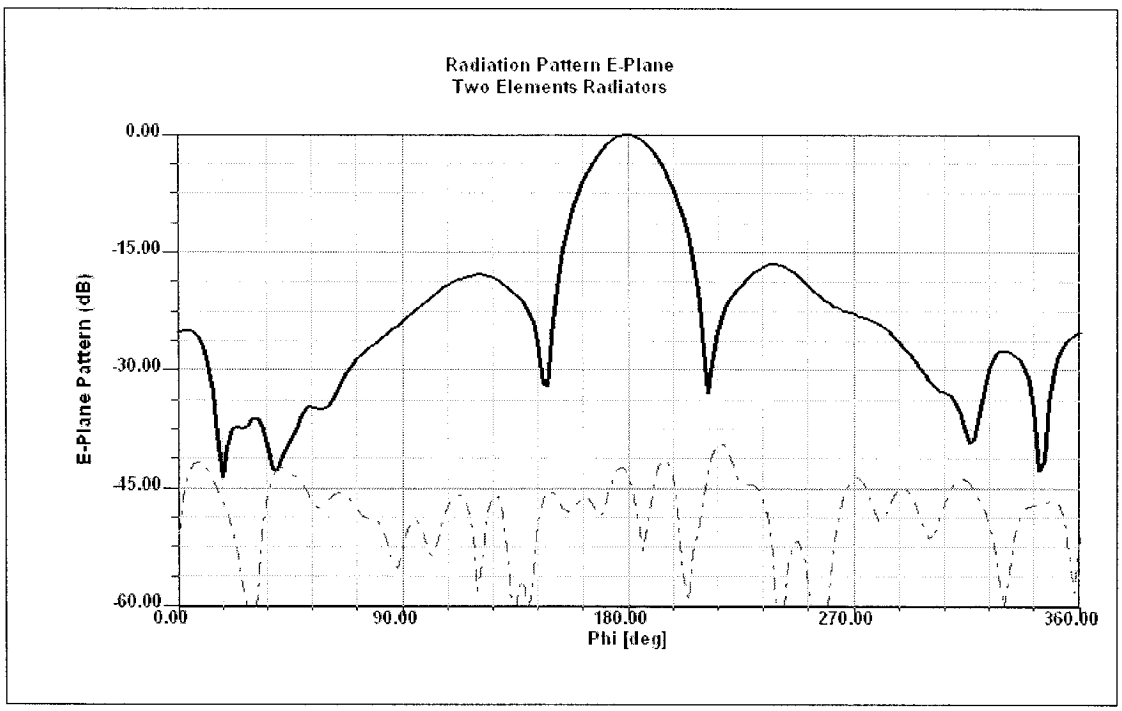

Fig. 5.20 (a) Simulated E-plane of the two-elements CUDR array fed by the multiple NRD-guide with $d_1 = 1.5mm$, $d = 0.38mm$, and $s = 8.788mm$

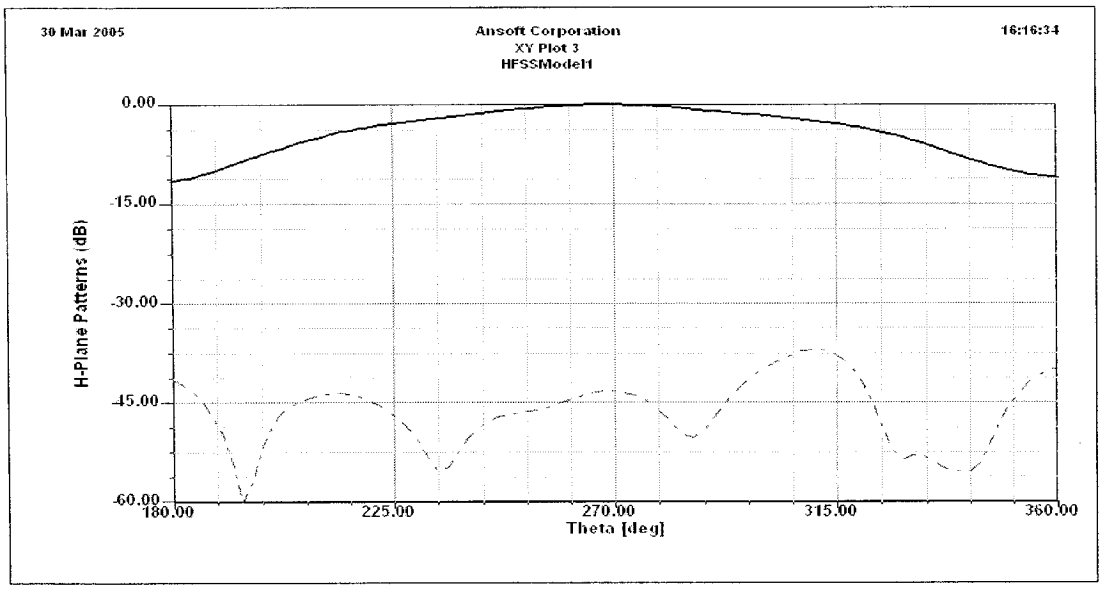

Fig. 5. 20 (b) Simulated H-plane patterns of the two-elements CUDR array fed by the multiple NRD-guide with $d_1 = 1.5mm$, $d = 0.38mm$, and $s = 8.788mm$

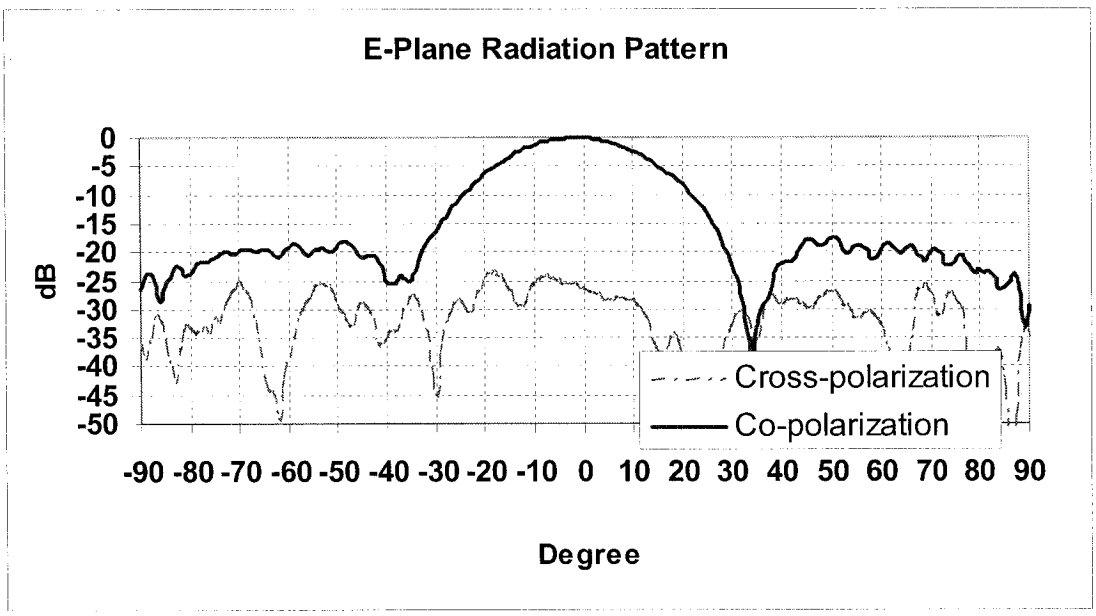

Fig. 5.21 (a) Measured E-plane patterns of the two-elements CUDR array fed by the multiple NRD-guide with $d_1 = 1.5mm$, $d = 0.38mm$, and $s = 8.788mm$

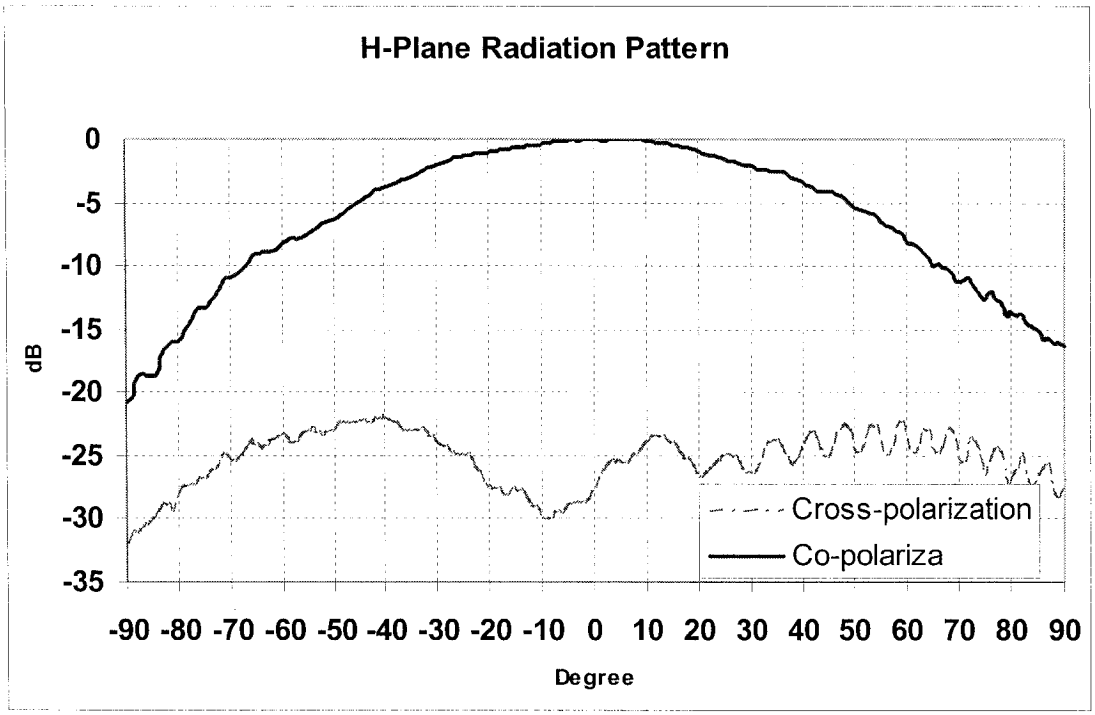

Fig. 5.21 (b) Measured H-plane patterns of the two-elements CUDR array fed by the multiple NRD-guide with distance $d_1 = 1.5mm$, $d = 0.38mm$, and $s = 8.788mm$

5.4.2 Single NRD-guide Side Coupling CUDR Array

Similarly, CUDR array can also be fed by a single NRD-guide, as shown in Fig.5.17. The material of radiators and NRD-guide are also polystyrene ($\varepsilon_r = 2.56$) with height of 4.953 mm, width of 3.556 mm and the resonators radius of 4.0 mm, while $d_2 = 1.01mm$, $d = 0.38mm$, and $s_1 = 10mm$. The resonant frequency of cylindrical dielectric resonator is 27.342 GHz as well as the desired resonance mode TE_{011} is excited.

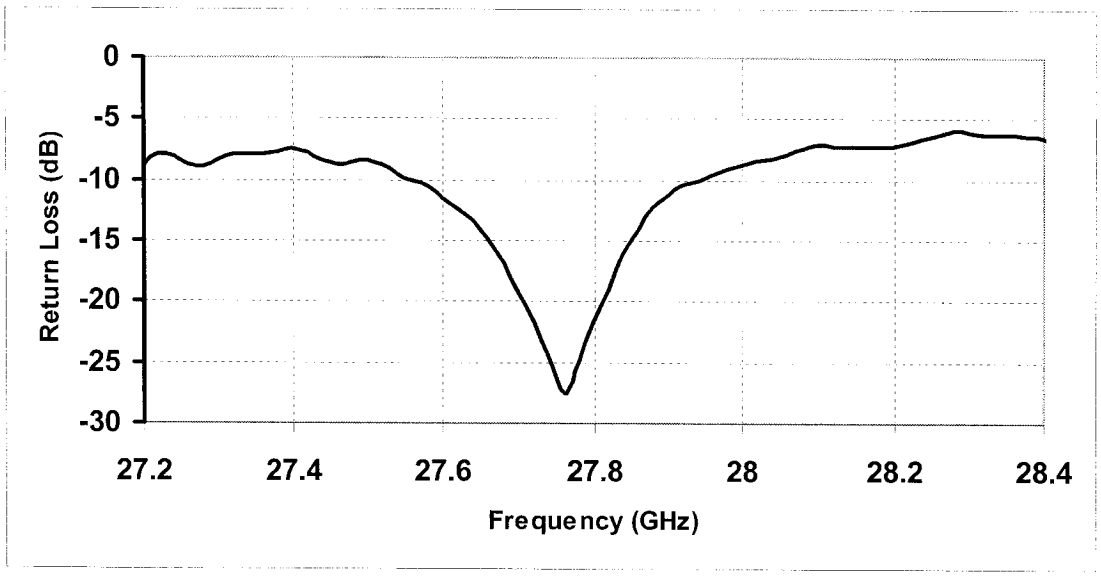

Fig. 5. 22 Measured return loss of the two-elements CUDR array fed by single NRD-guide with $d = 0.38mm$, $d_2 = 1.01mm$, and $s_1 = 10mm$

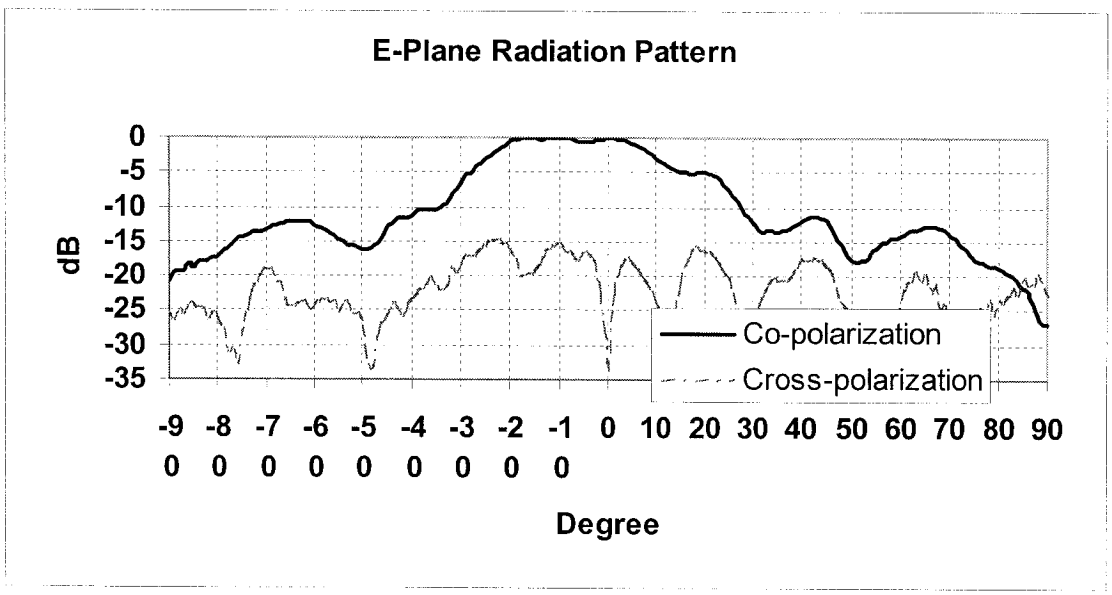

Fig. 5.23 (a) Measured E-plane radiation pattern of CUDR array fed by single NRD-guide with $d_2 = 1.01mm$, $d = 0.38mm$, and $s_1 = 10mm$

Fig. 5.22 shows the measured return loss of the two-element CUDR array fed by the single NRD-guide. It can be found that 10 dB return loss bandwidth of the two elements array is 0.4 GHz with a center frequency 27.76 GHz, which agrees with the calculated values of 27.342 GHz.

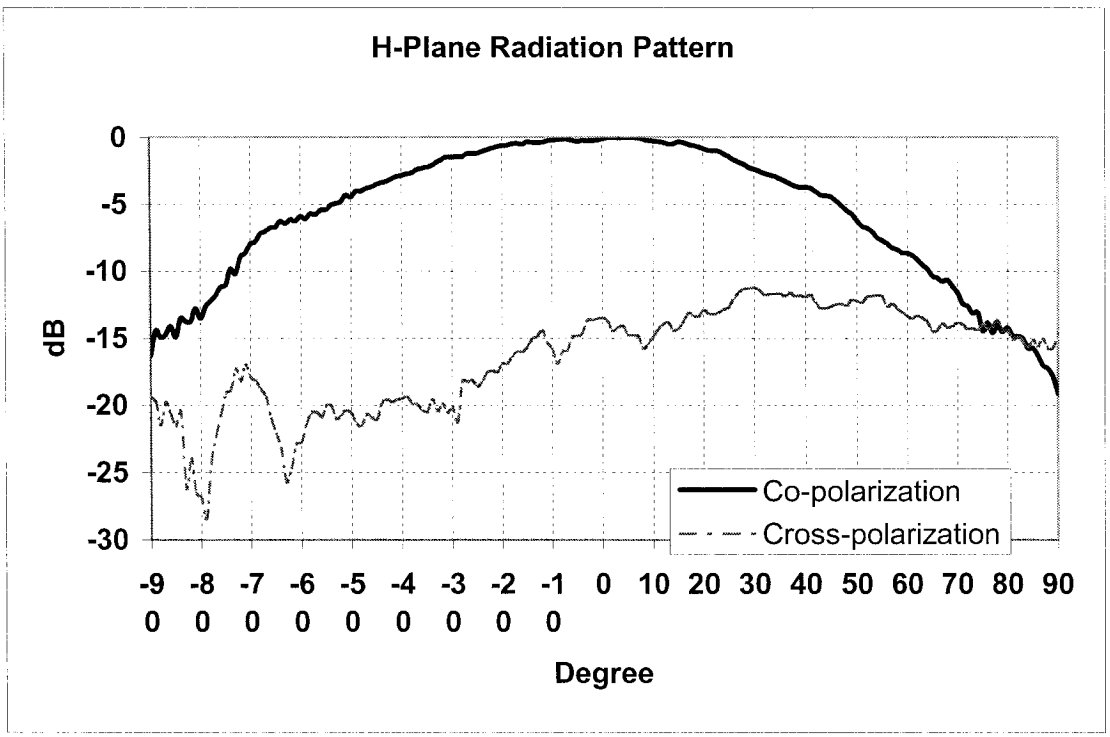

Fig. 5.23 (b) Measured H-plane radiation pattern of CUDR array fed by single NRD-guide with $d_2 = 1.01mm$, $d = 0.38mm$, and $s_1 = 10mm$

The measured radiation pattern of CUDR array fed by single NRD-guide with $d_2 = 1.01mm$, $d = 0.38mm$, and $s_1 = 10mm$ at the center frequency of 27.8GHz are shown in Fig. 5.23 (a) and (b), which can be found that realized gain for antenna array is measured as 13.42 dB, as well as the half power beam widths are 35° in E-plane and 75° in H-plane. As shown in Fig. 5.23 (a) and (b), an isolation of about 15 dB

between the E-plane co-polar and cross-polar patterns can be obtained. Meanwhile, the isolation between the H-plane co-polar and cross-polar pattern is about 12 dB. There are virtually slight side-lobe effects over the range of interest in the E-plane radiation pattern. The main beam direction of the radiation pattern in E-plane appears with a slight shifting.

5.5. Conclusion

Interesting performances of the CUDR antenna and its potential use in the design of CUDR array antenna are presented with theoretical and experimental results. The design of the antenna begins with the study and experiments of a simple CUDR antenna made with only one dielectric resonator. This step is followed by the integration of NRD-guide feeder and cylindrical dielectric resonators used as radiators that take the advantages of two schemes (Dielectric Resonant Antenna (DRA) and NRD-guide). The results have suggested that CUDR antenna can be used to make a very good directive antenna with low RF loss.

CHAPTER VI

CONCLUSIONS AND RECOMMENDATIONS

6.1 Conclusion

This thesis has presented new concept and technology of cylindrical unidirectional dielectric radiator (CUDR) and radiators array for applications in conjunction with microwave and millimeter wave circuits, which are based on low loss NRD-guide technology and high-Q cylindrical dielectric resonator technology. The associated feed blocks are based on NRD-guide components such as metal waveguide to NRD-guide transition, NRD-guide T-junction and NRD-guide bend, which allow the NRD-guide in direct coupling with the cylindrical dielectric resonators that can be arranged as cylindrical unidirectional dielectric radiators (CUDR). The structure has been investigated and verified both theoretically and experimentally. Following is a summary of the work addressed in this thesis.

Chapter II presents general expressions for the hybrid-mode LSM and LSE mode fields of NRD-guide. The fields and propagation characteristics of the NRD-guide has been discussed. Operating modes, and dispersion and bandwidth characteristics are also presented. Technical merits and limitations of the NRD-guide are also discussed. It shows that the NRD-guide structures can be applied in the design for low-loss and low-cost integrated microwave and millimeter-wave circuits.

Dielectric resonators (DR) in cylindrical and rectangular shapes are commonly employed at microwave and millimeter-wave frequencies in the design of filters, oscillators, radiators, and tuning elements. In Chapter III, cylindrical dielectric resonator (CDR) has been studied analytically and experimentally. Electromagnetic fields and the eigenvalue equation of dielectric rod are presented. Detailed results provide us a basic concept and guideline for the design of parallel-plate cylindrical dielectric resonator. The operating modes and resonant frequencies in the cylindrical dielectric

resonator can be determined once the dimensions of cylindrical dielectric resonator (CDR) are given. It is important to know these properties for the lowest order resonant mode and few higher order modes in order to enable the selection of a proper mode for a particular application and the incorporation of a suitable coupling mechanism to excite the mode. Knowledge of field distribution also helps in devising suitable techniques for suppressing or eliminating undesired modes, which may interfere with the desired mode.

In Chapter IV, the NRD-guide feeder network, including metal waveguide transition, NRD-guide T-junction and NRD-guide bend, has been proposed and developed. Simulated and measured results have shown the operating mechanism and preliminary performance of the NRD-guide feeder. The resonance and spikes were also discussed. This proposed structures is optimized for low return loss in achieving a good matching with the help of commercial software Agilent HFSS. The experiments verify the low-loss characteristic of the structure and the performances of NRD-guide transition, T-junction and bend demonstrated application for the construction of millimeter-wave circuits.

In Chapter V, the new concept of cylindrical unidirectional dielectric radiator and radiators array are presented. Two basic NRD-guide feeding structures are studied and fabricated that directly couple with CUDR and CUDR array and excite mode of interest in the radiators. Good performances of the CUDR antenna and CUDR array and its potential use in millimeter-wave circuits are shown. The design of the antenna begins with the study and experimentation of a simple CUDR antenna made with only one dielectric resonator that takes the advantages of two schemes (Dielectric Resonant Antenna (DRA) and NRD-guide). Next step is followed by integration of the NRD-guide feeder network and dielectric radiators to construct two kinds of cylindrical

unidirectional dielectric radiators arrays. The results have proven that CUDR and CUDR array can be used to make a good directive antenna with low RF loss.

6.2 Suggestions for Future Work

As known, a remarkable advantage of cylindrical dielectric radiator and radiators array is that this CUDR radiating element retains the attractive features of the NRD-guide technologies and dielectric resonator. The experiments results demonstrate the usefulness and interesting properties of radiation characteristics, which is suitable for millimeter-wave applications.

As mentioned previously this novel cost-effective technology is expected to be a promising fundamental building block for practical application in antennas. Such structure makes it possible to combine the dielectric antenna technology and NRD-guide technology and take advantage of both for different functions. Other interesting projects would be to incorporate this radiating component in systems such as millimetre-wave antenna and space power combining circuits.

In the design of the feeder block of CUDR, the new NRD-guide technologies (SISW, SICs, SINRD) can be applied and combined with CUDR. Meanwhile, CUDR and CUDR array can be designed at higher frequencies, which will demonstrate the superior electrical performance at millimeter-wave frequencies

REFERENCES

[1] K. R. Carver and J. W. Mink, "Microstrip antenna technology," *IEEE Tran. Antennas Propagat.,* vol. 29, pp. 2-23, Jan. 1981.

[2] D. M. Pozar, "Microstrip antennas," *Proc. IEEE,* vol. 80, no. 1, pp.79-91, Jan. 1992.

[3] J. Huang, "A *Ka*-band circularly polarized high gain microstrip array antenna," *IEEE Trans. Antennas Propagat.,* VOL. 43, PP. 113-116, Jan. 1995.

[4] S. Kitao, M. Yamayo, H. Ohmine, H. Aoki, and T. Haruyama, "Eradiation properties of triplate line fed microstrip array antenna with polarization grid in the 60-GHz," *IEICE Nat. Conv. Rec.,* vol. B-60, Sept. 1995.

[5] R. K. Mongia, A. Ittipiboon, P. Bhartia, and M. Cuhaci, "Electric-monopole antenna using a dielectric ring resonator," *Electron. Lett.,* vol. 29, no. 17, pp. 1530-1531, Aug. 1993.

[6] K. Wu, L. Ji, and R. G. Bosisio, "A low-loss unidirectional dielectric radiator (UDR) for antenna and space power combining circuits," *IEEE Trans. Microwave Theory Tech,* vol., 42, pp. 339-341, Feb. 1994.

[7] H. An, K. Wu, and R. G. Bosisio, "Analytic and experimental investigations of aperture coupled unidirectional dielectric radiator array (UDRA)," *IEEE Trans. Antennas Propagate.,* vol. 44, pp. 1201-1207, Sept. 1996.

[8] M. Belaid, J. J. Laurin, K. Wu, "Integrated active antenna array using unidirectional dielectric radiators," *IEEE Trans. Microwave Theory Tech.,* vol. 48, pp.1628-1634, Oct. 2000.

[9] T. Yoneyama and S. Nishida, "Nonradiative dielectric waveguide for millimeter-wave integrated circuits," *IEEE Trans. Microwave Theory Tech.,* vol. Mtt-29, pp.1188-1192, Nov. 1981.

[10] T. Yoneyama, "Millimeter-wave integrated circuits using nonradiative dielectric

waveguide," *Electron. Communicate. Jan. –Pt. 2,* vol. 74, no. 2, pp. 87-94, 1991

[11] Yoneyama T., Fujita S., and Nishida S., " Insulated nonradiative dielectric waveguide for millimeter-wave integrated circuits," *IEEE Trans. Microwave Theory Tech.,* vol. 31, pp. 1002-1008, 1983.

[12] T. Yoneyama, "Millimeter-wave integrated circuits using nonradiative dielectric waveguide," *Electron. Commun. Jpn.,* pt. 2, vol. 74, no. 2, pp. 20-28, 1991.

[13] Yoneyama T., "Millimeter-wave transmitter and receiver using the nonradiative dielectric waveguide," *IEEE MTT-S International Microwave Symposium Digest, Long Beach, CA,* pp.1083-1086, 1989.

[14] A. Sanchez and A. A. Oliner, "A new leaky waveguide for millimeter waves using nonradiative dielectric (NRD) waveguide – Part 1: Accurate theory," *IEEE Trans. Antennas Propagat.,* vol. 35, pp. 737-747, Sept. 1988.

[15] A. Sanchez and A. A. Oliner, "A new leaky waveguide for millimeter waves using nonradiative dielectric (NRD) waveguide – Part 2: Comparison with experiments," *IEEE Trans. Antennas Propagat.,* vol. 35, pp. 748-752, Sept. 1988.

[16] A. S. Rong and Z. L. Sun, "Radiation of millimeter waves from NRD leaky wave antennas with tapered transition and tuning aperture," *IEEE Trans. Antennas Propagat.,* vol. 39, pp. 1366-1371, Sept. 1991.

[17] C. E. Tong, R. Blundell, and M. C. Carter, "An NRD-fed dielectric rod antenna for the short millimeter wave band," *Int. J. Infrared Millimeter Waves,* vol. 10, pp. 1327-1337, Sept. 1993.

[18] K. Maamria, T. Wagatsuma, and T. Yoneyama, "Leaky NRD guide as a feeder for microwave planar antennas," *IEEE Trans. Antennas Propagat.,* vol. 41, pp. 1680-1686, Dec. 1993.

[19] M. T. Lee, K. M. Luk, K. W. Leung, and M. K. Leung, "A small dielectric resonator antenna," *IEEE Trans. Antennas Propagat.,* vol. 50, pp. 1485-1487, Oct. 2002.

[20] D. Kajfez, P. Guillon, *Dielectric resonators*, Artech House, INC, 1986.

[21] "Nonradiative dielectric waveguide," in *Infrared and Millimeter Wave, New York: Academic,* vol. 11, ch. pp.61-98, 1984.

[22] "Recent development in NRD-guide technology," Ann. Telecom,. Vol. 47, nos. 11-12, pp. 508-514, 1992

[23] T. Yoneyama, "Millimeter-wave integrated circuits using nonradiative dielectric waveguide," *Electron. Commun. Jpn.,* pt. 2, vol. 74, no. 2, pp. 20-28, 1991.

[24] K. Wu and L. Han, "Hybrid integrated technology of planar circuits and NRD guide for cost effective microwave and millimeter-wave applications," *IEEE Trans. Microwave Theory Tech.*, vol. 45, pp. 946-954, June 1997.

[25] T. Yoneyama, H. Tamaki, and S. Nishida, "Analysis and measurement of nonradiative dielectric waveguide bends," *IEEE Trans. Microwave Theory Tech.*, vol. MTT-34, PP.876-882, Aug. 1986.

[26] F. Boone and K. Wu, " Mode conversion and design consideration of integrated nonradiative dielectric (NRD) components and discontinuities," *IEEE Trans. Microwave Theory Tech.*, vol. 48, pp. 482-492, Apr. 2000.

[27] T. Yoneyama and S. Nishida, " Nonradiative dielectric waveguide T-junctions for millimeter-wave applications," *IEEE Trans. Microwave Theory Tech.*, vol. MTT-33, pp. 1239-1241, Nov. 1985.

[28] Y. Endo and T. Yoneyama, " Finite element analysis of discontinuities in nonradiative dielectric waveguide," *Electron. Commun. Jpn.*, pt. 2, vol. 72, no. 11, pp. 102-112, 1989.

[29] F. Kuroki and T. Yoneyama, " NRD-guide center-feed H-shaped five port at millimeter-wave-lengths," in *Proc. 3rd Asia- Pacific Microwave Conf.*, Tokyo, Japan, 1990, pp. 7-10.

[30] J. A. G. Malherbe and J. H. Cloete, "A transition from recon angular to nonradiating dielectric waveguide," *IEEE Trans. Microwave Theory Tech.*, vol. MTT-33, no. 6, pp. 539-543, June 1985.

[31] Y. Cassivi and K. Wu, "Hybrid planar NRD-guide magic-Tee junction," *IEEE Trans. Microwave Theory Tech.*, vol. 50, no. 10, pp. 2405-2408, Oct. 2002.

[32] F. Boone, "Etude et conception de composants passifs en technologie NRD pour applications en ondes millimetriques," Ph. D dissertation, Dept. Elect., Eng., Ecole Polytech., Montreal, QC, Canada.

[33] J. A. G. Malherbe, "Radiation from an open-ended nonradiative dielectric waveguide," *Microwave Opt., Tech., Lett.*, vol. 14, no. 5, pp. 266-268, Apr. 1997.

[34] "The design of a slot array in nonradiating dielectric waveguide, part I: Theory," *IEEE Trans. Antennas Propagat.*, vol. AP-32, pp. 1335-1340, Dec. 1984.

[35] J. A. G. Malherbe, J. H. Cloete, I. E. Losch, M. W. Robson, and D. B. Davidson, "The design of a slot array in nonradiating dielectric waveguide, Part II: Experiment," *IEEE Trans. Antennas Propagat.*, vol. AP-32, pp. 1341-1344, Dec. 1984.

[36] J. A. G. Malherbe, and H. F. V. Boshoff, "Planar slot array fed by coupled dielectric lines in a metal waveguide," *in 1987 IEEE AP-S Int. Antenna Symp. Dig.*, Blacksburg, VA, June 1987, pp. 372-375.

[37] T. Yoneyama, T. Kuwahara, and S. Nishida, "Experimental study of nonradiative dielectric waveguide leaky wave antenna," *in Proc. ISAP'85, Kyoto, Japan*, Aug. 1985, pp. 85-88.

[38] J. A. G. Malherbe, "A leaky-wave antenna in nonradiative dielectric waveguide," *IEEE Trans. Antennas Propagat.*, vol. 36, pp. 1231-1235, Sept. 1988.

[39] H. Shigesawa, M. Tsuji, P. Lampariello, F. Frezza, and A. A. Oliner, "Coupling between different leaky mode types in stub-loaded leaky waveguides," *IEEE Trans. Microwave Theory Tech.*, vol. 42, pp. 1548-1560, Aug. 1994.

[40] J. A. G. Malherbe, "An integrated antenna for nonradiative dielectric waveguide," *in Proc. ISAP'85, Kyoto, Japan*, Aug. 1985, pp. 69-72.

[41] S. A. Long, M. W. McAllister, and L. C. Shen, " the resonant cylindrical dielectric

cavity antenna," *IEEE Trans. Antennas Propagat.,* vol. AP-31, pp. 406-412, May 1983.

[42] J. T. H. St. Martin, Y. M. M. Antar, A. A. Kishk, A. Ittipiboon, and M. Cuhaci, " Dielectric resonator antenna using aperture coupling," *Electron. Lett.,* vol. 26, pp. 2015-2016, 1990

[43] K. W. Leung, K. M. Luk, K. Y. A. Lai, and D. Lin, "Theory and experiment of a coaxial probe-fed hemispherical dielectric resonator antenna," *IEEE Trans. Antennas Propagat.,* vol. AP-34, pp. 1439-1446, Dec. 1986.